



LUND UNIVERSITY

Growth and optical properties of III-V semiconductor nanowires:

Studies relevant for solar cells

Dagyte, Vilgaile

2018

Document Version:

Publisher's PDF, also known as Version of record

[Link to publication](#)

Citation for published version (APA):

Dagyte, V. (2018). *Growth and optical properties of III-V semiconductor nanowires: Studies relevant for solar cells*. [Doctoral Thesis (compilation), Faculty of Engineering, LTH]. Solid State Physics, Lund University.

Total number of authors:

1

Creative Commons License:

CC BY

General rights

Unless other specific re-use rights are stated the following general rights apply:

Copyright and moral rights for the publications made accessible in the public portal are retained by the authors and/or other copyright owners and it is a condition of accessing publications that users recognise and abide by the legal requirements associated with these rights.

- Users may download and print one copy of any publication from the public portal for the purpose of private study or research.
- You may not further distribute the material or use it for any profit-making activity or commercial gain
- You may freely distribute the URL identifying the publication in the public portal

Read more about Creative commons licenses: <https://creativecommons.org/licenses/>

Take down policy

If you believe that this document breaches copyright please contact us providing details, and we will remove access to the work immediately and investigate your claim.

LUND UNIVERSITY

PO Box 117
221 00 Lund
+46 46-222 00 00

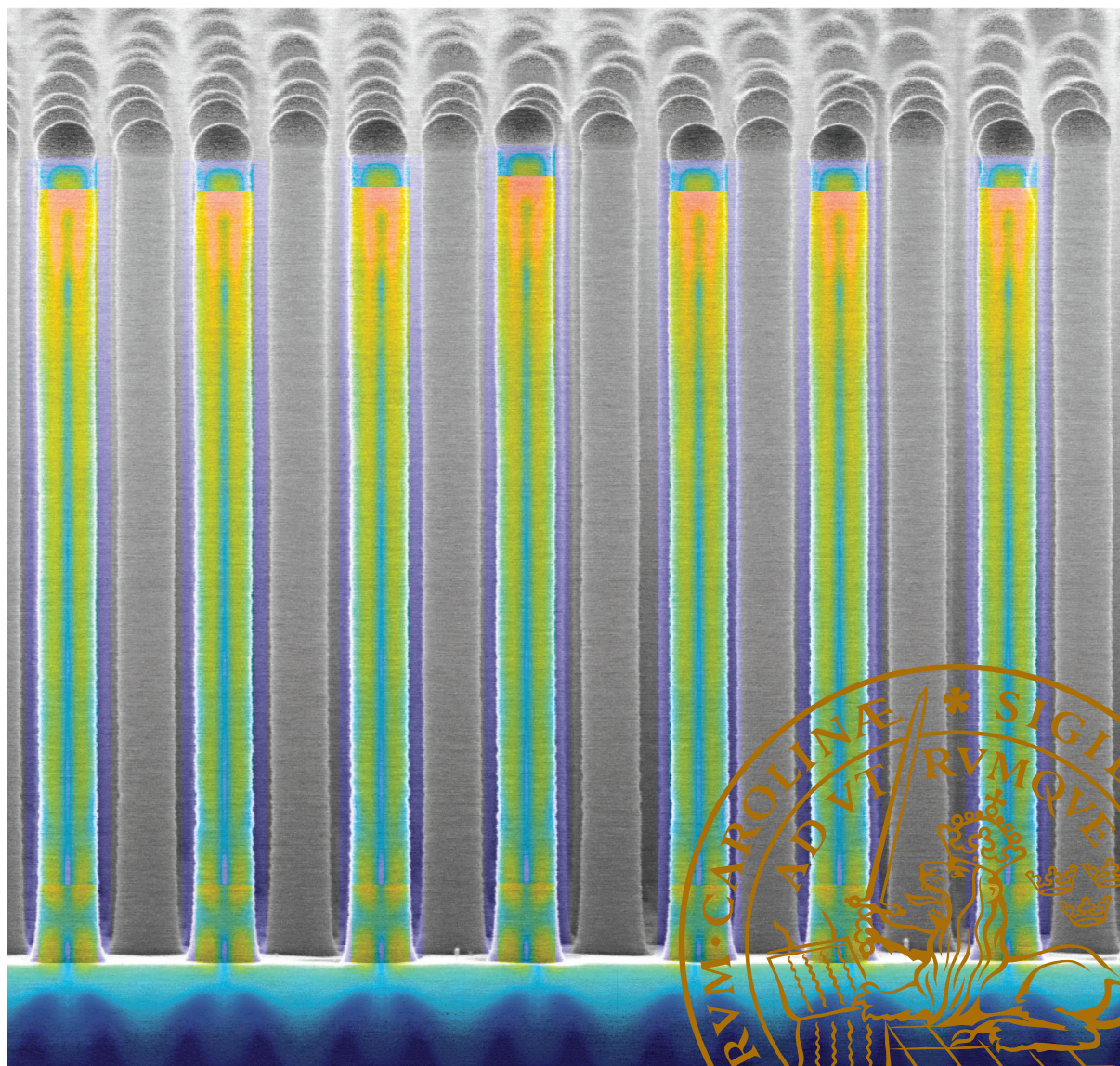


Growth and optical properties of III-V semiconductor nanowires:

Studies relevant for solar cells

VILGAILĖ DAGYTĖ

DEPARTMENT OF PHYSICS | LUND UNIVERSITY



Growth and optical properties of III-V semiconductor nanowires:

Studies relevant for solar cells

Vilgailė Dagytė



LUND
UNIVERSITY

DOCTORAL DISSERTATION

by due permission of the Faculty of Engineering, Lund University, Sweden.

To be defended on Friday, September 21st, 2018 at 9:15 in Rydbergsalen,
Sölvegatan 14, Lund, for the degree of Doctor of Philosophy in Engineering.

Faculty opponent
Prof. Erik Garnett

AMOLF, Netherlands

Organization: LUND UNIVERSITY	Document name:	DOCTORAL DISSERTATION
	Date of issue	2018-08-28
Author:	Vilgailė Dagytė	Sponsoring organization
Title and subtitle:	Growth and optical properties of III-V semiconductor nanowires: Studies relevant for solar cells	
<p>Abstract</p> <p>This thesis deals with epitaxial growth and optical properties of semiconductor nanowires with implications and insights about materials for solar cells. The chapters leading up to the papers give a broader background and an introduction to the field and include nanowires and their synthesis, semiconductor properties, solar cell operational principles, light interaction with a nanowire array, and optical characterization of such arrays.</p> <p>The nanowires were grown from gold seed particles using metal organic vapor phase epitaxy. Growth of ternary GaInP nanowires has been developed with a triethylgallium precursor that has not been commonly used before for this material structure in nanowires. We have achieved high yield and wide composition range nanowires with high control, which will be a crucial element for development of tandem solar cells where a high band-gap GaInP nanowire array could be the top cell.</p> <p>In terms of optical properties, lifetimes and carrier dynamics are important parameters for optoelectronic devices, including solar cells. We have investigated surface passivation of nanowires by capping GaAs nanowires with in-situ grown shells, at the same time evaluating the possibility of measuring time-resolved photoluminescence signal of as-grown nanowires, even when the substrate is made of the same material. We have identified that depending on doping levels in the substrate and the nanowires, excitation wavelength can be chosen to separate nanowire signal from the substrate signal. Moreover, we have preliminarily proposed a simple way to extract doping, which needs to be tested more extensively in the future. Such measurements of as-grown arrays could provide a fast and completely non-destructive characterization method for solar cell materials and allow further processing of the devices.</p> <p>Further, we have investigated reflectance and transmittance of flexible nanowire arrays embedded in a transparent polymer. Such flexible membranes could be interesting as flexible solar cells on their own, or could be incorporated on top of a lower band-gap material, for example silicon, to create a tandem solar cell. We have identified two potential issues with such structures. First of all, gold can absorb a significant fraction of the incoming light. The gold particles can be etched away, which recovers transmittance for the long wavelengths. However, a resonant reflectance peak is then observed. Through our work, we have identified that in-plane array modes arise in nanowire arrays embedded in a polymer that lead to resonant reflectance or absorbance in weakly absorbing materials. Such effect would be detrimental for transmitting long wavelengths to the bottom cell. Thus, we have investigated how these resonances depend on geometry in order to give guidelines for controlling this effect.</p>		
Key words: Nanowire, semiconductor, GaAs, GaInP, photovoltaics, epitaxy, optoelectronics		
Classification system and/or index terms (if any)		
Supplementary bibliographical information		Language: English
ISSN and key title		ISBN (print): 978-91-7753-773-1 ISBN (pdf): 978-91-7753-774-8
Recipient's notes	Number of pages: 228	Price
	Security classification	

I, the undersigned, being the copyright owner of the abstract of the above-mentioned dissertation, hereby grant to all reference sources permission to publish and disseminate the abstract of the above-mentioned dissertation.

Signature:



Date: 2018-08-13

Growth and optical properties of III-V semiconductor nanowires:

Studies relevant for solar cells

Vilgailė Dagytė

Doctoral Thesis

2018



LUND
UNIVERSITY

Division of Solid State Physics
Department of Physics
Lund University

Thesis advisors: Prof. Magnus T. Borgström, Prof. Lars Samuelson,
and Prof. Mats-Erik Pistol

Front cover: A GaInP nanowire array with *p-i-n* diode structure for solar cell devices, and GaP segment at the top as a window layer. The overlaid colors show modeled photogeneration rate due to absorption of sunlight.

Copyright © pp i-xxxi, 1-99, front and back covers by Vilgailė Dagytė

Paper 1 © IOP Publishing, CC BY

Paper 2 © IOP Publishing. Reproduced with permission. All rights reserved.

Paper 3 © IOP Publishing, CC BY

Paper 4 © by the Authors (Unpublished manuscript)


Division of Solid State Physics
Department of Physics
Lund University
SE-221 00 Lund
Sweden

ISBN 978-91-7753-773-1 (print)

ISBN 978-91-7753-774-8 (pdf)

Printed in Sweden by Media-Tryck, Lund University
Lund 2018



MADE IN SWEDEN 

Media-Tryck is an environmentally certified and ISO 14001 certified provider of printed material. Read more about our environmental work at www.mediatryck.lu.se

*“Promise me you’ll always remember:
You’re braver than you believe,
and stronger than you seem,
and smarter than you think.”*

- Christopher Robin to Winnie the Pooh

Contents

Preface	v
Acknowledgments	vii
Abstract	xi
Popular science short summary	xiii
Popular science extended summary	xv
List of papers	xxix
Abbreviations	xxxi
1 Introduction	1
1.1 Nanowires.....	1
1.2 Solar cells	3
1.3 Developing nanowires for solar cells	5
2 Basic semiconductor physics and solar cell operation	7
2.1 Semiconductors	7
2.1.1 Crystal structure.....	8
2.1.2 Band structure.....	8
2.1.3 Unintentional defects and intentional doping	12
2.1.4 Carrier concentration and recombination	16
2.1.5 <i>p-n</i> junction.....	22
2.2 Solar cells	23
2.2.1 Operational principles and main parameters	23
2.2.2 Main losses	25
2.2.3 Beyond the 33% single junction efficiency	26
3 Nanowire array synthesis	29
3.1 Metal-organic vapor phase epitaxy.....	30
3.1.1 Description of equipment	31
3.1.2 Gas phase processes.....	35
3.1.3 Processes on the surface	36
3.1.4 Thermodynamic and kinetic considerations	38

3.2	Considerations for nanowire growth	42
3.2.1	Periodic array preparation.....	42
3.2.2	Vapor liquid solid growth.....	43
3.2.3	Shell growth.....	49
3.2.4	Preparation after growth	50
4	Nanowire array optics	51
4.1	From bulk to nanowires.....	51
4.2	Geometric vs wave optics for nanowire arrays.....	53
4.3	Optical modes.....	55
4.3.1	Single nanowire	55
4.3.2	Nanowire array	57
4.4	Geometry dependent optical response.....	58
4.4.1	Enhanced absorption in nanowire arrays.....	59
4.4.2	Reduced reflection for tandem applications	60
5	Characterization techniques.....	63
5.1	Microscopy	63
5.1.1	Scanning electron microscopy.....	65
5.1.2	Transmission electron microscopy	65
5.2	X-ray diffraction.....	66
5.3	Photoluminescence	67
5.3.1	Steady state photoluminescence	68
5.3.2	Time-resolved photoluminescence	70
5.4	Absorption, transmission and reflection.....	73
5.5	In-situ optical reflectometry	77
6	Overview of results and outlook.....	81
6.1	Growth of ternary materials.....	81
6.2	Characterization of as-grown arrays.....	82
6.3	Optics of nanowire membrane.....	83
	References.....	87

Preface

In this thesis, my research on III-V semiconductor nanowires, including growth, optical characterization, and modeling of optical properties is presented. The contributions to the scientific field are contained in the articles and manuscripts included at the end of the thesis, whereas the chapters leading up to the papers give a scientific background and introduce the reader to the language and the field of the appended papers. Finally, before the introduction, you will find a popular science summary, where I attempted to give a taste of my research in more casual language, similar to what I have used during outreach presentations to general public and high school students. The short popular science summary gives just a quick overview of the topics I have worked with, whereas the extended summary gives more background, analogies, as well as details of my work and broader research area. I hope that all of you that open my thesis will find something of interest here.

Acknowledgments

4 years flew by so quickly that it feels like I just started at FTF and yet I have met so many wonderful people who helped me along the way. Just writing this acknowledgements section makes me smile from all the good memories and wonderful people I got to meet. Hence, I would like to extend a very warm Thank You to everybody at FTF for creating a wonderful, inspiring, caring and fun atmosphere, where, aside from the scientific topics, I learnt about Sweden as well as other cultures, and not the least, all kind of crazy facts about pretty much everything and anything during lunch breaks. There are some people, however, that I would like to extend special thanks to by saying a few words, even if words fail me to express the full extent of my appreciation for you being a part of my life.

First, my main supervisor, Magnus: You have really filled the whole scale, from being a great mentor, to being a great friend to chat with. You were always entertaining, sometimes bursting out with songs in the middle of a conversation, but, above all, always caring and helpful, always with the door open to devote your time to your students, no matter how stressed you were about your own deadlines. Thanks for all the long discussions and surviving my long reports, articles, and everything else. Also, for giving me the freedom to choose my research interests, which I believe helped me grow as an independent researcher.

Mats-Erik, you have been a supportive co-supervisor as well as a friend. Having you stumble into my office as if just in passing asking how my work is coming together, always having time to listen to me and giving some sane advice in addition to crazy stories really showed how much you care. Thanks for teaching me the importance of careful and realistic project planning.

Lars, I appreciate the opportunities to chat with you, filled with enthusiasm and eagerness to hear about what I have been working on, always happy to see me. You have always been very warm and fun to talk to and I knew that you were around as soon as I heard somebody happily whistling a tune in the corridor. Your kindness, experience, ideas, and stories are truly inspirational.

As most of you know, during these 4 years, I managed to try my hands on a lot of experimental techniques and I could not have done that without your help! My

biggest thanks goes to Gaute who took care of me already during the interviews and continued to do so by teaching me from basics such as how to handle tweezers (instilling me with a positive attitude even when I dropped his samples upside down on a hot susceptor) up to growing nanowires and much more. You have always been there to support me and I admire your work and life ethics, as well as your wittiness that always brightened my day. I have learnt a great deal from Magnus H. about growth, nanowires, TEM, and maybe most importantly, how to plan my experiments, keep organized and keep calm. I very much appreciated you casually coming by the lab just to see in case you could help or teach something, or just to ask how it was going. Alexander, you have always been very kind to discuss any growth related issues with. Xulu, we started at the same time and it has been a great journey to learn and work together with you. Enrique, your optimism and enthusiasm always puts a smile on my face – it is fun to work together with you. Pyry, although we only briefly worked on a project together, it has been nice learning from you and I am looking forward to working with you again. Lukas and Yuwei, you joined the group fairly recently, but we already had some good collaboration – thanks! Reza – thanks for helping out with imprint when I really needed it!

Neimantas, David L, Niklas S. - thank you for your kindness in helping me out with the optical measurements. Renato – thanks for teaching me processing and using a probe station. Olof – you were always very kind to discuss any questions I had about electrical properties and measurements as well as processing. Vishal – thanks for helping me with the EL measurements. Jesper – it was a lot of fun joining beam time at ESRF and learning to do measurements with synchrotron – I appreciate the opportunity you gave me. Colleagues at chemical physics, especially Arkady and Wei – you were so kind and devoted a lot of time teaching me about TRPL and discussing any topics related to it. Marcello – we have only recently started working together, but I find your enthusiasm and the care you put into experiments quite exceptional. To Sebastian – I appreciate your no-nonsense attitude and your help and advice in the lab. You made me feel encouraged that I am on the right path. Andrea – it has been a pleasure knowing you from the beginning of our PhD journey during interviews up until now. Thanks for your great attitude; it was fun having projects and courses together as well as to chat about topics beyond work.

Elke, Anette, Erik, Malin, Calle, Regina, Florinda, Oskar, Sara, Sudhakar, Laura, Martin J., Robert, Jason, Martin H., Damiano, Maryam, Steven, Ville – our scientific paths might have not crossed, but I definitely enjoyed the chats during breaks, lunches, summer schools, etc....

I would like to also extend gratitude to the technical and administrative staff that kept LNL and FTF running smoothly: Ivan, Maria, Peter, Håkan, Sara, Mariusz, George, Anders, David, Dmitry, Sören, Bengt, Abdul-Rehman, Charlotte, Mia, Margareta, Monica, Louise, Gerda, Line, Johanna and Janne. A lot of you taught me tips and tricks with technical equipment or administrative tasks and you made me feel that if I did not know how to do something, there was always somebody ready to help. Without you, FTF would turn into chaos. Also, thanks to Knut, Dan, Heiner and Anneli, both for their excellent job at organizing and leading people, as well as for some great conversation topics.

I would also like to thank Maria M. and Line for opportunities to do outreach activities that I really enjoyed. Also, thanks to Martin M., Olof, Laura, Marcus and Linus for great discussions and help with creating outreach content. Anny and Tim as well as the whole What Matter/s project and filming team – it was a very fun experience and I am grateful for the opportunity!

My office mates – Marcus, I-Ju, Xulu, Artis, Trung – most of us started at almost the same time and it was a lot of fun to share the office with all the PhD hardships, scientific knowledge and some completely off-topic entertaining discussions. The office has become so nice that I had to stay at home for writing thesis to not disturb you and distract myself. Thanks for the friendly atmosphere!

I would like to especially thank Neimantas, Milda, Vishal, Alexander, Xulu, Yang, Irene and Frida for the fun with badminton, tennis, board games, hiking, or simply chatting about topics beyond work.

I spent truly exciting and fun 4 months at Gaia Solar for an internship on building integrated photovoltaics, where I got the opportunity to learn about the solar cell market, real life solar module performance and manufacturing choices and challenges. Above all, the people at Gaia Solar made me so welcome that those months just flew by like a fun project rather than work. I would like to thank especially Jesper for teaching me so much and always being extremely enthusiastic, fun and supportive, Anders for getting me onboard, Michael G. for showing me the ropes around the manufacturing, Rikke, Sigurd, Michael P., Carsten, Jordan, Birgit, and Anne-Freja - you all created a wonderful and warm atmosphere with lots of laughter as well as seriousness. Finally, I am extremely grateful for the opportunity and the experience of making my own solar panel with my own hands, which even made it to the back cover of this thesis.

My friends from before PhD life – Ieva, Ieva, Julija, Arnoldas, Aistė – thanks for not forgetting me! It is always fun to meet you in Lithuania or whichever country

it might be. Also, I send thanks to friend/family Sam – thanks for being so awesome, your emails always make my day!

Love and Thanks always goes to my family: mum and dad, grandma, aunt Gražina, sister Girstautė with Massimo, Joris and Aras, and brothers Eigminas with Laura and Jonytė, Sirvydas with Toma, and Tolmantas for always supporting me, having interest in what I do, and always being there when I need you, or simply teasing me when I get too serious. Without you, life would not be the same. Finally, I have left out one person that started out as a colleague and helped me from the very beginning. A wonderful person that continues to support me at every step I take, believing in me ten times more than I believe in myself. I admire you as a scientist, I admire you as a person, and I love you. You bring so much joy to my life and you never get tired from trying new things. I cannot thank you enough for creating all the enthusiasm, happiness and love. Kiitos & Tack, Nicklas.

Abstract

This thesis deals with epitaxial growth and optical properties of semiconductor nanowires with implications and insights about materials for solar cells. The chapters leading up to the papers give a broader background and an introduction to the field and include nanowires and their synthesis, semiconductor properties, solar cell operational principles, light interaction with a nanowire array, and optical characterization of such arrays.

The nanowires were grown from gold seed particles using metal organic vapor phase epitaxy. Growth of ternary GaInP nanowires has been developed with a triethylgallium precursor that has not been commonly used before for this material structure in nanowires. We have achieved high yield and wide composition range nanowires with high control, which will be a crucial element for development of tandem solar cells where a high band-gap GaInP nanowire array could be the top cell.

In terms of optical properties, lifetimes and carrier dynamics are important parameters for optoelectronic devices, including solar cells. We have investigated surface passivation of nanowires by capping GaAs nanowires with in-situ grown shells, at the same time evaluating the possibility of measuring time-resolved photoluminescence signal of as-grown nanowires, even when the substrate is made of the same material. We have identified that depending on doping levels in the substrate and the nanowires, excitation wavelength can be chosen to separate nanowire signal from the substrate signal. Moreover, we have preliminary proposed a simple way to extract doping, which needs to be tested more extensively in the future. Such measurements of as-grown arrays could provide a fast and completely non-destructive characterization method for solar cell materials and allow further processing of the devices.

Further, we have investigated reflectance and transmittance of flexible nanowire arrays embedded in a transparent polymer. Such flexible membranes could be interesting as flexible solar cells on their own, or could be incorporated on top of a lower band-gap material, for example silicon, to create a tandem solar cell. We have identified two potential issues with such structures. First of all, gold can absorb a significant fraction of the incoming light. The gold particles can be etched away, which recovers transmittance for the long wavelengths. However, a

resonant reflectance peak is then observed. Through our work, we have identified that in-plane array modes arise in nanowire arrays embedded in a polymer that lead to resonant reflectance or absorptance in weakly absorbing materials. Such effect would be detrimental for transmitting long wavelengths to the bottom cell. Thus, we have investigated how these resonances depend on geometry in order to give guidelines for controlling this effect.

Popular science short summary

Nanoscience is rather a unifying concept over all disciplines than a specific branch of science. It simply refers to nanostructured materials and devices that are very small, thousand times smaller than the width of a human hair. This small size typically leads to a wide variety of new types of behavior, not observed in the large scale world. In that respect, any discipline can be combined with nanoscience, which leads to a variety of interdisciplinary projects where biology, medicine, material science, chemistry, and physics can meet on a daily basis. This thesis, however, focuses mostly on material science and physics, with particular emphasis on how light interacts with nanostructures and how what we learn could be useful for solar cells.

Solar cells are devices that convert sunlight into electricity. When sunlight falls on a solar cell, the energy from the sunlight is given to the particles (electrons) inside the solar cell material. The energetic electrons move around until, ideally, they reach the contacts, where electricity can be extracted. However, different materials can efficiently convert only part of the sunlight to electricity. Thus, to increase the electricity obtained from the same area, we could try to combine different materials in a stack, where the top cell would absorb the highest energy (e.g., UV or blue part) of the sunlight, and allow the lower energies (e.g., red) of the sunlight to pass through unhindered to the lower cells. Thus, it is important to investigate how light would interact with different parts of a solar cell and optimize material quality to maximize collection of sunlight's energy and its conversion to electricity.

This thesis deals primarily with the creation and control of high quality nanostructured materials for solar cells and investigation of how light interacts with the material, which can be rather different for small structures as compared to the large objects that we are more used to. In this thesis, we focus on structures called nanowires, which are essentially just a specific geometric shape – a tiny rod with a diameter of 200 nanometers and ten times longer length in our case. We investigate these nanostructures due to their promise for reduced material consumption thanks to efficient light collection (think of a radio antenna that collects signal from a larger area), as well as easier integration of different materials, which is needed to create the stack of solar cells for maximizing energy generation.

With this work, we have highlighted some issues, proposed solutions and expanded the knowledge for nanowire growth, optical measurement methods and nanowire solar cells stacked on top of other solar cells. If you are curious to learn more about the wonderful world of nanoscience as well as get a glimpse of my work in a casual everyday language, then, I hope that the following popular science extended summary will answer some of your questions.

Popular science extended summary

Researchers often focus on a specific, typically rather narrow, topic and dive into intricate depths of a problem in order to solve it or at least to gradually uncover some understanding. It happens rather often that when our curious friends and families would like to know more about our work, we suddenly lose the gift of speech. In the best case, we often mention an application, towards which we hope to contribute, which, in my case, is solar energy. I am always excited to talk about applications. However, behind the long term goal of solar cells lie a bunch of interesting concepts that I worked with, and I would not do justice to my work if I did not introduce some of those concepts as well. In this popular science summary, you will find my humble attempt to introduce, to all those curious minds that stumble upon my thesis, the beautiful world of nanoscience and give a short glimpse to my everyday work as well as larger goals I have been trying to reach.

What is nano?

Let's start with nanoscience, which has become a popular buzzword. Nanoscience deals with all things small, in particular, at the nanometer scale. How small is it really, you ask? One way to think about it is to imagine that if we shrank the Earth by 100 million times, it would look like a football, and if we shrank it yet another 100 million times, we would get down to the diameter of our DNA, which is just 2 nanometers. As nice analogy as this is, most likely it only depicts that Earth is huge and nanometer is tiny, still not giving us a good picture of what the nanometer scale really means. However, this is part of the everyday life in nanoscience – working with objects that cannot be seen with our eyes. Think of a human hair, which is typically around 10-200 micrometers (0.01-0.2 mm) in diameter - this is still 1000 times larger than the nanometer scale we are talking about. Here, I would like to remind you that an atom, the building block of all the ordinary matter, is just around one tenth of a nanometer. Hence, the nanometer scale deals with objects composed of only tens to thousands of atoms across. Thus, researchers working in nanoscience need to rely on various tools to enable both visualization as well as manipulation of objects at such a small scale.

In this thesis, I have worked with one type of nanostructures, called nanowires, which are essentially tiny rod like structures as you can see in Figure 1a (where they are arranged in a periodic array), but can also be a basis for more complicated

structure designs, such as nanotrees shown in Figure 1b (which I grew for a new concept of LEDs, outside the scope of this thesis). During my PhD studies, I have investigated how to create these tiny structures in a highly controlled way, analyzed what happens when light shines on such materials, and considered how to use the observed behaviors for improving solar cells.

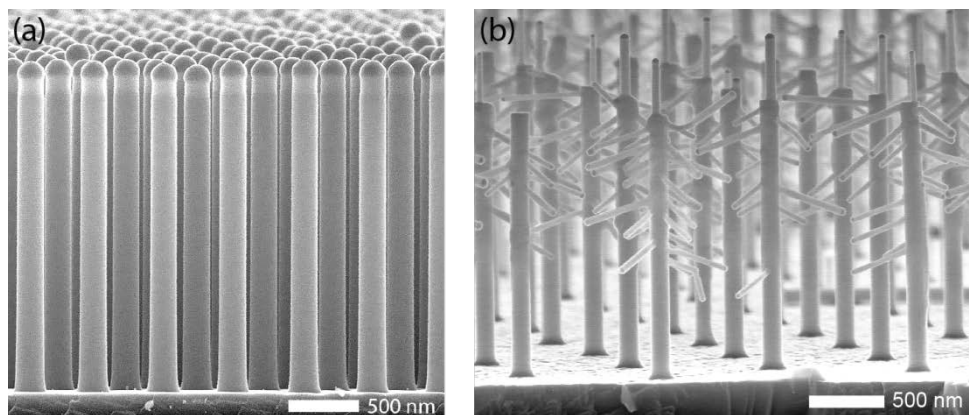


Figure 1. (a) A cross section view of a semiconductor nanowire array and (b) a nanotree array, obtained with a scanning electron microscope (described later).

What is so interesting about this nano-stuff?

The important thing to understand about nanostructures is that they are not just small, but also behave very differently due to their small size. One of the most common examples of nanostructures is gold or silver particles that have been used to create color in stained glass windows in churches for centuries. In order to understand the weird nature of nanoscience, let's start from a piece of gold, with its well-known yellowish shiny color. If we cut the gold piece into two, it still looks the same and has the same properties – no surprises here. However, if we keep cutting the gold into smaller and smaller pieces, the color will start changing when we get down to the nanometer scale. Note that at the small scale, we are typically not talking about a single particle anymore, because we would not be able to see it by eye. Instead, we are talking about many particles incorporated in some other material, for example glass or liquid, which gains the color due to inclusion of these small particles. For example, if we mix gold particles in a liquid, we could see colors from blue to red and transparent depending on particle size, shape and light direction. The change in color indicates incredible changes in material properties and ability to control them just by changing the size and shape of material, rather than changing its chemical composition (as, for example, one

does with regular paint, where different chemical elements are mixed together to achieve a certain color). In order to understand how this happens, we can roughly compare the metal particle to a guitar string. Whether you play a guitar or not, you probably know that when you strike a string, the sound will depend on where you put your finger on the string, which effectively changes the length of the string that vibrates. This vibration of the string has a frequency (how fast the string vibrates up and down) that depends on the length of the string, and the tone of the sound is determined by this vibration frequency. In a somewhat similar manner, depending on the size of the metal particle, the light can make the electron cloud in the metal particle vibrate, and this vibration frequency will determine which color we see in the stained glass.

A change in color, although with completely different physics (called quantum mechanics) behind, can also be achieved by semiconductor quantum dots (see Figure 2 for a photo). While semiconductors are a class of materials that I will talk about a little bit later, a quantum dot is essentially a special type of nanoparticle. Here, the quantum dots take in the energy of light and emit it back with a different color, specific to the material and the size of the particle. This is in contrast to metal particles, where the observed color is due to light that bounces off or passes through the material. Such quantum dots, as well as metal nanoparticles, are already used, for example, for medical imaging and quantum dot TV displays. Further, it is important to mention that nanostructures are on the biological scale of the building blocks of our bodies. Hence, designed nanostructures could efficiently interact with our cells and provide, for example, efficient drug delivery systems, implants and labs on a chip in the future.



Figure 2. A photo of semiconductor (cadmium selenide, CdSe) quantum dots under ultraviolet light illumination. All the vials contain the same material, but the shapes and sizes of the particles in the solutions differ (e.g., green solution contains particles of size 4 nm x 4 nm x 4 nm, whereas the red one - 6 nm x 6 nm x 12 nm).

Talking of biology, nature showcases some truly amazing nanostructures itself. For example, some butterflies and also peacock feathers have nanostructures that interact with light rather differently due to their small size, than most everyday objects. Without nanostructures, the peacock feather would actually be simply brown due to pigment (just like the color of our skin depends on the amount of melanin)! To ease the discussion of the rough principle behind this behavior, let's introduce two other common objects: a soap bubble, and a water puddle with oil on the street. I am sure you have seen and admired rainbow colors formed in both of them before, possibly even wondering why that happens. The concept is very well known in physics, and is called interference. The word itself, as you could guess from the regular phrase "to interfere" simply means that there is something else that gets in somebody's way and interferes with what they are doing. Imagine two people pushing a car: if they both push the car in the same direction, it is called constructive interference – they are helping each other and their strength is combined. However, if they were to push the car from opposite sides with equal force – the car would not move anywhere because their strengths would cancel out and we would get what is called destructive interference. Although we are definitely not talking about cars in this thesis, it illustrates the concept of the constructive and destructive interference where two phenomena can add or subtract.

To generalize the picture a little bit, think of the different pushing directions as positive and negative phenomena – in other parts of physics, the "negative" and "positive" does not always come from different directions. In this thesis, the term "interference" is used rather for light than for people pushing a car. Light can be described to consist of various colors, and each color has a property called wavelength (it is very closely related to frequency: for example, you might be used to microwave frequency to heat your food, which is also light, but with a very long wavelength of around ten centimeters compared to the visible light that has wavelengths in the range of a couple hundred nanometers). More mathematical definition follows from thinking of light as a sinusoidal wave, where the distance between two peaks, i.e., the oscillation period, is the wavelength. Armed with these new terms and analogies, we can now understand interference of light as two waves meeting each other. If the waves (might help to think of ocean waves) meet each other peak to peak – the wave becomes stronger since it becomes the sum of the two. However, if the peak meets a dip (negative "peak") – they cancel each other out. In terms of light, we said that a wave corresponds to a color. Thus, if two waves add up, we see a more intense color, whereas if they cancel out, that color might disappear. In the case of a soap bubble, we have the outer and the

inner surface of the bubble with very small thickness of the actual soap layer. The light can bounce between these two surfaces, where different colors of the light bounce slightly differently, which affects whether the waves meet peak to peak or not. Some colors thus cancel out and we see some other colors enhanced. Finally, a change in thickness of the film leads to different colors.

A similar effect is observed for our nanowire structures (Figure 3), where we initially see a shiny grey surface (Figure 3a), turning into a colorful pattern (Figure 3b) after nanowires are grown on that surface, due to light bouncing between the bottom and top of the nanowire array. Another related effect of light interacting with a periodic nanowire array can be seen in Figure 3c, where a green laser shines at a nanowire array and multiple spots appear on a tissue. This effect is well known for something called a diffractive grating (think of a CD, which is essentially lots of small hills and valleys to code ones and zeroes in), and occurs due to the presence of a periodic pattern of material with gaps in between, exactly like what we have with a nanowire array. If we shine the laser light at the sample in Figure 3a without the nanowires, we see just a single spot of light bounced off the sample. Hence, even though we cannot see nanowires themselves, we can deduce their presence and some properties from their interaction with light. Understanding how light interacts with such nanowire arrays forms a large part of this thesis.

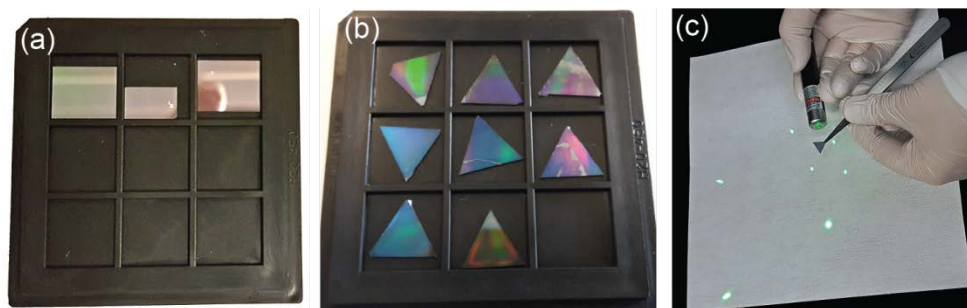


Figure 3. Photos of (a) samples without nanowires, (b) samples with nanowires creating colors, and (c) a pattern of multiple dots created by shining a green laser on a sample with nanowires.

So far, I have focused on introducing nanoscience examples related to light. However, nanoscience is a very multidisciplinary area that deals with everything that is on a small scale. Thus, there are many more exciting applications of nanoscience, such as nanoparticles used in water/dirt resistive coatings, sunscreen, paint, or even in a Spiderman costume (inspired by a gecko lizard with feet that can stick to surfaces so strongly that it can walk on ceilings). Finally, one of the

biggest areas, where you already are using nanotechnology every day, is transistors (the building blocks of computers) and data storage, which are all based on extremely small features in order to provide those powerful devices that fit into your pockets.

Nanowires, in particular, are just a specific shape of nanostructures, where their geometry leads to benefits for a rather broad range of possible applications. Nanowires could be used to scale down transistors even further, make small lasers, LEDs, solar cells with reduced material usage, various detectors and sensors, and the list goes on.

Semiconductors?

Having realized that nanowire is really just a specific geometry, we can come back to the title of the thesis, to notice that it says “*III-V semiconductor nanowires*”. The fact that I have worked with semiconductor materials underlines the whole thesis: from the way we make the nanowires and measure them to what applications they could be suitable for. Simply speaking, a semiconductor (for example, silicon, denoted by its chemical element symbol Si) is a material that has electrical conductivity between that of a conductor (metal) and an insulator (e.g., plastic casing of your electrical cables). In addition, semiconductor material properties depend on electricity, heat, light, etc., in such a way that by choice of materials, operating conditions and some additional material engineering, we can adjust its behavior to our needs. For example, a semiconductor transistor contains a gate (can be compared to a water dam), which has “on” and “off” states (dam lifted up or shut closed) that control whether electricity goes through or not. Thus, semiconductors allow creating sort of “traffic rules” for electricity, and are essential components of most electronic circuits.

Aside from the electronics and vast range of other applications, semiconductors are one of the main materials used for creating solar cells. Solar cells made from III-V semiconductor materials have consistently been the highest efficiency solar cells demonstrated, with the current highest efficiency of 46% [1], where *III-V* essentially narrows down the list of materials that we are talking about. The *III-V semiconductor* indicates that the material is made of a periodically repeated structure made of two types of atoms from chemical element table: group III atoms (e.g., gallium, Ga, or indium, In) and group V atoms (e.g., phosphorus, P, or arsenic, As). Combining different atoms together allows us to control various properties of the solar cells. In addition to III-V semiconductor solar cells, I should mention Si, which is actually in group IV of the chemical element table. This material has been developed for a long time, has manufacturing infrastructure

around the world, and is relatively cheap, which is why silicon solar cells dominate the solar energy market (in 2017, Si solar cells amounted to 95% of total production [2]), despite them being not the most efficient ones (current highest efficiency Si cell in the lab is 26.7% [1], while the average commercial Si module efficiencies are around 17% [2]).

How does a solar cell work?

As we all might know, a solar cell converts sunlight into electricity, but how does it actually work? For semiconductor solar cells, this behavior is enabled by a fundamental property of a semiconductor – the ability to absorb light that falls on the solar cell. What we mean by “absorption” is that when light falls on the solar cell, the energy contained in the light gets transferred into the material, and, more specifically, into the particles (electrons) inside the material. The electrons get excited with the extra energy and, provided suitable conditions, move towards the electrical contacts where they get collected and generate electricity.

In order to make a good solar cell, we need to be able to collect (absorb) as much light as possible and direct the created electrons towards the contacts. For this goal, we can use semiconductor properties to design a solar cell with certain “traffic rules” for how light interacts with the solar cell and where the electrons go.

Why would you make a nanowire solar cell?

Silicon is a cheap material that dominates the solar energy market, so why would we spend time researching new types of solar cells? The answer is mostly that we want higher efficiency, which means getting out more power using the same area. There are many scientists around the world working towards this goal, as well as towards making even cheaper solar cells, or solar cells designed for specific applications, where aesthetic design and additional functions could be also important (for example solar cells integrated in buildings, wearable electronics, cars, etc.).

Nanowires are promising for high efficiency solar cells due to two main benefits that stem from their small dimensions. First, the nanowires can absorb light very efficiently (think about radio antennas that gather signal from a larger area), without needing to cover the whole surface with material, thus leading to reduced material consumption. Second, it is much easier to combine different materials in small size as compared to the traditional large blocks of material. This is very important for achieving high efficiency solar cells, since every specific material can only absorb a certain fraction of the incoming sunlight, and even then only part of it will be efficiently converted to electricity (the other part will result in

heating up and some other processes). Thus, it becomes crucial to stack different materials on top of each other, making so called multi-junction or tandem structures that collect solar energy more efficiently and convert it to electricity efficiently. In such a stack, the traffic rules will dictate that the highest energy light (e.g., UV and blue) will be absorbed by the solar cell at the top and the lower energy light (e.g., red) by the lower cells.

How do you make the nanowires?

The ways to make things can be categorized into top-down and bottom-up approaches. A top-down approach is when a sculptor takes a stone and carves a figure out of it. In principle, we could make the nanowires in the same way, as after all, a nanowire on its own is just a geometric shape. However, our way of building nanostructures is more like building a house, or playing with Lego. It can even be compared to how growth in nature starts by putting a seed to the ground and then providing right conditions of sun, water and nutrients. This approach is called bottom-up and allows higher control of material properties, while at the same time reducing the amount of materials needed.

In particular, to grow nanowires in our laboratory, we start from a so called substrate of a semiconductor material, which is essentially a “big” flat and grey looking piece of material, as shown by the photo in Figure 3a and electron microscope (i.e., magnified) image in Figure 4, left. We coat this substrate with light sensitive materials and use the top-down approach to sculpt out openings in a repeated pattern, optimized for solar cell performance. After evaporating some gold everywhere, we can use different chemicals to get rid of the coatings. In such a way, we are left with a periodic array of gold particles on the semiconductor substrate (Figure 4, middle). We can place such substrate in a growth reactor (Figure 5), which essentially is a very sophisticated version of an oven where pipes with control valves are used to adjust how much and what gases are sent into the reactor. We grow nanowires using different gases that mix only in the oven when they reach the surface, instead of using ingredients already mixed into dough as one would do when baking. When we increase the temperature and let the gases into the reactor, the gases (made of molecules, which are in turn made out of atoms) would like to land on the surface and attach the constituent atoms to already existing material (grow a crystal) to minimize energy. The gold particle, however, acts as a preferred site for the crystal to form. The material from gas form mixes with the gold particle, which becomes a liquid alloy. When the particle saturates, it cannot accept more material and thus the material is expelled to form a solid crystal underneath the particle (for comparison, imagine adding sugar into

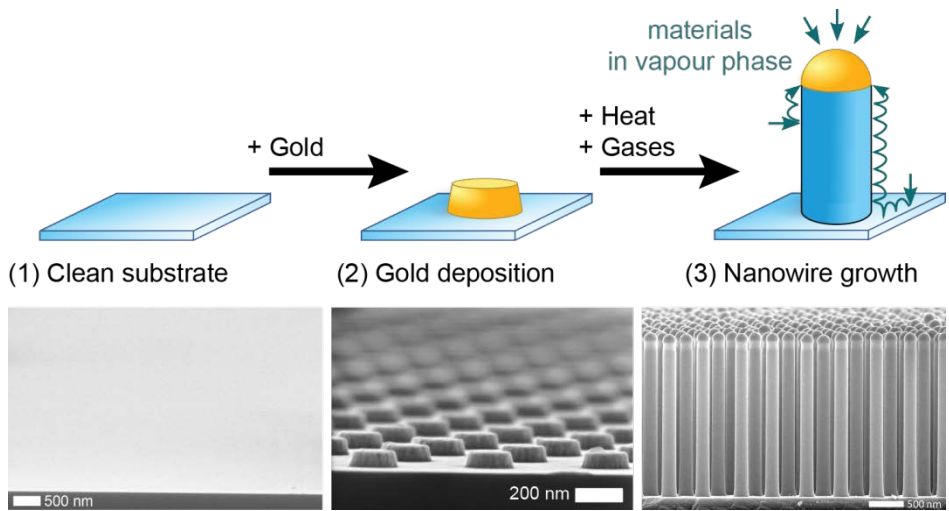


Figure 4. Schematic and corresponding scanning electron microscope images of the nanowire growth process starting with (1) a clean substrate, on which we (2) deposit gold, and then (3) grow nanowires.



Figure 5. Photos of the growth equipment, the growth reactor, and me in lab clothes for sample preparation before growth.

coffee – it melts in the coffee at first, but when there is too much sugar, it will settle down at the bottom as a solid sugar). This leads to material growing only under the gold particles, thus creating these cylindrical shapes (Figure 4, right), where the length depends on how long we keep the gases on.

If they are so small, how can we see them?

As I said earlier, we work with structures that are not seen by eye, which strictly means that we cannot resolve the tiny nanowires: if there was a single nanowire – you would not think there was anything there, whereas with a lot of them arranged together, you could see a dark color because of how light interacts with them. One might then wonder - how do we know that the nanowires are there, and what properties they have? A large part of my PhD was using various tools that allow seeing and characterizing this small scale world. You are most likely familiar with an optical microscope. However, a regular optical microscope can only help you see things down to maybe a few hundred nanometers in size, which is usually not enough to get required information about our structures. Instead of an optical microscope, we use electron microscopes, which are in principle quite similar to optical microscopes, but have magnetic fields instead of optical glass lenses to focus electrons instead of light. Most of the images in this thesis are taken by such electron microscopes. See Figure 6 for comparison of how a single nanowire looks like in an optical microscope and two types of electron microscopes. Optical microscope, in Figure 6a, only allows us to identify location of a specific broken-off nanowire, which helps for performing different measurements on the same nanowire. It could also be used to check for some irregularities in patterns. Figure 6b, on the other hand, allows us to see the shape and size of every nanowire as well as, in some cases, contrast between different materials. Transmission electron microscope (Figure 6c) provides the highest magnification that allows us to see how the crystal is formed from layers of atoms, where some microscopes can resolve even single atoms. It can also be used to identify what mixture of elements the nanowire is made of.

In addition to getting a physical image of the object, there are many other characterization tools that allow us to learn about specific properties of the material. For example, one might use x-rays to learn about material composition, i.e., the fraction of different elements that the material is made of. Or one could add electrical contacts and see what happens when electricity is sent through the material (if it is an LED, we could measure the light that comes out for example). Alternatively, one could shine light on the sample and see what happens afterwards, where typically some light comes out again and can be measured.

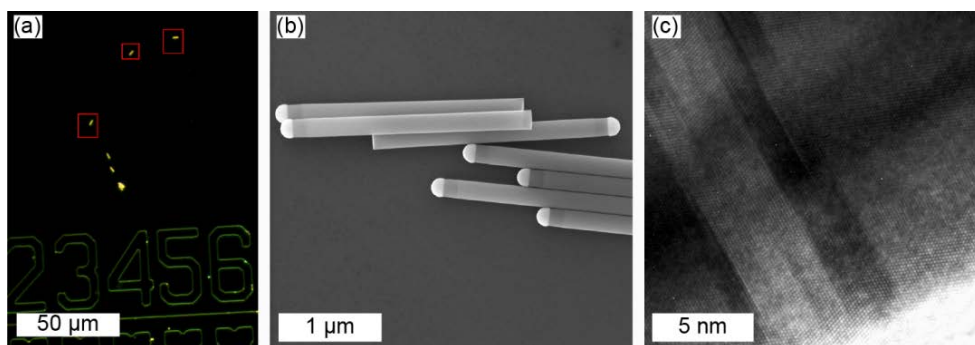


Figure 6. Broken-off nanowires with three different microscopy techniques: (a) a dark field optical microscope image where single nanowires are marked by red squares, (b) a scanning electron microscope image, and (c) a transmission electron microscope image zoomed-in to a small part of a nanowire.

So what has my work really been about?

As I tried to get across with the paragraphs so far, my work has been focused on working with nanostructures: creating and controlling them, preparing them for different experiments, using various tools to allow seeing or describing the properties of such materials. I have also tinkered with trying to compute how nanostructures in certain geometries would react to light. This section will thus attempt to give a bit more detailed account of the results I obtained that are contained in the articles included at the end of this thesis.

Growth of nanowires

The basics of the nanowire growth that I described earlier, hopefully, sound nice and simple; one might even say that it is a piece of cake! However, just like baking a cake, not all nanowire samples turn out the way you want and it takes a lot of experience and trial and error to adjust the ratios of the different gases, the materials used, temperature, pressure, growth time and so on in order to make exactly what you want. Understanding how every different adjustment influences the growth is then an extra step, which is extremely complicated because multiple processes can occur at the same time. As a simplified example, imagine you have a recipe of lemon curd, which contains eggs, butter, sugar, and lemon juice to produce a sort of thick jam-like spread. Let's say after a few tries you managed to make it, but maybe you want it to be more sour? So you add some lemon juice, but suddenly the lemon curd is not thickening anymore! You could add some sugar and egg and butter again to make it thicken, but then it will be sweet again. But maybe it would thicken with just addition of egg without sugar? Or maybe we can add cornstarch? Or heat it more? This gives a very simplified picture of growth in

the lab where one tries to understand which parameters affect which properties in order to obtain exactly what is needed.

One of my papers [Paper II] deals exactly with that – optimizing growth of nanowires with specific properties and trying to understand how different parameters affect the growth. For a while, we have faced a problem that for a material called GaInP, which is well suited to be a top cell in a tandem solar cell (remember, we want to stack different materials on top of each other, where each material will take a part of the solar energy), some of our nanowires grow very differently than others. We called them ultra-long nanowires, because they tended to be several times longer than the others. Such nanowires had poor properties and could completely destroy solar cell performance. In order to get rid of them, I have investigated growth where a different type of gas was used to provide the same atoms for the nanowires. The new type of gas turned out to work much better, and I went on to investigate what happens to the nanowires when temperature is changed and the ratios of the different gases are varied. Analyzing the data then led to a deeper understanding of how the growth of the nanowires proceeds, which, in turn, resulted in a higher control of growth to design nanowires with desired properties.

Optical studies

I have mentioned before that in order to learn about the materials we make, one can shine light on the sample to see what happens. I also mentioned that semiconductor materials are special in the way they interact with light, which then defines methods that can be used to measure and analyze the materials. In one of my papers [Paper II], I investigated what happens to the material on extremely fast timescale just after light hits the sample. When light hits the sample, it gives its energy to electrons that get excited and start moving around. However, everything that gets excited should calm down at some point and go back to a balanced, relaxed situation. The measuring technique used in this paper, in principle, allows extracting information about how quickly these electrons calm down and also in which way they calm down, i.e., where the energy goes to. This is especially important for solar cells, where we want to keep the electrons excited long enough so that the energy would travel through the sample into the electrical circuit. The difficulty with such optical measurements, however, is that the measurement is indirect and there can be many complex processes and components that contribute to the measured signal. For example, in this paper, we have faced a challenge of telling apart the signal of the nanowires and the substrate on which the nanowires were grown, because both of them were made from the same material. We have

identified certain settings for the experiments that allowed distinguishing the two signals. Such possibility could be important for getting information about solar cells during their production without damaging the sample in any way.

The last two papers also deal with how light interacts with the nanowires. However, in this case, we were interested in nanowires embedded in a polymer membrane (a sort of transparent, flexible plastic). This configuration is important for making flexible solar cells as well as to transfer the nanowires from the substrate they were grown on to other, cheaper, or more beneficial surfaces, for example on a silicon solar cell in order to get an even higher power from the same area. In Paper III, we have measured how light bounces off, travels through, and gets absorbed in such a nanowire membrane. We found out that the gold particles used for growth of nanowires are detrimental to the optical properties and should be removed after growth. However, after removing the gold particles, we have observed another issue – suddenly some of the light reflected (bounced back) from the sample more efficiently than could have been expected. In order to understand what was happening, we turned to numerical calculations and modeling of the system [Paper IV]. Remember our discussion about light bouncing between the two surfaces of a soap bubble? In this case, we have the plastic, as well as the periodic array of the nanowires, where light can travel along the nanowires, or it can bounce between the top and bottom surfaces in such a way that it can look like light is travelling perpendicular to the nanowires. In the end, depending on geometry and material parameters, the different waves can interact in such ways as to enhance absorption or reflection of the light. Thus, through this work, we have provided some guidelines for design of the nanowire arrays, especially when they should be used as a top cell in a tandem solar cell configuration.

Finally, to summarize this thesis in a simplified picture, let's turn to the image of traffic. Think of a semiconductor nanowire as an object, where, by picking materials and geometry, we can create a set of traffic rules for both light and electricity. During my PhD studies, I have attempted to get a grasp of these traffic rules as well as see if we can design better ones. In terms of bigger motivation, all of the work presented in this thesis has been done with solar energy in sight. In more technical description, the work presented in this thesis has contributed towards three areas: (i) the optimization of growth with a new gas precursor that reduces material consumption and allows easier control of high quality growth; (ii) investigation of optical properties of nanowires as well as optical methods for measuring them; and (iii) numerical calculations and deeper understanding of light interaction with nanowires in a membrane, which is particularly relevant for flexible or tandem solar cells.

List of papers

This thesis is based on the following papers, which will be referred to by their roman numerals in the text:

I. Growth kinetics of $\text{Ga}_x\text{In}_{(1-x)}\text{P}$ nanowires using triethylgallium as Ga precursor

V. Dagtýè, M. Heurlin, X. Zeng, and M. T. Borgström, *Nanotechnology*, 29 (39), 2018

I planned and performed nanowire growth, as well as optical, XRD, and SEM measurements. I was responsible for analyzing the data and for writing the paper.

II. Time-resolved photoluminescence characterization of GaAs nanowire arrays on native substrate

V. Dagtýè, E. Barrigón, W. Zhang, X. Zeng, M. Heurlin, G. Otnes, N. Anttu, and M. T. Borgström, *Nanotechnology*, 28 (50), 2017

I participated in the planning of the growth of the nanowires and performed some SEM imaging. I performed optical measurements and was responsible for analyzing the data, as well as for writing the paper.

III. Absorption and transmission of light in III-V nanowire arrays for tandem solar cell applications

N. Anttu, V. Dagtýè, X. Zeng, G. Otnes, and M. T. Borgström, *Nanotechnology*, 28 (20), 2017

I grew the nanowires, etched gold particles and performed SEM imaging. I participated in the transmission, absorption, and reflection measurements and performed the photoluminescence measurements. I wrote the parts related to growth, gold etching, SEM, and photoluminescence.

IV. Modal analysis of resonant and non-resonant optical response in semiconductor nanowire arrays

V. Dagtýè and N. Anttu, *submitted*

I performed numerical simulations, contributed to data analysis, prepared the figures and wrote most of the text.

The following papers are not included since their content is outside the main focus of the thesis:

V. Doping evaluation of InP nanowires for tandem junction solar cells

F. Lindelöw, M. Heurlin, G. Otnes, V. Dągytė, D. Lindgren, O. Hultin, K. Storm, L. Samuelson, and M. T. Borgström, *Nanotechnology* 27, 065706 (2016)

VI. InP nanowire *p*-type doping via zinc indiffusion

T. Haggren, G. Otnes, R. Mourão, V. Dągytė, O. Hultin, F. Lindelöw, M. T. Borgström, and L. Samuelson, *Journal of Crystal Growth* 451, 18-26 (2016)

VII. GaAsP nanowire solar cell development towards nanowire/Si tandem applications

E. Barrigón, Y. Chen, G. Otnes, V. Dągytė, N. Anttu, L. Samuelson, and M. T. Borgström, *Proceedings of the 44th IEEE Photovoltaic Specialists Conference, 2017*

VIII. Electrical and optical evaluation of *n*-type doping in $\text{In}_x\text{Ga}_{(1-x)}\text{P}$ nanowires

X. Zeng*, R. T. Murão*, G. Otnes*, O. Hultin, V. Dągytė, M. Heurlin, M. T. Borgström, *Nanotechnology*, 29 (25), 2018

* These authors contributed equally

IX. Nanobeam X-ray fluorescence dopant mapping reveals dynamics of in situ Zn-doping in nanowires

A. Troian, G. Otnes, X. Zeng, L. Chayanun, V. Dągytė, S. Hammarberg, D. Salomon, R. Timm, A. Mikkelsen, M. Borgström, and J. Wallentin, *submitted*

X. Spectrally resolved X-ray beam induced current in a single InGaP nanowire

L. Chayanun, V. Dągytė, A. Troian, D. Salomon, M. T. Borgström, and J. Wallentin, *submitted*

Abbreviations

AlGaAs	Aluminum Gallium Arsenide	MOCVD	Metalorganic Chemical Vapor Deposition
AlInP	Aluminum Indium Phosphide	MOVPE	Metalorganic Vapor Phase Epitaxy
AR	Anti-reflective	NIL	Nanoimprint Lithography
Au	Gold	PL	Photoluminescence
CB	Conduction Band	PV	Photovoltaics
CCD	Charge Coupled Device	SEM	Scanning Electron Microscope
DEZn	Diethylzinc, $Zn(C_2H_5)_2$	Si	Silicon
e-h	electron-hole	SQ	Shockley-Queisser
FWHM	Full Width at Half Maximum	SRH	Shockley-Read-Hall
GaAs	Gallium Arsenide	SSPL	Steady-State Photoluminescence
GaCl	Gallium Chloride	TE	Transverse Electric
GaInP	Gallium Indium Phosphide	TEGa	Triethylgallium, $Ga(C_2H_5)_3$
H₂	Hydrogen	TEM	Transmission Electron Microscope
HBr	Hydrogen Bromide	TM	Transverse Magnetic
HCl	Hydrogen Chloride	TMGa	Trimethylgallium, $Ga(CH_3)_3$
HE/EH	Hybrid electromagnetic	TMIn	Trimethylindium, $In(CH_3)_3$
InAs	Indium Arsenide	TRPL	Time-Resolved Photoluminescence
InCl	Indium Chloride	UV	Ultraviolet
InP	Indium Phosphide	VB	Valence Band
IR	Infrared	VLS	Vapor Liquid Solid
LED	Light Emitting Diode	VSS	Vapor Solid Solid
MCP	Microchannel Plate	WZ	Wurtzite
MFC	Mass Flow Controller	XRD	X-Ray Diffraction
MO	Metalorganic	ZB	Zinc-blende

1 Introduction

1.1 Nanowires

Semiconductor nanowires are tiny rod like single crystalline structures that are not resolved by the naked eye (Figure 1.1). Thus, various imaging and spectroscopy techniques play a crucial role in understanding their properties. In more technical terms, nanowires are high aspect ratio nanostructures with a radial scale of a few to a few hundred nanometers and lengths on the order of micrometers and display geometry dependent properties due to their small size and unique structure.

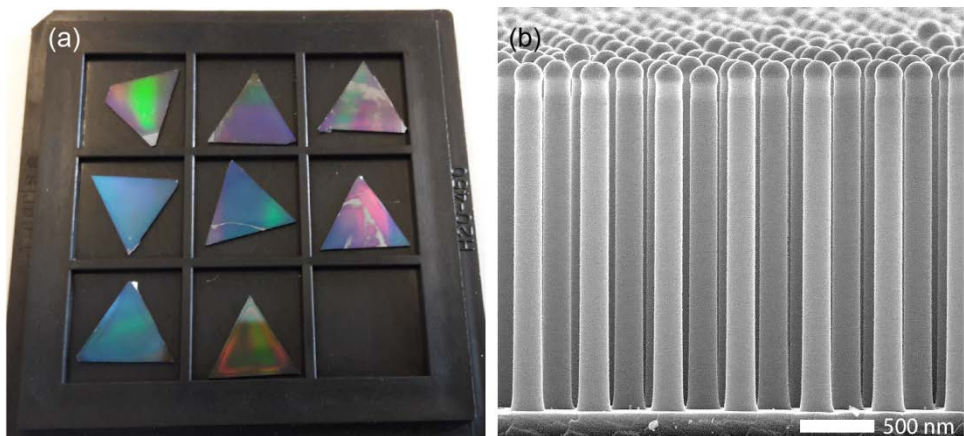


Figure 1.1. (a) A photograph of several samples with nanowires on native growth substrates. The nanowires are grown on a semiconductor substrate in a periodic array, which diffracts the incoming light as well as creates interference effects, which, together, result in different colors visible in the image. The grey patches correspond to defect areas where pattern was not transferred and hence nanowires were not grown. (b) A scanning electron microscope image of nanowires acquired by cleaving the sample and looking at the cross-section.

Research of semiconductor nanowires can be traced back to the studies on the vapor-liquid-solid (VLS) growth of whiskers of silicon (Si) and other materials in 1960's and 1970's [3-7]. At first, most research focused on understanding the growth mechanism and morphology of such whiskers. Then, three major breakthroughs happened in 1990s and early 2000s that sparked the nanowire research field of today: (i) epitaxial growth of $p-n$ junctions within nanowires [8],

(ii) control of both diameter and length of nanowires during growth [9-13], and (iii) growth of defect-free lattice-mismatched heterostructures that would not be possible in the conventional bulk materials [14-17]. These major breakthroughs, together with other benefits due to unique nanowire geometry, gave rise to the interest in using nanowires for various applications, which in turn increased the research efforts on the fundamental properties of the nanowires. During the past 20 years, research has branched out into many areas and remarkable progress has been achieved, which is reflected in the increase of the number of articles published on the topic of nanowires in general (Figure 1.2). It is important to realize here that the special properties of nanowires originate purely from their geometry, and thus geometry benefits can be combined with various materials as well as applied as a new platform for numerous bulk devices, which thus reflects in the large number of publications for the keyword “nanowire*”. In this thesis, we focus on a narrower field of nanowires - III-V semiconductor nanowires and, in particular, nanowire arrays with dimensions suitable for solar cells.

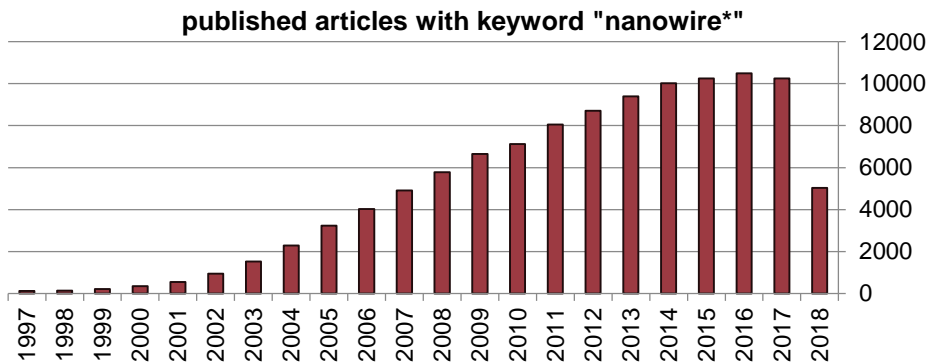


Figure 1.2. Number of papers published on the topic of nanowires. The search was performed with the keyword “nanowire*” in the Web of Science on 6th of July 2018.

In general, semiconductor nanowires show promise for various future electronics and optoelectronics applications within life-sciences, renewable energy and information technology, as well as miniaturization of devices into the nanoscale, which is currently of high interest in many areas, and especially for transistors [18,19]. The large surface area of the nanowires results in high potential for sensitive detectors, for example, label-free, real-time, selective detectors of a wide range of chemical and biological species [20,21]. The nanowire crystal structure and degree of quantum confinement can be tailored during growth to alter the band structure, suggesting promising optoelectronic applications as well as an interesting platform for fundamental studies. Tunable nanowire dimensions and

flexible choice of heterostructure materials due to efficient strain relaxation via the free surface are particularly promising for optoelectronic applications such as lower cost, efficient solar cells, light emitting diodes, detectors, and single nanowire lasers.

1.2 Solar cells

In 2015, around 160 000 TWh of energy was produced globally [22], whereas about 120 000 TWh of energy is received by Earth from the sun every hour [23]. Despite the abundance and versatility of solar energy, we use only a small fraction of it: roughly 500 TWh was produced in 2017 by photovoltaics (PV), which represents only about 2% of the world electricity demand [24], although some countries have rapidly reached significant percentages. This indicates a vast untapped potential of solar energy that can play a central role in reducing fossil fuel consumption, where PV is one of the approaches to harvest this solar energy. Currently, most of the terrestrial solar cell market is based on single junction planar solar cells, almost completely dominated by Si solar cells [2,25]. Single *p-n* junction solar cells, however, are limited by the Shockley-Queisser (SQ) limit [26] to about 33% PV energy conversion efficiency under 1-sun at 300 K (assuming perfect absorption where 1 photon generates 1 electron-hole (e-h) pair, and a perfect black body emission to the top side with no emission to the bottom side). The origin of the main losses as well as the basic operation principles and main parameters of the solar cells, together with some approaches for reaching higher efficiencies, will be discussed in Section 2.2, whereas here, main benefits of nanowires are introduced that make them a promising platform for high efficiency and low cost solar cells [23,27-31].

As we have seen in Section 1.1, nanowires offer a variety of benefits as well as possibilities to investigate new physics and tune some material properties. In terms of solar cells, the most important and interesting properties of nanowires are probably the geometry-tunable resonant absorption [29,32-37] (Chapter 4), and efficient strain relaxation via the free surface [16,17,38].

As nanowire dimensions are below visible wavelengths, geometrical optics does not apply, and wave optics description has to be used when considering light interaction with the nanowire arrays [34,39,40] (see Section 4.2). This leads to the benefit of tunable absorption resonances, which, together with anti-reflecting properties of nanowire arrays, enhances the ability of nanowires to efficiently

absorb light – a property that is crucial for optoelectronic devices such as detectors and solar cells. Indeed, the promise and progress of III-V semiconductor nanowires for PV has been demonstrated by numerous research groups [31,40-51]. In particular, high efficiency epitaxially grown InP [40,50] and GaAs [41] nanowire solar cells have been reported with nanowires covering only a fraction of the substrate surface while still showing bulk-like photocurrent generation [40].

The second important benefit of nanowires for solar cells is efficient strain relaxation via the free surface due to the low dimensional nature of the nanowires [16,17,38]. In monolithic bulk solar cells, the layer by layer growth of different materials is limited by the matching of the lattice parameters. If the lattice parameters differ too greatly, the material becomes strained, which leads to defect formation that can diminish the optical quality of the material and reduce efficiency of the solar cell. In nanowires, strain relaxation can allow a combination of normally incompatible lattice-mismatched materials for optimal functionality. This is particularly important for solar cells as their efficiency is ultimately limited by the balance between absorption and emission, which results in a 1-sun SQ limit of 33% if a single band-gap solar cell is used. A common way to go beyond this SQ limit is to combine several band-gaps into one cell. Due to efficient strain relaxation, nanowires could allow a more flexible choice of materials in order to optimize solar cell efficiency.

Additional important aspect of the nanowires is the large surface to volume ratio, which can be good for surface-functionalized sensors, but can be bad for solar cells. For example, GaAs is known to have a high surface recombination velocity [52], which can be detrimental for the optoelectronic quality of the material [42,53-55]. Specifically, high surface recombination velocity can reduce minority carrier lifetime, which typically leads to a reduction in the open circuit voltage [54,55]. Furthermore, surface recombination can in some cases prevent separation of photogenerated e-h pairs, which would reduce the short circuit current [54,55]. Compared to bulk solar cells, this problem is further enhanced in nanowires due to the larger surface to volume ratio. A common way to improve the surface quality of GaAs nanowires is by passivating them with an epitaxial shell grown around the GaAs core [56-68]. Paper II, included at the end of this thesis, investigates optical measurements of such core-shell nanowire arrays.

Even though nanowire solar cells are still in research phase, several nanowire properties and research directions show promise for reducing the cost of nanowire solar cell production. First, efficient absorption leads to reduced material consumption as compared to planar III-V solar cells [29,37,40,69]. Second,

efficient strain relaxation as well as in some cases preferential nucleation under assisting particle provide opportunity to grow nanowires directly on low-cost abundant material substrates, which can also allow for better integration with other devices [70,71]. Third, embedding the nanowires into a polymer and peeling them off from the substrate allows both flexible devices and reuse of expensive III-V substrate, which could substantially reduce material consumption and cost [31,72-74]. Finally, aerotaxy, a gas phase nanowire growth technique, shows potential for high-throughput of nanowires completely without using expensive growth substrates, which may enable low-cost fabrication of high quality nanowire-based devices on an industrial scale [75,76].

1.3 Developing nanowires for solar cells

This thesis deals with epitaxial growth and optical properties of dense III-V semiconductor nanowire arrays with a focus towards applications in PV. Thus, Chapter 2 provides a short summary of most relevant concepts in semiconductor physics and solar cell operational principles.

In order to make a good solar cell, we need to consider both manufacturing limitations and optimal designs in terms of optical and electrical properties. A good solar cell should absorb light efficiently, and convert absorbed solar energy to electricity by efficiently splitting the photogenerated carriers.

The most successful bottom-up grown nanowire solar cells so far have been synthesized by gold (Au) catalyzed VLS mechanism in a metal organic vapor phase epitaxy (MOVPE) system [40,41,50]. The position of the Au particles and thus position, as well as to a large extent diameter, of the nanowires has been defined via a nano imprint lithography (NIL) technique (see Section 3.2.1 and Refs. [70,77]). Although aerotaxy [75,76] promises a cheaper and faster method for producing nanowires with control over array geometry afterwards during alignment process, the method is still under optimization and development. Hence, in this thesis, we focus on the VLS grown nanowires in MOVPE [Papers I-III]. Chapter 3 contains a summary of main concepts of MOVPE for nanowire array synthesis, as well as description of the growth process and some steps in sample preparation. Growth of ternary GaInP nanowires has been discussed in detail in Paper I, where high yield and composition control has been obtained, which is needed for development of a top cell in a tandem solar cell configuration.

The high control of array geometry, provided by the NIL, is used for optimizing light interaction with the nanowire array, which is discussed in Chapter 4. In particular, reflection, transmission and absorption of light in III-V nanowire arrays embedded in a polymer and relevant for tandem solar cell applications have been investigated experimentally in Paper III, and theoretically in Paper IV. In these articles, we have observed resonant optical effects in non-absorbing wavelength region that could be detrimental for tandem solar cell applications. We have analyzed the origin of such effects and proposed directions of geometry design in order to avoid them.

In addition to the absorption of light, lifetimes and carrier dynamics are also important parameters for optoelectronic devices, including solar cells. Time resolved photoluminescence (TRPL) (section 5.3.2) can be used to evaluate lifetime of the carriers, which can provide information about the materials and surface quality. In Paper II, we have investigated the possibility of measuring TRPL signal of as-grown nanowires, even when the substrate is made of the same materials. We have identified that depending on doping levels in the substrate and the nanowires, excitation wavelength can be chosen to separate nanowire signal from the substrate signal. Such measurements of as-grown arrays could provide a fast and completely non-destructive characterization method for solar cell materials and allow further processing of the devices. Furthermore, doping is the most common way to control carrier splitting in semiconductor solar cells, and in Paper II, we have preliminary proposed TRPL as a non-destructive method for measuring doping levels in nanowires, including nominally intrinsic nanowires with low level of doping that can be cumbersome to measure with other non-destructive optical methods.

In addition to the TRPL, various other characterization techniques are used to develop solar cells and the main techniques used in the included papers are described in Chapter 5. In this thesis, characterization has been done on nominally intrinsic nanowires, in order to understand material and optical properties that can be tuned for improving and understanding behavior of materials meant as a platform for solar cells.

Finally, Chapter 6 provides an overview of the results discussed in the included papers.

2 Basic semiconductor physics and solar cell operation

The fact that I have worked with semiconductor materials carries through the whole thesis from the way we make the nanowires and measure their properties to the way devices work. Thus, in this chapter, we cover some fundamental background physics that is most relevant to the scope of this thesis. It includes a short overview of the most important semiconductor concepts in Section 2.1 and a glimpse to solar cell basics in Section 2.2.

2.1 Semiconductors

Semiconductors are the foundation of the electronic industry as well as many other devices that we use every day [78]. Light emitting diodes, solar cells, transistors, motion sensors, cameras, gas detectors, and lasers are but a few examples of devices that would not be possible without the knowledge of semiconductors. A semiconductor is essentially a material with properties between those of an insulator and a metal (conductor). By choosing the type of atoms and the order in which they are arranged (see Section 2.1.1 for crystal structure), we can affect a semiconductor's band structure (see Section 2.1.2), which governs the most important optical, as well as, to some extent, electrical, properties of the semiconductor. Band-gap, in particular, is an important parameter of the band structure that can be tuned by material composition in order to adjust fundamental properties of a semiconductor, such as its conductivity, light absorption and emission. Materials with zero band-gap are metals or semimetals, while those with an energy gap larger than 3-4 eV are often classified as insulators [79,80].

It should be mentioned that semiconductors can be either crystalline or amorphous solids, where a crystalline solid implies a periodic arrangement of its constituents, whereas amorphous solids lack long-range periodic order [81]. In this thesis, we focus on epitaxially grown crystalline semiconductors.

2.1.1 Crystal structure

The stable crystal structure of most III-V bulk semiconductors is zinc-blende (ZB), which is a face-centered-cubic lattice structure with two different atoms at each basis point (if the two atoms are the same, then it is called a diamond lattice) [81]. The nitride based materials are an exception and are stable in wurtzite (WZ) crystal structure, which is a hexagonal-close-packed lattice structure with two different atoms at each basis point. The WZ and ZB crystal structures are actually quite similar if we compare them along the cubic $[\bar{1}\bar{1}\bar{1}]$ and hexagonal [0001] directions, which are equivalent and correspond to the typical growth direction of nanowires. Along this direction, both crystals are made of bi-layers that are equivalent from crystallographic point of view, and only the stacking sequence differs. Thus, a common way to illustrate the two crystal structures is by denoting the stacking sequence of the bi-layers A, B, C of III-V atom pairs. In such a picture, WZ has stacking sequence ABAB... along the [0001] direction, whereas ZB is expressed by ABCABC... along the $[\bar{1}\bar{1}\bar{1}]$ direction. Misplacement of bi-layers results in defects as well as alternating crystal structures. III-V nanowires, unlike their bulk counterparts, allow both crystal structures and have a tendency to grow in a mixed WZ/ZB crystal structure [82-85]. Under specific growth conditions, however, it is possible to achieve nanowires with a desired single crystal phase, or controlled crystal structure heterostructures [85-89].

As the electronic band structure (Section 2.1.2) and thus many semiconductor properties depend on the crystal structure of the material, the ability to manipulate crystal structure of nanowires allows band engineering and control of optoelectronic properties [84,86,90-92]. This can lead to advanced structure designs as well as open up for investigations of fundamental physics.

2.1.2 Band structure

The property which distinguishes semiconductors from other materials concerns the behavior of their electrons and, in particular, the existence of gaps in their electronic excitation spectra [79]. The behavior of electrons in a solid is most conveniently specified in terms of the electronic band structure, which is also a convenient way to illustrate processes occurring in a semiconductor. For an overview of band structure formation, Claus Klingshirn, *Semiconductor Optics*, Ch. 8 [80] is recommended, whereas here, we discuss some key concepts and parameters related to common representation of the band structure.

A representation of a simplified semiconductor band structure with two bands is shown in Figure 2.1a. The band that is completely filled with electrons at $T = 0$ K is called the valence band (VB), while the empty band is called the conduction band (CB). The situation at $T > 0$ K will be described in Section 2.1.4. Between the CB and the VB lies the forbidden gap, where no stationary electron states exist. The width of this forbidden gap is called the band-gap (E_g) and is one of the most important properties of a semiconductor. In addition to the band-gap value, which is the smallest distance between the band extrema, the band-gap is classified as either direct or indirect. A direct band-gap semiconductor is indicated in Figure 2.1a and defined via its band structure where the CB minimum and VB maximum are aligned in k -space, where k is crystal momentum, and thus k -space is momentum space. This k -space is often referred to as reciprocal space, in which a reciprocal lattice (the Fourier transform of the direct lattice) exists. For an indirect band-gap semiconductor, the CB minimum is offset from the VB maximum, as illustrated in Figure 2.1b. In this case, to absorb a photon with energy close to the band-gap, additional momentum needs to be provided. This is typically achieved by lattice vibrations that can be described by particles called phonons. The indirect band-gap transition thus involves an additional particle, which makes the absorption weak in comparison to that in the direct band-gap semiconductors.

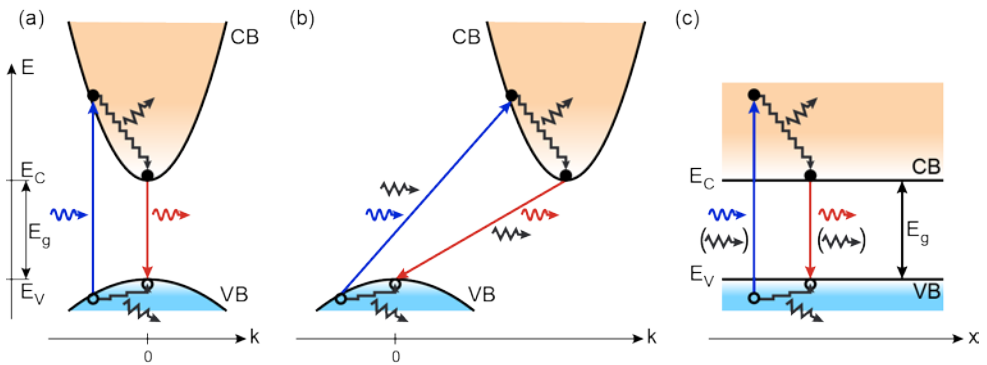


Figure 2.1. Common representation of simplified (a) direct and (b) indirect band-gap semiconductor band structures in k -space showing parabolic conduction (CB) and valence (VB) bands, and (c) a band diagram in real-space where only the band edges are drawn. All figures illustrate absorption of a high energy photon (blue), thermalisation of the created e-h pair by emission of phonons (black), and a subsequent radiative recombination with emission of a band-gap energy photon (red). The indirect transitions require assistance by phonons, as illustrated by the black arrows. Vertical axis corresponds to energy and is common for all figures.

In a direct band-gap semiconductor, photons with energy higher than the band-gap are strongly absorbed. When a high energy photon is absorbed, an electron is excited from the VB to the CB (leaving a hole behind in the VB) and an electron-hole (e-h) pair is created. (Note that while absorption of lower energy photons could be possible via different mechanisms, it is often weak and gives negligible creation of e-h pairs.) This electron (hole) then has kinetic energy, which is quickly dissipated by phonon scattering as the electron (hole) thermalizes to the bottom (top) of the CB (VB). Such thermalisation process usually occurs on a timescale much faster than any recombination processes. Hence, the band edges are often most important for the optical and transport properties. Thus, instead of a band structure, a band diagram is often used, as shown in Figure 2.1c. It is important to note that a band structure is drawn in the k -space, whereas a band diagram is drawn in the real space (x) where possible spatial variation of the CB minimum and the VB maximum is shown. The vertical axis is common to the two representations and indicates energy levels, where, in particular, the CB edge energy level (E_C) and the VB edge energy level (E_V) are worth mentioning as the band-gap is given by $E_g = E_C - E_V$.

Band structure engineering and modifications

Since the band structure formation stems from the periodicity of the crystal, modifications of the crystal also change the band structure and the connected properties. In Section 2.1.1, the idea of band structure engineering by tuning the crystal structure of the semiconductor was introduced. Another possibility of adjusting band-gap and material properties is by mixing two or more solids to an alloy, where an alloy with two, three and four components is called a binary, ternary and quaternary alloy, respectively. A common approach to estimate the lattice constant as well as other properties of an alloy is by using a virtual crystal approximation where properties of a random alloy formed by atoms A and B on a (sub-) lattice are replaced by a single kind of atoms whose properties are assumed as a linear average of those of A and B [93]. Such an approximation yields the commonly used empirical Vegard's law, which states that at a constant temperature, a linear interpolation exists between the crystal lattice constant of an alloy and the concentrations of the constituent elements [93]. For example, for a ternary (or often called pseudobinary) alloy $A_xB_{(1-x)}C$ the lattice constant of the alloy is then given by:

$$a_{\text{alloy}}(x) = xa_{AC} + (1-x)a_{BC}, \quad (2.1)$$

where a_{AC} and a_{BC} are the lattice constants of the binary materials AC and BC.

Other material properties, for example, the band-gap, are sometimes assumed to follow the same linear dependence. In reality, however, the behavior can be more complex and a common approach to account for the deviation from the linear interpolation of virtual crystal approximation is by introducing a bowing parameter E_{bow} , so that the band-gap of a ternary material is given by [94]:

$$E_g(A_xB_{(1-x)}C) = xE_g(AC) + (1-x)E_g(BC) - x(1-x)E_{\text{bow}}. \quad (2.2)$$

Introduction of different materials or change of crystal structure in a single semiconductor material are called heterostructures and result in a modified band structure. There are three types of band alignments as shown in Figure 2.2: type I (straddling gap), type II (staggered gap), and type III (broken gap) and the exact alignment of the bands depends on both the materials as well as their doping levels. It is worth noting that type I transitions give rise to direct band-gap transitions (with both electrons and holes gathering to the lower band gap material), whereas type II can give rise to spatially indirect transitions at the interface between the two materials (with, in Figure 2.2b, electrons in the right material with lower E_C and holes in the left material with higher E_V).

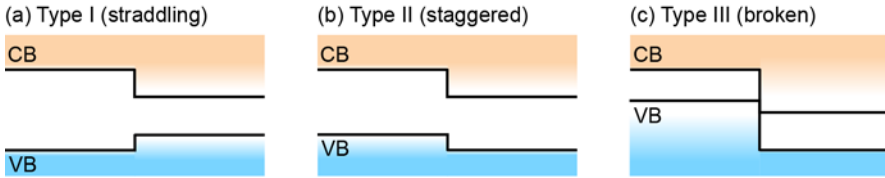


Figure 2.2. Three types of band alignments in semiconductor heterostructures: (a) Type I (straddling), (b) Type II (staggered), and (c) Type III (broken).

Temperature is another factor that modifies the band structure. The band-gap of most semiconductors tends to increase with decreasing temperature, which can be understood from thermal expansion of the lattice and temperature-dependent electron-lattice interactions. Such temperature dependence can be represented by the empirical Varshni's model [95]:

$$E_g(T) = E_0 - \frac{\alpha T^2}{T + \beta}, \quad (2.3)$$

where E_0 is the band-gap value at $T = 0$ K, whereas α and β are adjustable, empirical parameters specific for each semiconductor.

2.1.3 Unintentional defects and intentional doping

In semiconductor crystals, any disturbance of the periodicity is considered to be a defect and, in fact, every real semiconductor typically contains a lot of crystal or lattice defects. These defects can be classified into point defects, one-dimensional or line defects (e.g., dislocations), two-dimensional or surface defects (e.g., stacking faults, grain boundaries, twin planes), and three-dimensional defects (e.g., precipitates, voids) [80]. The surface that terminates a three-dimensional crystal can also be considered to be a two-dimensional defect and the electronic states introduced by such surfaces are usually called “surface states” [79]. Usually, point defects, such as vacancies, interstitials, substitutionals, antisites, and Frenkel defect pairs (see Figure 2.3) are considered to be most important for semiconductors, since they tend to determine the properties of the devices [79,80]. Due to exceptionally large surface-to-volume ratio of the nanowires, however, surface states tend to be the dominating factor in recombination of carriers in the nanowire materials [96,97], which can be detrimental for the optical performance of the nanowires.

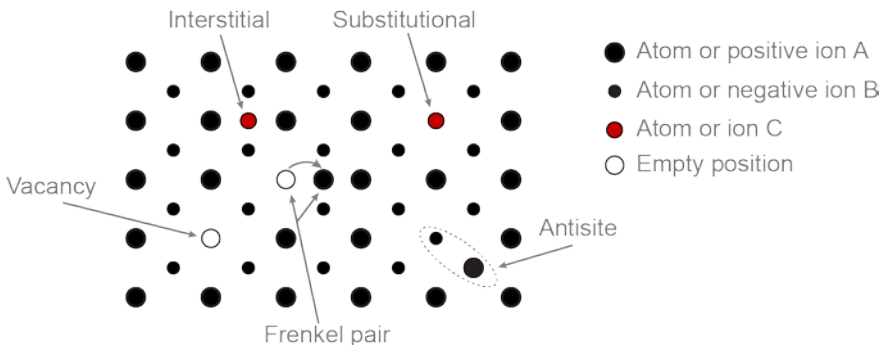


Figure 2.3. Sketch of a lattice of a binary semiconductor AB containing various types of point defects.

Most of the defects are typically unintentional. However, introduction of impurities as point defects is a crucial property of semiconductors, needed to form *p-n* junction devices (Section 2.1.5), such as is commonly used for semiconductor solar cells (Section 2.2). Additionally, while a crystal phase change can be an undesired defect, it can also sometimes be used intentionally for band structure engineering, as mentioned in Section 2.1.1.

Doping

One of the attractive properties of semiconductors is the band-gap, and the possibility to tune it by combining different materials into alloys. However, pure semiconductors are neither very good conductors nor good insulators. If nothing is done to a semiconductor, the bands are flat, and the only way for the electrons and holes to be extracted to external contacts is by diffusion, which is a slow process that is hard to control. Adding impurities (foreign atoms) to the semiconductor is called doping and results in important control of the optoelectronic properties. A pure semiconductor is called intrinsic, whereas when impurities are included that introduce additional free carriers, the semiconductor is called extrinsic.

Dopants can occupy one of the point defect locations as illustrated in Figure 2.3, which defines the effect of the dopant on the semiconductor. Defects that can contribute free electrons to the host crystal are known as donors, while defects that can contribute holes are known as acceptors. As an example, for group III-V semiconductors, if group II substitutional atoms are incorporated in group III sub-lattice, the impurity atoms have one less valence electron than the group III atoms, which can be depicted as free holes associated with negative ions (Figure 2.4, *p*-type). Alternatively, addition of group VI substitutional atoms on group V sub-lattice can result in extra free electrons associated with positive ions (Figure 2.4, *n*-type). Semiconductors with excess free electrons are called *n*-type, whereas those with excess free holes are called *p*-type.

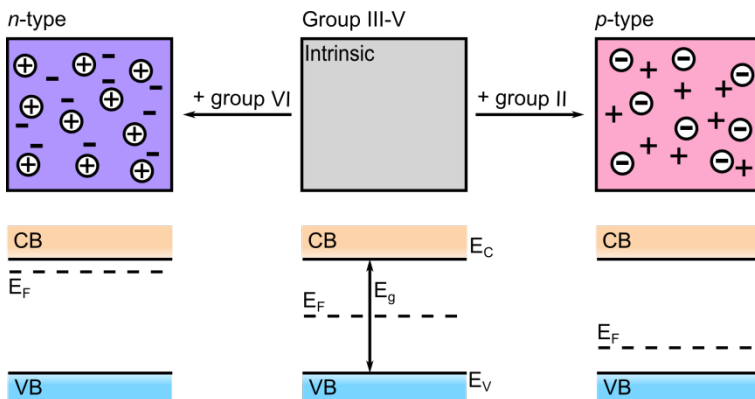


Figure 2.4. Illustration of intrinsic and doped III-V semiconductors along with schematics of band diagrams showing position of the Fermi level E_F in each case. The "-" and "+" signs indicate free electrons and holes, whereas encircled "-" and "+" indicate fixed ions.

We note that not all of the impurities result in desired doping. The effect of impurities will depend on the dopant energy level. In particular, mid-gap states typically result in loss of excess carriers in a solar cell circuit and thus are considered as parasitic defects. However, dopants with energy levels close to the bands can be activated and provide free electrons or holes.

The mathematical way of calculating electron and hole concentrations in the semiconductor that are important for both electrical and optical properties will be introduced in Section 2.1.4. Here, we only mention that the Fermi level energy, E_F , for an intrinsic semiconductor is close to the middle of the band-gap (where Fermi energy is the energy at which the probability of occupation by an electron is exactly 50%). With p -type doping, the Fermi level is situated closer to the VB due to an increased number of free holes, whereas with n -type doping, the Fermi level is situated closer to the CB as illustrated in Figure 2.4. Apart from moving the Fermi level, the dopants also give rise to additional states within the band-gap that can be occupied by electrons and holes. Semiconductors with the Fermi level below/above the CB/VB are called non-degenerate, whereas a degenerate semiconductor has high level of doping, where the Fermi level enters the bands. Note that for weakly doped semiconductors, impurities are assumed to not disturb the lattice and intrinsic semiconductor band structure is often used. When dopant concentration increases, and especially for degenerate semiconductors, modifications due to many-body interactions between the carriers need to be considered.

Surface states

Surface states are electronic states found at the surface of materials due to sharp transition from solid to air (or at an interface between two materials), which interrupts the periodicity of the crystal and leaves dangling bonds at the surface. The dangling bonds are unsatisfied, ‘free’ atom bonds whose energies often lie within the semiconductor band-gap [98]. Due to the exceptionally large surface-to-volume ratio of the nanowires, surface states are especially important and have a significant influence on the optoelectronic properties of nanowires [42,53-55,99].

Surface states can act as donor/acceptor levels that can capture holes/electrons. For many semiconductors, the energies of surface states lie within the band-gap and the density of states is high, such that addition or removal of some electrons does not change the occupation distribution at the surface significantly. This can result in a Fermi level ‘pinning’ leading to band bending (see Figure 2.5). For example, for an n -type semiconductor with a surface containing surface states (assumed to

be acceptor-like states) within the band-gap, the situation before equilibrium can be pictured as in Figure 2.5a. Since the bulk Fermi level E_F is above the surface Fermi level $E_{F,s}$, the free electrons flow to the surface resulting in a negative charge at the surface. Due to charge imbalance, electrostatic potential at the surface goes up resulting in a built-in potential that is illustrated by the bending of the bands. The area with the band bending, in this example, is depleted of the electrons and positively charged ions are left behind, forming a so called space charge region (depletion region in this case). This process continues until thermal equilibrium is reached, which is depicted by a constant Fermi level from bulk to surface [79], as shown in Figure 2.5b.

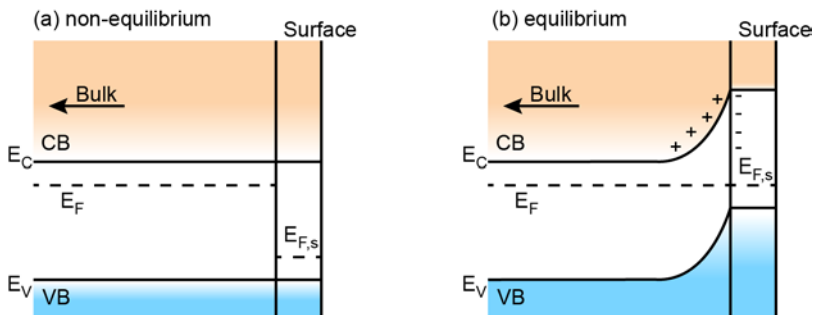


Figure 2.5. Example of band bending due to surface states for an n -type semiconductor with surface states (here illustrated as acceptor states) within the band-gap: (a) the system is not in equilibrium, Fermi levels are not aligned, which makes electrons flow from the bulk to the surface; (b) the system reaches equilibrium when the Fermi level is constant throughout the system, and the bands are bent. Note that, in this example, high density of surface states is assumed, so that the surface Fermi level $E_{F,s}$ does not move considerably when states at the surface get filled by electrons.

Besides the inherent defects from the break in periodicity, the surface is very sensitive to any impurities. Thus, surface impurities may also be a source of surface states and may coexist with the dangling bond states.

Surface states can be detrimental to the optical and electronic properties of semiconductor nanowires [42,53-55,99]. They can increase the probability of nonradiative transitions, thus reducing radiative efficiency of the material, especially near the band-edge. Band bending can also suppress the direct band-gap transition. In terms of solar cell parameters, surface states can reduce minority carrier lifetime, which typically leads to a reduction in the open circuit voltage [54,55]. Furthermore, surface recombination can in some cases prevent e-h pair separation, which would also reduce the short circuit current [54,55].

The removal of dangling bonds and impurities at the surface and their associated interface states is called passivation. The passivation process should include two

steps: (i) prevent a semiconductor from reacting with the atmosphere during the entire lifetime of the device, and (ii) eliminate the surface states from the band-gap, and prevent their formation. It should also take into consideration the application of the device, which, in optoelectronic applications, typically requires the passivation layer to be a low-absorbing material that provides an adequate barrier to prevent the loss of electrons and photons in the passivation layer. Ex-situ chalcogenide (especially sulfur) passivation by wet-chemical techniques is one widely investigated passivation approach for improving the performance of III-V semiconductor devices [100,101]. However, stability of such passivation methods still requires further work [101]. Another widely used passivation method, which was also used in this thesis for GaAs nanowires, is in-situ epitaxial growth of a high band-gap passivating shell around the nanowire core [56-68] (see Section 3.2.3). Such passivation method essentially displaces the dangling bonds from the nanowire core surface to the shell surface, which is then typically not part of the electrically active device structure.

Crystal Structure

In Section 2.1.1, we have pointed towards the uniqueness of nanowires in terms of possibility of growing crystals in the WZ and ZB structures. At the same time, this possibility often results in nanowires with a mixed crystal structure [82-85]. Such mixed crystal structure breaks the symmetry of the crystal and falls within the category of defects that can affect the optical quality of the material, for example, by reducing the quantum efficiency, carrier lifetime, and carrier mobility [60,84,91,102-105]. On the other hand, as mentioned in Section 2.1.1, controlled crystal structure engineering can lead to new types of devices and interesting fundamental physics.

2.1.4 Carrier concentration and recombination

Equilibrium carrier concentration

In Section 2.1.2, we have introduced the concept of band structure where we said that at zero temperature, the VB is completely filled with electrons, whereas the CB is completely empty. At non-zero temperature, on the other hand, continuous thermal motion results in the excitation of electrons from the VB to the CB and leaves behind an equal number of holes in the VB. In order to get a quantitative value of electron and hole concentrations in the bands, one needs to consider the density of states (number of allowed energy states per energy range per unit

volume) and the probability that a state is occupied at a certain temperature, which is given by the Fermi-Dirac distribution function [78]:

$$F(E) = \frac{1}{1 + e^{(E-E_F)/k_B T}}, \quad (2.4)$$

where k_B is the Boltzmann constant, T is the absolute temperature in Kelvin, and E_F is the energy of the Fermi level, which can be considered as a hypothetical energy level of an electron that would have a 50% probability of being occupied at any given time at thermodynamic equilibrium, as already mentioned in Section 2.1.3. For an intrinsic (undoped) semiconductor, the Fermi level lies close to the middle of the band-gap, whereas, as we saw in Figure 2.4, for a doped semiconductor, the Fermi level moves towards one of the bands depending on the doping type.

For most non-degenerate semiconductors, the approximation $(E - E_F) \gg k_B T$ can be used, which simplifies the Fermi-Dirac statistics to Boltzmann statistics:

$$F(E) \approx e^{-(E-E_F)/k_B T}. \quad (2.5)$$

Such an approximation allows us to express the equilibrium electron density n_0 in the CB, and the equilibrium hole density p_0 in the VB by:

$$n_0 = N_C \exp\left(-\frac{E_C - E_{F0}}{k_B T}\right), \quad (2.6)$$

$$p_0 = N_V \exp\left(-\frac{E_{F0} - E_V}{k_B T}\right), \quad (2.7)$$

where N_C and N_V are the effective density of states in the CB and the VB respectively and E_{F0} is the Fermi level energy at thermal equilibrium.

For an intrinsic semiconductor, $n_0 = p_0 = n_i$, where n_i is the intrinsic carrier density. In general, a mass action law applies: $n_0 p_0 = n_i^2 = N_C N_V \exp\left(-\frac{E_g}{k_B T}\right)$ for non-degenerate semiconductors in thermal equilibrium.

Carrier recombination

The equilibrium carrier concentrations n_0 and p_0 were given by Eqs. (2.6) and (2.7) respectively, whereas if light shines on a semiconductor, photogenerated e-h pairs are created (at a rate G) and the carrier concentration of nondegenerate semiconductor is then described by the nonequilibrium electron and hole concentrations:

$$n = n_0 e^{(E_{Fn} - E_{F0})/k_B T} \text{ and } p = p_0 e^{-(E_{Fp} - E_{F0})/k_B T}, \quad (2.8)$$

where E_{Fn} and E_{Fp} are the electron and hole quasi-Fermi levels that split due to the non-equilibrium distribution of carriers.

Generally, for any semiconductor material [106], the photogeneration rate $G(\mathbf{r}, t)$, the electron concentration $n(\mathbf{r}, t)$, and the hole concentration $p(\mathbf{r}, t)$ contain both spatial and temporal dependence. For a quantitative description of the carrier recombination dynamics, knowledge of the drift and diffusion of the carriers as well as of the possibly spatially varying recombination characteristics within the nanowire are needed [107]. However, such a complete characterization of carrier dynamics in a nanowire is outside the scope of this thesis.

If, after the photogeneration of carriers, the light source is switched off (as is done in time resolved photoluminescence, TRPL, measurements – see Section 5.3.2), the system is driven towards thermodynamic equilibrium. This results in excess carrier decay via various recombination paths that can be split into radiative and non-radiative recombination processes. A more extensive description of different radiative and non-radiative recombination transitions can be found in textbooks [79,108], whereas here, we just briefly mention some more relevant ones for the III-V nanowires.

Radiative recombination is accompanied by emission of a photon after recombination of an electron and a hole. Such emitted photons can then be detected by photoluminescence (PL) techniques as described in Section 5.3. Thus, radiative recombination forms the basis for understanding the behavior of measured PL intensity, as will be described in the next section.

In many semiconductors, however, a nonradiative transition is the dominant recombination process. The most common nonradiative processes are Shockley-Read-Hall (SRH) recombination and the Auger recombination. The SRH recombination is a two-step process via an energy level in the forbidden gap created by the presence of bulk defects, impurity states or surface states, and accompanied by an emission of phonons. The Auger recombination involves three carriers where the energy released by a recombining e-h pair is immediately absorbed by another electron or hole, which then usually dissipates the energy by emitting phonons. Auger recombination becomes increasingly dominating as the carrier concentration increases. Such nonradiative recombination processes can be treated as parasitic processes that waste the energy of the system. Thus, in order to improve the quality of devices, the nonradiative processes need to be minimized,

which can be done by improving the growth to obtain defect-free, direct band-gap semiconductors with passivated surfaces.

The total recombination R can be written as a sum of the main recombination channels and expressed by a commonly used parametric model [109-111]:

$$R = R_{\text{SRH}} + R_{\text{rad}} + R_{\text{Aug}} = \left(\frac{A}{n + p + 2n_i} + B + C(n + p) \right) (np - n_i^2), \quad (2.9)$$

where the first term R_{SRH} is the bulk SRH recombination [112,113], the second term R_{rad} is the radiative recombination [106], and the third term R_{Aug} is the Auger recombination [114]. The constants A , B and C are the respective recombination coefficients and it has been assumed that SRH recombination rates are equal for electrons and holes, that the electron and hole densities in the impurity level, responsible for SRH recombination, are equal to the intrinsic carrier density, and that the Auger coefficients are equal for electrons and holes.

An additional term that should be included in the Eq. (2.9) is the surface recombination that is assumed to follow the SRH model applied at the surface, where the SRH recombination coefficient A with units of s^{-1} effectively gets replaced by the surface recombination velocity v_{sr} with units of cm/s [115]:

$$R_{\text{surface}} = \frac{v_{\text{sr}}}{n + p + 2n_i} (np - n_i^2). \quad (2.10)$$

If the diffusion length of the carriers is larger than the diameter of the nanowire, d_{NW} , surface recombination can be transformed to effective bulk recombination [115,116], which can then be added to Eq. (2.9):

$$R_{\text{surface}}^{\text{eff}} = \frac{4v_{\text{sr}}/d_{\text{NW}}}{n + p + 2n_i} (np - n_i^2). \quad (2.11)$$

By probing carrier recombination rates, we can learn how fast different recombination processes occur and which of them dominate. TRPL is one characterization technique used in this thesis (see Section 5.3.2) that can probe carrier dynamics. To enable a discussion of some of the important physical processes underlying the overall recombination dynamics within nanowires, an approximate, volume-averaged description of the carrier dynamics can be employed [106,117]. Then, the recombination of electrons and holes can be described by the rate equations:

$$dn/dt = G_{\text{av}}(t) - R_n(n, p), \quad (2.12)$$

$$dp/dt = G_{\text{av}}(t) - R_p(n, p), \quad (2.13)$$

where G_{av} is the volume averaged photogeneration rate of e-h pairs in the semiconductor, and R_n and R_p are the recombination rates of the electrons and the holes, respectively. For simple electron-hole recombination: $R_n = R_p = R$, where possible trapping of either type of carriers is neglected.

In nanowires, and in particular GaAs nanowires studied by TRPL in Paper II, the surface recombination is typically the limiting factor, which means that the recombination is dominated by the nonradiative surface recombination [96,97]. We assume that this surface recombination can be described as an effective bulk recombination with recombination lifetime τ in the low injection regime (where the photogenerated excess carrier concentration is lower than the equilibrium carrier concentration) [105,118]. In this case, the dynamics takes on a simple form:

$$dn/dt = G_{\text{av}} - (n - n_0)/\tau, \quad (2.14)$$

with $(n - n_0) = \Delta n$ the excess electron concentration. Note that with the above assumption of $R_n = R_p = R$, we have similarly for the holes $dp/dt = G_{\text{av}} - (p - p_0)/\tau$ with $(p - p_0) = \Delta p$ the excess hole concentration.

Radiative recombination intensity

The recombination of electrons and holes can be described by the rate equations; however, it does not describe what is detected as a PL signal. PL measurements (see Section 5.3), by definition, detect photons originating from radiative recombination and we assume that the PL intensity can be described as [106]:

$$I_{\text{PL}}(t) \propto B \times [n(t) \times p(t) - n_i^2], \quad (2.15)$$

where B is the radiative recombination coefficient, which is specific for each semiconductor bulk material, and n_i is the intrinsic carrier concentration with $n_0 p_0 = n_i^2$ for a non-degenerate semiconductor. Note that we assume for Eq. (2.15) that the material behaves as a bulk material where the radiative recombination is dominated by spatially direct recombination. In other words, we neglect quantum confinement effects, which ought to be a good approximation due to the large diameters of the nanowires investigated in this thesis, as well as possible charge separation due to, for example, band-bending [119].

The nonequilibrium carrier concentrations in Eq. (2.8) can be expanded as:

$$n(t) = \Delta n(t) + n_0, p(t) = \Delta p(t) + p_0, \Delta n = \Delta p, \quad (2.16)$$

where $\Delta n(t)$ and $\Delta p(t)$ are the photogenerated excess carrier concentrations, which, in a TRPL experiment, are set at $t = t_{\text{pulse}}$ by the TRPL laser pulse, where the t_{pulse} marks the initial interaction of the pulse and the sample. Note that $\Delta n(t_{\text{pulse}}) \propto P$, and $\Delta p(t_{\text{pulse}}) \propto P$, where P is the excitation power. In steady state PL (SSPL), the steady state excess carrier concentrations are maintained by the continuous wave laser excitation, where, similarly as in TRPL, one often assumes $\Delta n_{\text{SSPL}} \propto P$ and $\Delta p_{\text{SSPL}} \propto P$ with P now the SSPL excitation power. However, strictly, for SSPL, this linear proportionality applies only if the lifetime is independent of the excitation power.

By comparing Eqs. (2.15) and (2.16), it can be seen that the PL intensity in Eq. (2.15) in general has a nonlinear dependence on the carrier concentration. This means that the decay of the TRPL signal is not always directly proportional to the decay of carrier density, which can lead to inaccurate lifetime extraction. To exemplify possible differences in the decay of excess carriers and the decay of the TRPL signal, we look into the low and high injection regimes. For example, for a p -type doped semiconductor ($p_0 = N_A$, $n_0 \ll p_0$, where N_A is the acceptor concentration in the semiconductor) at low injection ($\Delta p \ll p_0$), Eq. (2.15) simplifies to:

$$I_{\text{PL}} \propto \Delta p \times N_A. \quad (2.17)$$

In this case, the PL intensity depends linearly on the photogenerated carrier density, and thus I_{PL} decays in the same manner as Δp . In contrast, at high injection ($\Delta p \gg p_0$), Eq. (2.15) simplifies to:

$$I_{\text{PL}} \propto \Delta p^2, \quad (2.18)$$

where I_{PL} decays twice as fast as Δp .

Some level of intentional or unintentional doping is usually present in semiconductors. In some cases, and in particular for unintentional doping, it can be difficult to estimate the doping concentration and thus the injection regime, which can lead to a possible misjudgment of instantaneous lifetime of excess carriers by a factor of up to 2.

2.1.5 *p-n* junction

In Section 2.1.3, we discussed that doping is important for controlling the conductivity of semiconductors. However, the greatest benefit of doping occurs when *p*- and *n*-type semiconductors are brought together. Due to the concentration gradients, the majority holes from the *p*-type material diffuse across the junction, and electrons diffuse from the *n*-side to the *p*-side (Figure 2.6a). During this process, the free electrons leave positive ions uncovered and free holes leave negative ions uncovered, thus creating a positive charge on the *n*-side, and a negative charge on the *p*-side (Figure 2.6b). This area is called the space charge (or depletion) region. Due to such charge separation, an electric field is set up that now creates a drift force, which opposes diffusion. In the end, equilibrium is reached with the space charge region and a built-in potential across the junction (Figure 2.6b,d). This potential difference now acts as a barrier, creating a diode that allows current to flow one way but not the other. This potential difference is the property that allows power extraction when light is applied to the *p-n* junction as will be seen in Section 2.2.

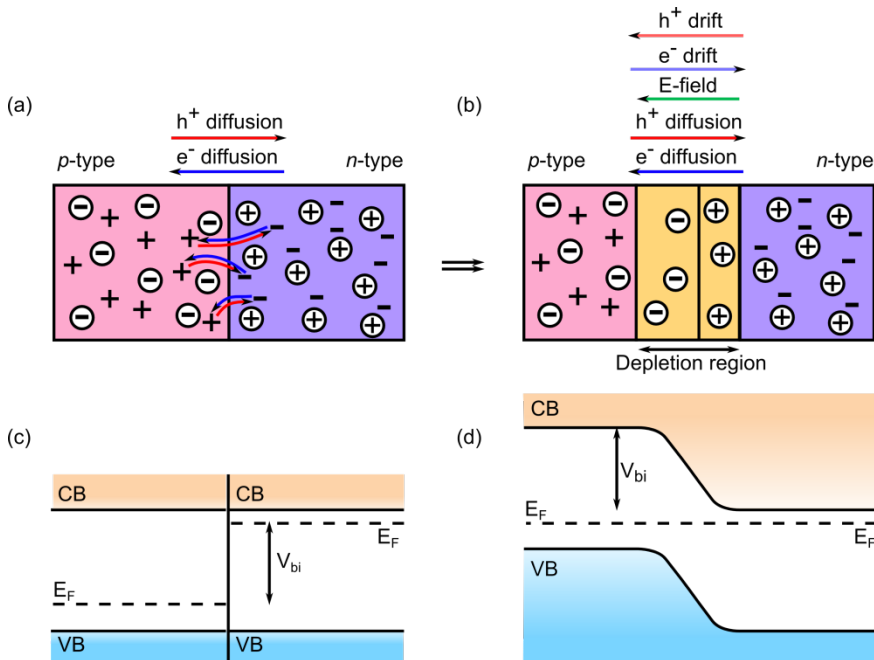


Figure 2.6. Schematic of a *p-n* junction with electron and hole drift and diffusion directions shown in the top figures and band diagrams of the *p-n* junction shown in the bottom figures: (a,c) before equilibrium and (b,d) in thermal equilibrium.

2.2 Solar cells

A solar cell is an optoelectronic device that directly converts sunlight into electricity. The concept of converting light to electricity was first introduced with the discovery of the photovoltaic (PV) effect by Edmond Becquerel in 1839. PV energy conversion requires only a material in which the absorption of light raises an electron to a higher energy state, and a way to move this higher energy electron into an external circuit where the electron dissipates its energy before returning to the solar cell. Although a variety of approaches are possible for PV energy conversion, a semiconductor p - n junction is the most common solar cell platform. Thus, only p - n junction solar cells are discussed in this thesis.

2.2.1 Operational principles and main parameters

In Section 2.1.5, we have discussed the basic principles of p - n junction formation and its band diagram in thermal equilibrium in the dark (Figure 2.6d, and repeated in Figure 2.7a). In the case of applied light, photons, absorbed by the solar cell, excite electrons from the VB to the CB while leaving holes in the VB. Then, the electrons and holes diffuse until they recombine or reach the depletion region. If the e-h pairs are created far from the depletion region, the probability is higher for them to recombine before reaching the depletion region. However, if the e-h pair is created in the depletion region or within a few diffusion lengths from it, the electric field can separate the e-h pair by sweeping the electrons to the n -side and holes to the p -side (Figure 2.7b). Such carrier separation allows extracting the built-in potential as usable voltage if a load is connected to the solar cell (Figure 2.7c).

The case when there is no load connected to the solar cell is called short circuit (Figure 2.7b). In such a case, the resistance is assumed to be zero and there is no voltage drop across the solar cell, which is shown by the same Fermi level position at the two contacts. The electrons are thus driven through the external circuit and result in a short circuit current (I_{sc}).

When a highly resistive load is connected to a solar cell, it operates at an open circuit condition (Figure 2.7c). In this case, the carriers cannot escape from the solar cell through the external circuit and accumulate by the contacts. Such accumulated charges act to reduce the electric field across the p - n junction until

equilibrium is reached. This then leads to splitting of the quasi-Fermi levels where the difference between them gives the limit to the potential that can be extracted from the solar cell, which is called the open circuit voltage (V_{oc}).

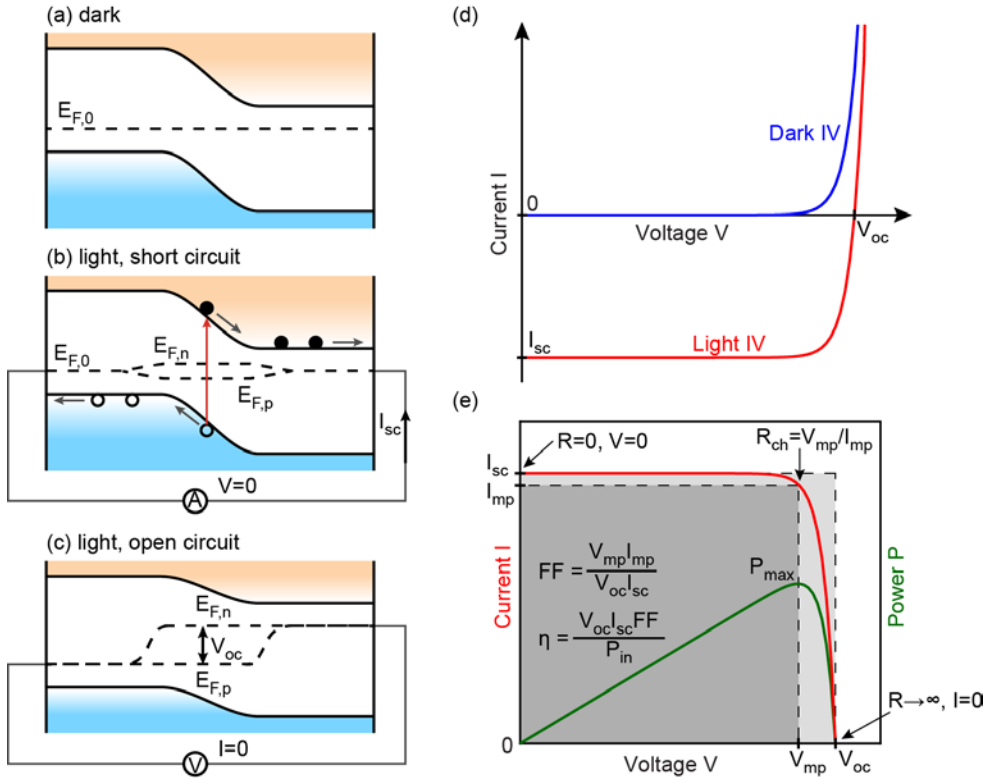


Figure 2.7. Schematic of a p - n junction band-diagram (a) in dark with a constant thermal equilibrium Fermi level, (b) under illumination at the short circuit condition, (c) under illumination at the open circuit condition showing the splitting of the quasi-Fermi levels and production of open circuit voltage. Typical photodiode I-V characteristics are shown (d) in dark (blue) and under illumination (red), as well as (e) with inverted axes according to the solar cell convention due to power production (green); key parameters of a solar cell are also illustrated in the figure (e).

In both cases, however, no power is produced, since either the voltage or the current is zero and power is given by the product of the two. Power generation occurs when a load resistance is tuned between the two cases. The current and voltage obtained by tuning the load can be illustrated by the I-V characteristics as shown in Figure 2.7d,e and described by the diode equation under illumination:

$$I = I_L - I_0 \left(\exp(qV/n_{IF}k_B T) - 1 \right), \quad (2.19)$$

where series and shunt resistances are not taken into account, in which case the photogenerated current $I_L = I_{sc}$, I_0 is the dark saturation current that represents recombination under thermal equilibrium, and n_{IF} is the ideality factor that accounts for different types of recombination mechanisms and typically varies between 1 and 2. The maximum power P_{max} output is obtained by tuning the load to the characteristic resistance value $R_{ch} = V_{mp}/I_{mp}$, where V_{mp} and I_{mp} are the voltage and current obtained at the maximum power point (Figure 2.7e).

The efficiency of a solar cell (η) is then defined by the ratio between the maximum power produced by the solar cell (P_{max}) and the incident light power (P_{in}), and can be expressed as:

$$\eta = \frac{P_{max}}{P_{in}} = \frac{I_{mp}V_{mp}}{P_{in}} = \frac{I_{sc}V_{oc}FF}{P_{in}}, \quad (2.20)$$

where FF is called the fill factor and is given by the ratio between the maximum output power (dark grey rectangle in Figure 2.7e) and the product of the I_{sc} and V_{oc} (light grey rectangle in Figure 2.7e).

2.2.2 Main losses

As has been mentioned in Section 1.2, the single p - n junction solar cell efficiency is limited by the SQ limit to around 33% at 1-sun and 300 K [26]. The main losses originate from thermalisation (inability to utilize full energy of above-band-gap photons) and transparency (inability to absorb photons with energy below band-gap) as illustrated in Figure 2.8. Both of the losses are connected to the band-gap of the semiconductor. Larger band-gap materials can more efficiently use the energy of high energy photons and thus have a larger V_{oc} , but they are transparent to a larger part of the solar spectrum and the photons below band-gap are lost. Narrow band-gap materials, on the other hand, absorb most of the photons, and thus have a larger I_{sc} . However, very little energy is extracted from the high energy photons, which in turn reduces the V_{oc} . The two opposing effects need to be balanced in order to obtain the maximum efficiency, which, for single band-gap solar cells, is achieved with a band-gap close to 1.1-1.4 eV. InP, GaAs, and Si materials are thus well suited for single junction solar cells.

Additionally, in a single-junction solar cell, thermalized carriers cannot be extracted at the bandgap energy, that is, V_{oc} is below E_{bg}/q . This efficiency

limitation originates from the fact that the solar cell must, by reciprocity, emit light since it absorbs light. This emission is enhanced exponentially by the voltage over the solar cell, and it is the recombination mechanism that must remain even when no non-radiative recombination occurs. In other words, the emission sets the lower limit on I_0 in Eq. (2.19) and, in this radiatively limited case, gives $n_{\text{IF}} = 1$ [26]. Then, if emission occurs into all the directions on the top incidence side, the single-junction SQ limit of 33% for 1 sun illumination is obtained [26]. The actual device efficiency is further affected by additional loss mechanisms such as reflection, nonradiative recombination, losses at the contacts, resistance of the semiconductor material itself, and heating of the whole solar cell.

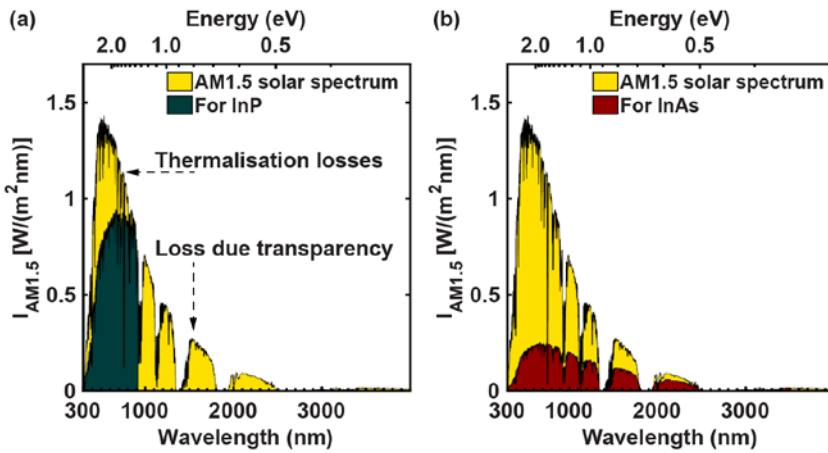


Figure 2.8. Illustration of the AM1.5 direct and circumsolar spectrum intensity (1000 W/m^2) (yellow) [120] overlaid with the intensity usable by (a) an InP solar cell (green), and (b) a lower band-gap, InAs solar cell (red) after thermalisation and transparency losses.

2.2.3 Beyond the 33% single junction efficiency

The 33% SQ efficiency limit of a single junction solar cell can be exceeded by violating one or more of the assumptions of the SQ calculation, in order to avoid losses such as those described in the previous section. For going beyond the 33% limit, the most relevant aspects are the assumption of a single band-gap material that cannot absorb photons below band-gap and cannot efficiently use high energy photons as their energy is lost by thermalisation, and the mismatch between the incident and emitted light cone angles.

In order to lift the last limitation, we note that direct sunlight is incident from a small cone of 0.26° half-angle. In this case, the reciprocity between absorption and

emission requires emission of light only into that small cone. Thus, emission into angles outside of that cone is an additional, unnecessary loss. The incidence and emission cones can be matched by two approaches: (i) Light concentration, which increases the half-angle of the incidence cone of light and the intensity of the light on the cell. The higher light intensity directly increases the I_{sc} , which, in turn, increases the V_{oc} (as seen from Eq. (2.19)). (ii) Emission angle restriction, which, under radiative recombination limit, decreases the I_0 in Eq. (2.19) and hence increases the V_{oc} . The light concentration method is commonly used and increases the theoretical limit for a single junction solar cell under maximum concentration (46 000 suns) to 44%, which is also the limit obtained by restricting the emission to the 0.26° half-angle cone for direct sunlight. Importantly, the light concentration increases solar cell efficiency even when the solar cell is non-radiatively limited (since the I_{sc} is increased). In contrast, for emission angle restriction to show a practical benefit, the external luminescence efficiency should be above 10% [121].

Aside from the incidence and emission angle matching, most approaches for reaching higher efficiencies are based on several new band structure and energy conversion concepts. These approaches can be roughly split into three categories: (i) multiple energy levels (multijunction/tandem solar cells), (ii) multiple carrier generation per high energy photon or single carrier pair generation with multiple low energy photons (multiple exciton devices in quantum dot solar cells, intermediate band solar cells, impurity photovoltaics, up and down converters combined with solar cells), and (iii) capture of carriers before thermalisation (hot carrier solar cells) [25,122,123].

Tandem solar cells are by far the most popular approach, which in bulk materials has resulted in efficiencies exceeding the 33% single junction efficiency limit (current world record at 1-sun intensity is 38.8% [1]). In this approach, higher band-gap materials are stacked on top of the lower band-gap materials so that the higher energy photons are more efficiently absorbed in the high band-gap solar cell with minimized thermalisation losses while being transparent to the lower energy photons that are then absorbed by the lower band-gap materials.

Nanowire arrays for solar cells

Although other approaches are also being investigated, multijunction concept remains the most researched one for nanowire platform as well. Nanowire array single junction solar cells have reached efficiencies (current epitaxially grown record is 15.3% [41]) where it becomes feasible to talk about creating tandem solar cells in order to achieve even higher efficiencies. The approach for

multijunction solar cells containing nanowire arrays can be split in two main directions: (i) tandem solar cell fully within the nanowire platform, containing an Esaki tunnel diode [124,125] connecting the two cells in each nanowire, and (ii) nanowire array top cell integrated with a Si (or possibly other material) bulk bottom cell [126]. In either case, nanowire arrays with higher band-gap materials are needed, which, in most cases, requires ternary materials. This thesis is to a large extent focused on the growth of ternary GaInP materials [Paper I] and their optical properties [Paper III, IV]. In particular, Papers III and IV investigate properties of a nanowire array embedded in a membrane, which is an example of a top cell for the second tandem solar cell direction.

In terms of efficiency losses, in Paper II we have used TRPL measurements to investigate nonradiative recombination, whereas in Paper III, we have observed that the Au particles, used for assisting nanowire growth, can absorb low-energy photons strongly [Paper III], which would be detrimental for tandem solar cells. The removal of Au particles can recover transmission of low energy photons. However, then a reflectance peak can show up due to resonant back-scattering of light from in-plane waveguiding modes for peeled-off samples [Paper III,IV]. Such effect can be avoided by tuning the geometry of the nanowires so that the resonant excitation of the in-plane waveguide modes is suppressed.

3 Nanowire array synthesis

Nanowires can be synthesized in either top-down [49,127] or bottom-up [127,128] approaches. In the top-down approach, nanowires are obtained by a combination of lithography and etching from a bulk material. The bottom-up approach involves chemical/physical synthesis of nanowires from smaller building blocks, which is typically preferred due to reduced material consumption, flexibility in structure design on a small scale, and possibility to control nanowire properties during growth.

Bottom-up nanowire growth approaches can be categorized by two properties: (i) type and presence or lack of an assisting particle often split into groups with (a) Au particle assisted growth [4], [Paper I, II, III], (b) other metal particle assisted growth [129], (c) self-assisted (or self-seeded) growth [130-132] where a particle, native to the grown semiconductor, is formed during growth, and (d) particle-free growth, usually combined with the selective area growth [133,134], which is part of the second property – (ii) the presence or lack of a growth mask, where the presence of a growth mask is often called selective area growth. It should be noted that particle assisted growth can be combined with a selective area growth mask in order to improve pattern preservation [77], as has been used in Paper II also. The particle assisted growth is most common since it helps to preserve a preferential vertical growth of the nanowire, including nanowire position and diameter and allows easier formation of axial heterostructures. However, particle-free growth is quickly gaining interest, especially for radial structures and growth on Si [135,136]. Additionally, growth without a metal particle can also be achieved by an oxide assisted growth method in laser ablation as well as by thermal evaporation techniques [137], where presence of oxides in the target materials lead to generation of semiconductor oxides in the vapor phase that then decompose at high temperature and play a crucial role in the nucleation and growth of nanowires.

When an assisting particle is used, the growth mechanism is usually described by either vapor-liquid solid (VLS) mechanism [3-7], where growth occurs from a liquid alloy particle, or vapor-solid-solid (VSS) mechanism [138,139], where growth occurs from a solid particle. Most often for Au-assisted nanowires and typical growth conditions, VLS is the dominating mechanism. However, in-situ

transmission electron microscope (TEM) measurements show that in some cases both VLS and VSS growth mechanisms of nanowires are possible for the same system with the state depending on temperature, pressure of the precursor and growth history [138].

When it comes to the Au particles used for nanowire growth, there are several ways of forming them on a substrate: aerosols or colloid deposition, thin film layer evaporation, nanoimprint lithography (NIL), electron beam lithography, deep UV lithography, block copolymer evaporation, and electroplating are some of the more common examples [27,140,141]. NIL is particularly promising for high-throughput and low-cost patterning for nanowire array growth since NIL can be used to deposit Au particles in a periodic pattern of independently controlled array symmetry, pitch and nanowire diameter parameters, over large areas and in large batches, compatible with the requirements of PV industry [77,142]. Other patterning techniques that show promise for ordered, position and size controlled arrays are listed by Otnes et al. [31] and described in references therein.

Finally, a diversity of synthesis techniques can be used for nanowire growth, where the most commonly used techniques are metalorganic vapor phase epitaxy (MOVPE), and molecular beam epitaxy, whereas chemical beam epitaxy, laser-assisted catalytic growth, and chemical vapor transport techniques have also been used for nanowire growth. A review of these growth techniques can be found in Ref. [140].

This thesis focuses on nanowire arrays grown by VLS method in an MOVPE from NIL patterned substrates [Paper I, II, III]. Thus, in the following sections, we describe the fundamental principles of MOVPE (Section 3.1) and more relevant considerations for nanowire array growth (Section 3.2).

3.1 Metal-organic vapor phase epitaxy

MOVPE (also referred to as MOCVD – metalorganic chemical vapor deposition, which is technically a broader term since it does not imply epitaxial process) is an epitaxial technique for growth of semiconductor crystals from vapor phase materials and is commonly used in semiconductor industry for optoelectronic and electronic devices. It is, thus, well established and offers possibility of high throughput. The term *epitaxial* refers to the growth of a crystalline, i.e., ordered, structure on a crystalline substrate. Thus, the substrate provides the crystal's “building plan” according to which the atoms order themselves on the surface. The

MO, metalorganic, part of the name refers to the fact that at least one of the precursor materials is supplied as molecules that consist of a metal atom bonded to organic ligands, such as methyl, CH_3 , and ethyl, C_2H_5 , molecules in the case of trimethylgallium (TMGa, $\text{Ga}(\text{CH}_3)_3$) and triethylgallium (TEGa, $\text{Ga}(\text{C}_2\text{H}_5)_3$) precursors for example.

Growth of crystals by MOVPE technique is a complex process with several interdependent steps. A more extensive description of MOVPE, as well as crystal growth in general, can be found in various textbooks [93,143], whereas here we will only introduce some main concepts to provide an overview for those that are less familiar with crystal growth and MOVPE. We thus start with a description of the MOVPE tool and main process flow in Section 3.1.1. Thereafter, we consider what happens when a gas is introduced in the reactor (Section 3.1.2), and what interactions with the surface could be expected (Section 3.1.3). Finally, we introduce some fundamental principles of thermodynamics and kinetics (Section 3.1.4.).

3.1.1 Description of equipment

A schematic of MOVPE system used in this thesis (Aixtron 200/4) is given in Figure 3.1, which we can divide into two parts – the left hand side (colored light blue) contains a complex network of lines in order to obtain the required amounts of specified materials as well as keep the system stable during the whole process, whereas the right hand side (colored light red) contains the growth reactor with in-situ reflectometry system. If we only looked at the growth reactor part, the main principle of operation is rather straightforward: The gases get mixed together just before flowing into the reactor, after which a laminar flow extends past the sample, finally exiting the reactor to the exhaust. The sample is placed on a highly conductive graphite susceptor that is heated by infrared (IR) lamps from outside the reactor. In order to prevent linear gradients and keep the growth homogeneous across the sample, the susceptor can be rotated.

In-situ measurement techniques in our system include a thermocouple inserted into the susceptor to keep track of the temperature, and an in-situ reflectometry system used for monitoring growth rate and nanowire dimensions in real time (see Section 5.5 for a more detailed description). Note that a thermocouple measures the susceptor temperature, and the real growth temperature at the sample is expected to be lower due to the flow of cooler gases.

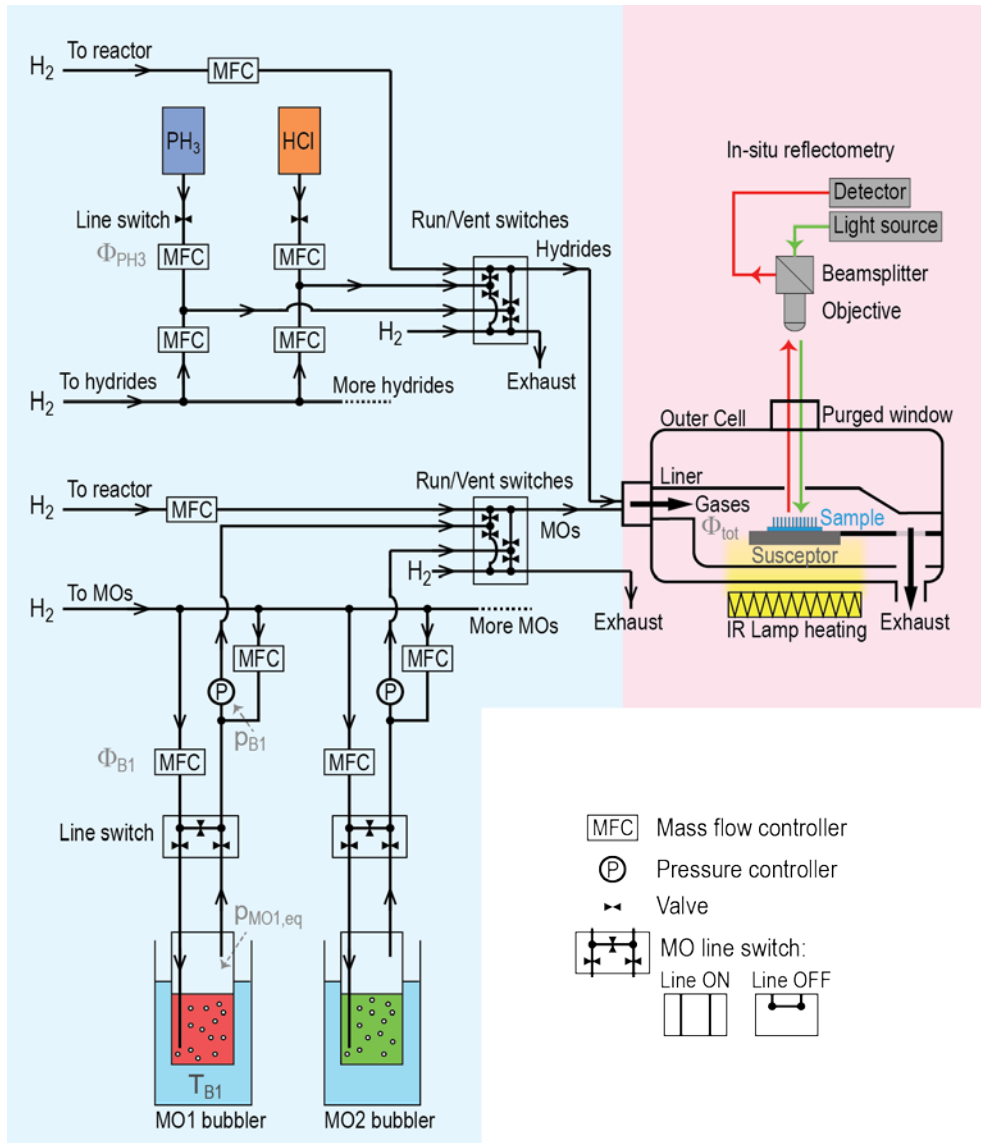


Figure 3.1. Schematic of an MOVPE system (based on Aixtron 200/4) illustrating the principle of metalorganic (MO) precursor bubblers, hydride gases, and a reactor with a sample and an in-situ reflectometry system. The variables used in Eqs. (3.1-3.3) are indicated in gray.

If we now look at the network of gas lines on the left side of the reactor, we see that, in our system, hydrogen (H_2) carrier gas is used for growth. The carrier gas is split into several lines and sent to “pick-up” MO precursors or hydrides, supply a base flow to the reactor and exhaust lines, control rotation of the susceptor, or to

purge the optical reflectometry window and the liner (last three parts are not shown in the figure). Overall, it leads to a messy network that can be hard to follow at first and we will highlight only some parts of the design.

In MOVPE, as the name suggests, the growth proceeds with supply of material in vapor phase. However, not all materials start in the vapor phase. Furthermore, in MOVPE, the group III and V constituents are not supplied as elements but in the form of so called precursor molecules. Group V materials are often supplied in the form of hydride gases, e.g., phosphine (PH_3) or arsine (AsH_3). The group III precursors, however, are typically supplied as MOs, such as trimethylindium (TmIn , $\text{In}(\text{CH}_3)_3$), trimethylgallium (TmGa , $\text{Ga}(\text{CH}_3)_3$), and triethylgallium (TEGa , $\text{Ga}(\text{C}_2\text{H}_5)_3$) that have been used in this thesis. These precursors are typically in liquid (TEGa , TmGa) or solid (TmIn) form at around room temperature, and thus the so called bubblers are used to extract materials in gas form (see Figure 3.1 bottom left).

A bubbler is essentially a cylinder filled with a specified material in liquid or solid form and with an inlet and an outlet for gases to flow, or bubble through the material. The equilibrium vapor pressure in the cylinder ($p_{\text{MO1,eq}}$) depends only on the liquid material and temperature. Thus, the MO cylinder is placed in a liquid (water/glycol) bath for temperature-control. In this thesis, hydrogen (H_2) is used as a carrier gas, which flows into the bubbler through the MO material with a flow value Φ_{B1} set by the mass flow controller (MFC). An equal flow of vapor then leaves the cylinder from the top part, at a bubbler pressure (p_{B1}) fixed by the pressure controller. The actual concentration of the MO precursor in the flow is then determined by the input flow Φ_{B1} , bubbler temperature T_{B1} and pressure p_{B1} .

Description and control of material flows

The growth process is controlled by setting reactor and bubbler temperature and pressure as well as carrier gas flow values sent to the MOs and gas flow values for hydrides. Typically, the flow values are set as volume flow in units of standard cubic centimeters per minute (sccm). In the case of MOs, this flow value only specifies the amount of carrier gas sent into a bubbler, not the actual amount of growth material sent to the reactor. In order to relate the two values, one needs to consider the vapor pressure of the material as well as the temperature and pressure of the bubbler. All in all, it is convenient to describe the material entering the

reactor in terms of a molar fraction, which is independent of reactor total flow as well as other settings, and thus can easily be applied for reproducing the growth by other researchers. The molar fraction of a metalorganic precursor, χ_{MO} , is given as a ratio of the MO partial pressure in the reactor (p_{MO}) and the total reactor pressure (p_{tot}), which can be further expressed as:

$$\chi_{\text{MO}} = \frac{p_{\text{MO}}}{p_{\text{tot}}} = \frac{p_{\text{MO,eq}}(T_{\text{B}}) \times \Phi_{\text{B}}}{(p_{\text{B}} - p_{\text{MO,eq}}) \times \Phi_{\text{tot}}}, \quad (3.1)$$

where Φ_{B} and Φ_{tot} are the carrier gas flux into the bubbler, and total gas flux in the reactor respectively, p_{B} is the regulated bubbler pressure, and $p_{\text{MO,eq}}$ is the equilibrium vapor pressure of MO, which depends on the bubbler temperature T_{B} , and is given by:

$$p_{\text{MO,eq}} = 10^{(a-b/T_{\text{B}})} \times \frac{1013.25}{760}, \quad (3.2)$$

where the first term is a parametric form for vapor pressure calculation, defined by empirical parameters a and b that are known for common metal organic precursors (see Table 3.1 below for the parameters of the precursors used in this thesis). The second term is conversion from Torr pressure units to mbar, since the parametric equation gives pressure in Torr, whereas we prefer to use mbar.

Table 3.1. Vapor pressure parameters of metal organic precursors used in this thesis (data from AkzoNobel product data sheets [144-146])

	a	b (K)
TMIIn	10.98	3204
TMGa	8.07	1703
TEGa	8.08	2162

For precursors already in the gas phase, the situation is even simpler, since the partial pressure of the gas, p_{gas} , is directly proportional to gas input flow rate, Φ_{gas} . Thus, the molar fraction for gaseous precursors is given by:

$$\chi_{\text{gas}} = \frac{p_{\text{gas}}}{p_{\text{tot}}} = \frac{\Phi_{\text{gas}}}{\Phi_{\text{tot}}}. \quad (3.3)$$

An important part of the flow design is to keep the flow constant and balanced, in order to avoid fluctuations and transient effects that can be especially detrimental

to heterostructure abruptness. In this respect, in an Aixtron 200/4 system, whenever a carrier flow is set for the source, another flow is set with a second MFC to keep the sum of the two values constant (see Figure 3.1). Additionally, line and run/vent switches are implemented in order to allow stabilization of the materials before sending them to the reactor, as well as to balance the flows when materials are switched between the reactor and exhaust. Note that this switching and subsequent mixing of the gases is done as close to the reactor inlet as possible in order to avoid any parasitic pre-reactions in the gas lines.

3.1.2 Gas phase processes

A gas is just a collection of molecules, whereas a molecule consists of atoms bonded to each other in a specific way. Different atoms are thus introduced into the growth reactor by bonding them with various other atoms to achieve certain properties of the molecules. For example, every molecule requires different amount of energy to break it apart. Pyrolysis, in particular, is thermal decomposition of a molecule at elevated temperatures. A temperature at which the molecules are fully pyrolysed (group III/V atoms free from the organic components) is typically referred to as pyrolysis or thermal decomposition temperature. However, one should be aware that pyrolysis depends on temperature exponentially and there is a range of temperatures where precursors can be partially pyrolysed. Too low pyrolysis temperatures can lead to immediate pyrolysis and parasitic deposition of the material on the gas lines and reactor walls, thus contaminating the reactor as well as wasting material. In addition, if growth temperature is much higher than the pyrolysis temperature, desorption could dominate and stop the growth process. On the other hand, too high pyrolysis temperature can lead to inefficient use of materials as the precursors go to exhaust without incorporating into the crystal.

In Paper I, we have used TEGa precursor instead of TMGa due to its lower pyrolysis temperature. In particular, TEGa is expected to fully pyrolyse at $\approx 350^\circ\text{C}$, TMGa at $\approx 480^\circ\text{C}$, and TMIIn at $\approx 350^\circ\text{C}$ (see Figures 5.11, 5.9, and 5.4 respectively in Stringfellow et al. [143] and references therein for precursor percentage pyrolysis as a function of temperature in various ambients). Since particle assisted nanowire growth in MOVPE is typically carried out at relatively low temperatures (e.g., $\approx 440^\circ\text{C}$ [147]), considerations of precursor pyrolysis temperatures become important. For GaInP nanowires, only a narrow growth window exists due to very different pyrolysis temperatures of TMIIn and TMGa:

TMIn gets increasingly more difficult to incorporate into the crystal above $\approx 450^\circ\text{C}$ [148], whereas TMGa precursor is not fully pyrolysed at temperatures below $\approx 480^\circ\text{C}$, which leads to both more complex growth processes, as well as to inefficient precursor consumption. Therefore, TEGa precursor, especially in combination with TMIn, could be expected to perform better; and in Paper I, we have demonstrated versatility of TEGa precursor by synthesis of high yield GaInP nanowire arrays, with a materials composition tunable over a wide range by the group III input flows. It is worth noting here that another benefit of TEGa precursor, in comparison to TMGa, is expected reduced carbon incorporation in growth of layers [143]. This is often attributed to the larger ethyl molecule that decomposes in a different pathway than the methyl molecule, which is expected to be the main contributor to carbon incorporation. For growth of nanowires with a Au particle, however, this consideration is less relevant, since carbon solubility in Au is low and thus the particle acts as a filter for carbon impurities [89]. Nonetheless, carbon could incorporate at the sidewalls, and it would also be relevant for selective area growth of nanowires where a particle is not used [149].

As the gas enters the reactor, it can pyrolyse already in the gas phase (homogeneous pyrolysis) if temperature is high enough. However, typically, most of the pyrolysis happens at surfaces (heterogeneous pyrolysis), where thermal decomposition energy is reduced by the presence of a surface. In reality, there is a mixture of both homogeneous and heterogeneous pyrolysis, and to make matters even more complicated, different precursors and their radicals interact with each other and can increase pyrolysis rates even further as well as combine to form new adducts with different decomposition properties. For example, the decomposition temperatures of AsH_3 and PH_3 are significantly lowered when introduced together with TMGa or TMIn due to methyl radicals, whereas decomposition temperature of TMGa and TMIn can be at the same time lowered by AsH_3 and PH_3 due to hydrogen radicals (e.g., [150,151]). For more details on complex kinetics of precursor chemical reactions, see Chapter 5 in Stringfellow et al. [143] and references therein.

3.1.3 Processes on the surface

Temperature as well as concentration gradient across the reactor leads to the flow of materials towards the sample on the susceptor. Thus, a portion of precursors and the products of full or partial pyrolysis end up at the semiconductor surface. When close to the surface, the precursors can diffuse in the gas phase until they either

pyrolyse to some degree and incorporate into the crystal, exit to the exhaust, or get adsorbed to the surface. The adsorbed molecule (or atom) is only weakly bound to the surface by van der Waals forces, which means that the available thermal energy is enough to break the attractive forces and allow the molecule (or atom) to diffuse on the surface until it incorporates into the crystal or gets desorbed back to the gas. Note that if the molecule is not fully pyrolysed before incorporation into the crystal, some elements of the molecule can be added to the crystal as dopants.

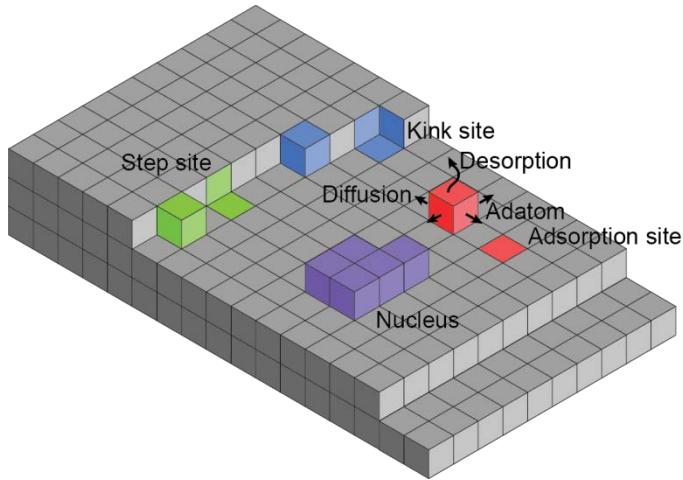


Figure 3.2. Illustration of important sites of an atom on a crystal surface as described in the main text. An atom attracted from the gas and weakly bonded to the crystal at an adsorption site is called an adatom (red) and can then either diffuse on the crystal surface or desorb back to the vapor phase. Diffusing adatom can then incorporate at a kink site (blue), step site (green), or create a new nucleus (violet) by coordination of several adatoms that then result in new step and kink sites, which lead to the growth of the nucleus.

A simple and intuitive way to imagine crystal growth is to think of atoms as cubes (more generally, the building blocks could be atoms, ions, or molecules – however, here we assume that the molecules were fully pyrolysed and only atoms remain on the surface). Such a description of the crystal is referred to as the Kossel crystal [93], where the number of free faces of a cube relates to the energy required to create that surface area in order to incorporate the atom into the crystal at that location. Replacing an identical surface at the incorporation site is considered to not cost any energy as no new surface is created. In such a picture, higher number of free surfaces refers to a higher energy state and thus the adsorbed atom (adatom) (red in Figure 3.2), which has 5 of the faces exposed, will look for an incorporation site where it can minimize the energy of crystal formation. A kink site (blue in Figure 3.2) is the most energetically favorable site

for incorporation into the crystal, followed by the step site (green), whereas nucleation of a new nucleus (violet) is the most energy costly path, since it requires creation of the largest new surface area as well as coordination of several adatoms to form a stable nucleus. Thus, growth can proceed in a so called terrace step kink model, where first an adatom is added to a step and then other adatoms incorporate to kink sites in order to complete the step before starting a new step. However, if diffusion length is short compared to the distance between steps, the preferred incorporation route depends on the position of the adatom.

3.1.4 Thermodynamic and kinetic considerations

Vapor phase epitaxy of a crystalline solid consists of a transition from a vapor phase to a solid crystal phase. Such a phase transition can be described by thermodynamics on a larger scale. However, understanding growth phenomena requires kinetics as well, where processes on an atomistic scale are considered. In other words, thermodynamics describes the potential for crystal growth, whereas kinetics governs the rates at which the growth processes occur, where, in particular, the slowest (rate-limiting) step determines the growth rate behavior.

Concentration gradient of materials above the substrate surface can be controlled by growth temperature and input flows, which in turn describes the presence of a driving force for material growth. In thermodynamic terms, the driving force for growth of a solid crystal is described by the chemical potential difference, where chemical potential of a species in a mixture is defined as the rate of change of the free energy (Gibbs energy G) of a thermodynamic system with respect to the change in the number of moles (n_i) of the species i that are added to the system:

$$\mu_i = \left(\frac{\partial G}{\partial n_i} \right)_{T,p,n_{j \neq i}}, \quad (3.4)$$

where T and p are temperature and pressure respectively. Thermodynamics equilibrium is defined by the minimum of the Gibbs energy, and thus in equilibrium, chemical potentials of all phases and all components are equal. In order to make a reaction happen, a driving force is established by a chemical potential difference. In vapor phase epitaxy, this difference is between the chemical potential of the vapor (μ_v) and that of the solid crystal (μ_s):

$$\Delta\mu_{vs} = \mu_v - \mu_s, \quad (3.5)$$

where a positive $\Delta\mu_{\text{vs}}$ indicates a driving force for material to move from the vapor to the solid crystal, whereas a negative value would indicate the reverse process, which is called etching or desorption of atoms. Such a phase transition and chemical potential difference can typically be achieved by varying the actual vapor pressure, p , of input material, which, for the simplest case of an ideal gas in a single component, can be expressed as:

$$\Delta\mu_{\text{vs}} = RT \ln\left(p/p_{\text{eq}}\right), \quad (3.6)$$

where R is the universal gas constant, T is the temperature, p_{eq} is equilibrium (also called saturation) vapor pressure of the solid, and p/p_{eq} is the supersaturation ratio of the gas.

In addition to chemical potential difference, the formation of a new phase in the initial stage of growth requires nucleation, i.e., small clusters of particles forming a stable nucleus of the solid. After a stable nucleus is formed, the crystal can grow from it by attaching atoms to an edge or kink as described in Section 3.1.3. The process of nucleation requires overcoming a nucleation energy barrier due to creation of new interfaces. Although nucleation can occur spontaneously and randomly in a homogeneous initial phase (e.g., forming a solid or liquid nucleus in the vapor), the drive for nucleation is strongly facilitated by the presence of preferential nucleation sites, such as inhomogeneity like a substrate or suspended particles, where some energy is released by destroying pre-existing interfaces. In epitaxial growth, which implies a presence of a substrate, nucleation typically only happens at the surfaces. The nucleation barrier that needs to be overcome to create a nucleus can be expressed by the difference in the Gibbs free energy:

$$\Delta G = \Delta G_{\text{V}} + \Delta G_{\text{S}}, \quad (3.7)$$

where the first term represents released energy by formation of a volume, whereas the second term represents the energy cost for surface creation (we ignore any strain in the nucleus here). The two energies thus need to be balanced, which leads to a critical nucleus size as illustrated in Figure 3.3 for the case of an unstrained, spherical nucleus in a homogeneous surrounding, where the total change of Gibbs free energy is given by:

$$\Delta G = -\frac{\Delta\mu}{V_{\text{m}}}\frac{4\pi r^3}{3} + 4\pi\gamma r^2, \quad (3.8)$$

where $\Delta\mu$ is the supersaturation between the initial and final phases (note that $\Delta\mu$ is positive here for formation of a solid, which leads to reduced nucleation

barrier by the first term), V_m is the mole volume of the new phase, r is the radius of the spherical nucleus, and γ is surface free energy, which can be regarded as reversible work to form a unit area of a surface. As a simplification, the surface energy of any solid can be taken to be proportional to its number of dangling bonds, which is then proportional to the number of free faces of the cube in the Kossel crystal model as we described in Section 3.1.3.

In Figure 3.3, the change in the total Gibbs free energy initially increases due to creation of a new surface, until a critical radius (r^*) is reached where the volume term starts to dominate. ΔG^* is thus the critical work needed to form a stable nucleus. If the size of the nucleus is smaller than the critical size, the nucleus is unstable and tends to disband, whereas if it is larger, the nucleus is stable against decomposition and the growth is now limited by mass transport or kinetic reactions rather than nucleation.

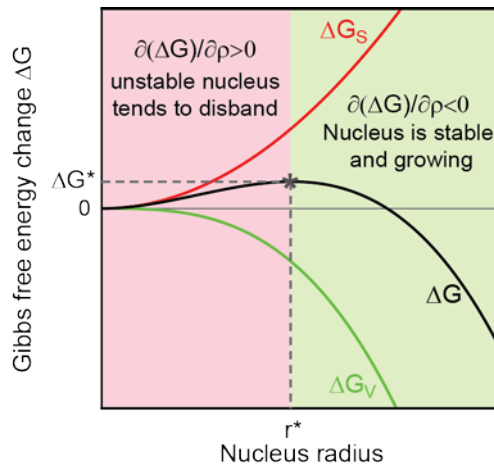


Figure 3.3. Gibbs free energy change as a function of nucleus radius for the case of a homogeneous nucleation of a spherical nucleus. Surface (ΔG_s) and volume (ΔG_v) formation contributions are shown as red and green lines respectively.

For the heterogeneous nucleation, one needs to adjust the volume term to take into account the actual shape of the nucleus, which depends on the wetting properties of a surface, and one needs to split the surface term to describe all the different interfaces available. The difference between the interfacial energies and the shape of the nucleus thus defines the preferential sites for nucleation. This consideration is especially important to explain the highly anisotropic growth of nanowires, as will be described in more detail in Section 3.2.

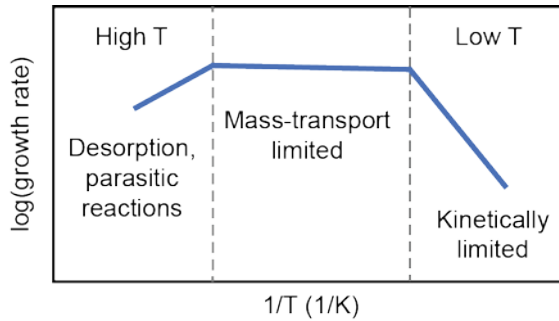
Temperature dependence

Figure 3.4. A logarithmic dependence of growth rate on inverse of temperature for a typical MOVPE process. At low temperatures, growth rate increases exponentially with temperature as a result of temperature activated, kinetically limited, reactions. At intermediate temperatures, growth rate is only weakly dependent on temperature and the process is governed by mass-transport. At high temperatures, growth rate starts decreasing with temperature, typically, due to desorption of growth materials from the crystal surface or parasitic reactions in the reactor.

Finally, three important epitaxy regimes defined by temperature ranges should be introduced here. Without considering the detailed growth mechanisms, the limiting regimes can be identified by investigating growth rate dependence as a function of temperature (Figure 3.4). High quality thin films are typically grown at intermediate growth temperatures, where growth rate is limited by the material transport through the vapor phase to the growth interface. Particle assisted nanowires, on the other hand, are typically grown at lower temperatures, in kinetically limited regime, where the gas phase supplies precursors to the surface at a rate much higher than the rate of growth reactions. Here, the growth rate increases exponentially with temperature, indicating that thermally activated processes limit the growth rate. In particular, precursor pyrolysis and interface growth reactions can be the cause for such temperature dependence, where the slowest reaction limits the growth rate, which can be expressed by an Arrhenius equation:

$$k \propto \exp\left(-\frac{E_a}{RT}\right), \quad (3.9)$$

where k is the rate constant (or growth rate), R is the universal gas constant, T is temperature, and E_a is the activation energy for the limiting reaction. Activation energy is commonly specified for various reactions, which can help with identifying the limiting process [143]. With increased temperature, thermally activated processes become faster (due to exponential temperature dependence) in

comparison to the diffusion in the gas phase, which depends only weakly on the temperature (diffusion coefficient $\propto T^{3/2}$). Thus, intermediate temperatures lead to the mass transport limited regime, where growth rate is nearly independent of temperature. Radial growth of nanowires can be achieved in this regime, as will be introduced in Section 3.2.3. At even higher temperatures, due to enhanced desorption of molecules and parasitic deposition at the reactor walls, growth rate starts decreasing.

3.2 Considerations for nanowire growth

While the fundamental principles of vapor phase epitaxy apply to the growth of particle-assisted nanowires as well, there are some specific considerations that result in very different structures. At the heart of this difference are both the presence of an assisting metal particle, and the small dimensions of the nanowires with a large surface area and different crystallographic facets. Thus, in this section, we add some details of fabrication and general growth processes of Au-particle seeded nanowire arrays that have been used for the work in this thesis.

3.2.1 Periodic array preparation

The nanowire arrays in this thesis have been grown with geometry and materials in mind for development of nanowire solar cells in the future. Hence, as solar cells require large area, high-throughput, and highly absorbing materials, the NIL patterning technique and the nanowire array optics guidelines (Chapter 4) have been employed to obtain patterned substrates of desired dimensions.

The NIL process can be described step by step as follows [152]: (i) A wafer, on which growth will be carried out, is spin coated with double layer resist structure, where the first resist is a lift-off resist that is easily dissolved with a remover chemical, whereas the second, top resist layer is an imprint resist into which the pattern is transferred. (ii) A prepared stamp with the inverse of the desired structure is then pressed onto the wafer with the resists and the pattern is transferred into the top-resist. (iii) The compressed residual layer is removed by oxygen plasma and then a wet chemical etching step is used to partially etch the bottom lift-off resist so that the wafer surface is exposed and an undercut profile is created to aid the lift-off process later by separating Au particles of the pattern from the unwanted Au film deposition on the resist. (iv) Finally, Au is evaporated,

and (v) remover chemical is used to dissolve the lift-off resist resulting in a defined pattern of Au discs (see Figure 3.5a and 3.6a) with the diameters defined by the imprint stamp and the oxygen plasma etching step, whereas the height of the discs is defined by the thickness of the evaporated Au layer. The volume of the Au particle then defines the diameter of the nanowire depending on the semiconductor material and growth conditions [9,142].

3.2.2 Vapor liquid solid growth

When the Au particle pattern is defined on a wafer, the wafer can be cleaved into smaller pieces (like in Figure 1.1a), which are then placed inside the MOVPE growth reactor on the graphite susceptor (see Figure 3.1). The growth procedure (Figure 3.5) typically starts with increasing the susceptor temperature under group V and carrier H₂ pressure in order to anneal the substrate and remove native oxides before the actual growth of the nanowires is started. Otnes et al. [77] have shown that a two-step pre-nucleation procedure can improve pattern preservation. In such a case, a pre-anneal nucleation step is used where group III precursors are supplied to the growth chamber at a temperature below the intended growth temperature. During the supply of the group III and V precursors at low temperature, the Au particle is alloyed with the group III material, which reduces the effective melting temperature of the Au alloy particle and thus forms depressions in the substrate surface that prevent thermally activated movement of the Au alloy particle and hence preserve the pattern [77]. Group III precursor supply is switched off during the annealing step, and turned back on after annealing and reduction of temperature to that of the growth.

The growth mechanism of semiconductor nanowires from Au particles, in our work, is governed by the vapor liquid solid (VLS) growth principle, initially introduced by Wagner and Ellis [4], which can be described as follows: A vapor phase semiconductor source (group III precursor) is pyrolysed and dissolves into the Au particle, creating an eutectic alloy (Figure 3.5b), which means that the alloy has a lower melting point than its constituents individually. If growth temperature is above the Au/semiconductor alloy eutectic point, the particle is liquid. However, for growth below the eutectic point, it has been observed that whether the particle is liquid or solid depends on temperature and specific materials, as well as precursor pressure and thermal history [138]. The alloying of the Au particle with the group III material continues until supersaturation is reached and the chemical potential between the vapor-liquid and liquid-solid interfaces acts as a driving

force for nucleation of the solid semiconductor [28] (Figure 3.5c). The nanowire continues to grow with the continued flow of chosen precursors (Figure 3.5d, 3.6b). At this point, group III or V precursors can be switched to different ones in order to create axial heterostructures. Additionally, other group elements can be introduced in order to dope the semiconductor. In general, group V/III ratio, temperature, and precursor pressures can be adjusted in order to control the growth rate, crystal structure and material quality of the nanowires [153]. At the end of the growth process, group III source is switched off and the system is cooled down under group V and H_2 carrier pressure. During this cool down, however, growth can still continue as the Au-alloy particle precipitates group III material stored in the particle during growth.

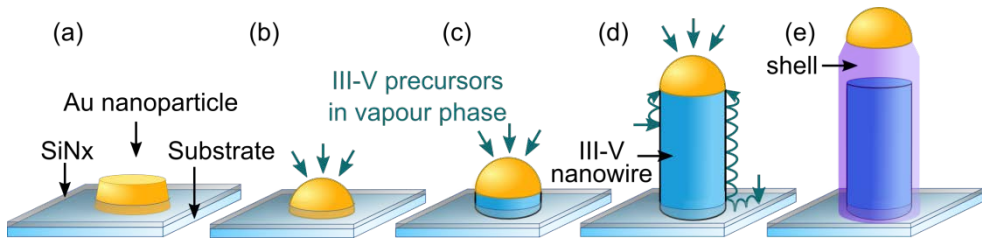


Figure 3.5. A schematic illustration of MOVPE VLS growth: (a) Au particles deposited on the substrate covered by patterned SiN_x mask, (b) introduced vapor phase precursors alloy with the Au particle, (c) nucleation takes place at the substrate-nanoparticle interface, (d) nanowire continues to grow with the flow of chosen precursors, (e) shell growth is carried out by increasing the growth temperature and adjusting the precursor flows (see Section 3.2.3).

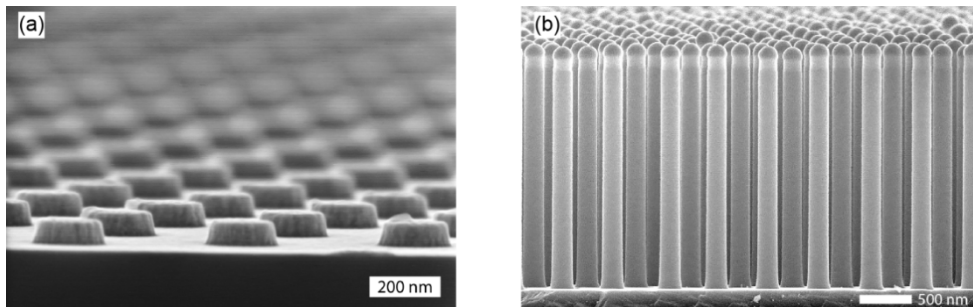


Figure 3.6. Scanning electron microscope images of (a) Au-particle array after NIL process and (b) nanowire array after growth.

Back to thermodynamic and kinetic considerations

To grow a crystal in the form of a nanowire, extremely anisotropic growth is required, i.e., growth in one direction needs to be strongly preferred. However, if we consider just the chemical potential differences that were introduced in

Section 3.1.4, the relation between chemical potentials in each phase for the VLS growth is expected to be: $\mu_v > \mu_l > \mu_s$ for the vapor, liquid and solid phases, respectively. Thus, the biggest chemical potential difference is between vapor and solid, which would lead to preferential growth directly from vapor to solid, without involvement of a liquid particle. Such pure thermodynamic considerations, therefore, do not explain the role of the liquid particle for nanowire growth. In some systems, the seed particle has been observed to act as a catalyst for decomposition of precursors [154-156], which could explain why crystal grows under the particle as well as why particle assisted nanowires typically grow in the kinetically limited regime. However, catalytic behavior where a particle lowers the activation energy compared to planar growth is not always observed, which could mean either that the particle is not catalytic, or that the catalyzed reaction is not rate limiting. Furthermore, nanowires can also be grown from a seed particle in molecular beam epitaxy, where materials are introduced as elements and thus no thermally-activated processes exist to be catalyzed. Thus, even if the particle might be catalytic, catalytic behavior cannot be treated as a general, system independent mechanism for explaining the anisotropic growth of nanowires [157,158]. Instead, we need to look more in depth and consider nucleation events in the VLS system, as has been described in detail by Wacaser et al. [158].

Here, the liquid particle introduces interfaces between the different phases with different interfacial energies. Assuming a simplified, flat particle-solid interface model, four distinct nucleus positions for VLS growth are depicted in Figure 3.7a: (I) on the substrate or (II) nanowire surface, where the nucleus has interfaces with the solid and vapor, (III) inside the particle, where the nucleus interfaces are with solid crystal and liquid particle, and (IV) at the triple phase interface inside the particle, where the nucleus has interfaces with vapor, liquid and solid at the same time. The sites I and II are very similar, with a difference only in the facet orientation for the created surfaces, which can affect surface energies that we disregard here. If we use the classic nucleation theory, briefly introduced in Section 3.1.4., we can compare the change in Gibbs free energy for sites I, III, and IV (we adapt the equations now for a 2D nucleus as a single monolayer cylinder with height h and perimeter P):

$$\Delta G_{\text{I,II}} = -\Delta\mu_{\text{vs}}n + Ph\gamma_{\text{vs}}, \quad (3.10)$$

$$\Delta G_{\text{III}} = -\Delta\mu_{\text{ls}}n + Ph\gamma_{\text{ls}}, \quad (3.11)$$

$$\Delta G_{\text{IV}} = -\Delta\mu_{\text{vs}}n + P_{\text{vs}}h\gamma_{\text{vs}} + P_{\text{ls}}h\gamma_{\text{ls}}, \quad (3.12)$$

where $\Delta\mu$ is the chemical potential difference per mole of atoms added to the nucleus at an interface between the two phases given by the indices v for vapor, l for liquid, and s for solid, n is the number of moles added to the nucleus, γ is the surface energy at the respective interface indicated by the indices, whereas P_{vs} and P_{ls} refer to the partial perimeter of the nucleus, only along the respective interfaces. Note that only the side surfaces play a role in the surface energy terms, because the top surface interface is considered to be the same as the one replaced at the bottom of the nucleus.

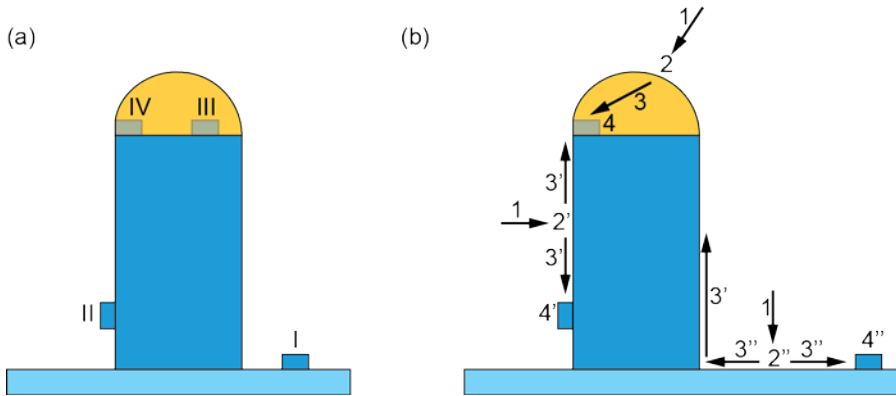


Figure 3.7. Schematics of (a) the main nucleation sites and (b) possible material supply pathways during VLS nanowire growth, as described in the main text.

If we considered only supersaturation, then site I would be preferential over site III in Figure 3.7a since $\Delta\mu_{vs} > \Delta\mu_{ls}$. However, the difference in the surface energies at the two sites can make nucleation at site III preferential. At the triple phase interface (site IV), the change in Gibbs free energy for formation of a nucleus could be very low, because supersaturation is high, and the nucleus as well as the liquid particle, can adjust its shape and contact angle in order to minimize surface energy terms [158].

Note, however, that the actual situation is even more complicated, as it has been observed that the particle solid interface is not always flat [159,160]. Instead, the interfaces at the nanowire sides can be truncated, in which case the main nanowire-particle interface facet does not reach the triple face interface. In this case, nucleation was suggested to start at a site III, at the corner of the truncation. After formation of a nucleus at the particle-solid interface, addition of new atoms proceeds with a reduced energy barrier, since fewer or no new interfaces need to be created. Nanowire growth then typically proceeds in a layer by layer (or birth

and spread) manner, where a nucleus is followed by a quick completion of the full layer, during which the particle gets depleted from the precursors, which results in reduced supersaturation and halts the growth. New nucleation event happens after an incubation period where particle supersaturation is increased by continued supply of precursors [161,162].

The different pathways for supply of precursors to particle assisted nanowire growth as well as processes parasitic to the axial nanowire growth are illustrated in Figure 3.7b. The processes can be split into 4 categories: (i) gas-phase diffusion (1), (ii) precursor decomposition reactions at the assisting particle (2), nanowire sidewall (2'), or substrate (2'') surface, (iii) diffusion of reactants through the assisting particle (3), on the nanowire sidewall (3'), or on the substrate (3'') surface, and (iv) nucleation and subsequent growth of a solid crystal at the liquid-solid interface (4), at the nanowire sidewall resulting in shell growth (4'), or at the substrate surface resulting in thin film layer growth. Every process has a different dependence on temperature, precursor flows and total flow, which can help identify which processes are limiting in different situations (for an example, see Verheijen et al. [154]).

Diffusion considerations

Due to high vapor pressures, group V precursors, such as AsH_3 and PH_3 , typically incorporate into the crystal by direct impingement to the Au particle/growth interface. Group III precursors, however, have lower vapor pressures and longer surface diffusion lengths. Hence, as shown in Figure 3.7b, group III precursors can attach at the nanowire sidewall or substrate surface and then diffuse towards the growth interface in addition to the direct impingement pathway. Taking these considerations into account, we can roughly describe how nanowire axial growth rate will change with time, i.e., increasing nanowire length. In the very beginning, the growth rate is slow until the particle reaches the steady state supersaturation. Once the nanowire starts growing at a steady state, most of the material is collected from the substrate, defined by the substrate surface diffusion length λ_s of the diffusing species. As the nanowire continues to grow, the collection area on the substrate decreases (pink area on the substrate in Figure 3.8a), whereas additional collection area on the nanowire sidewalls shows up. However, since the substrate collection area decreases with the square of the nanowire length L , whereas the nanowire sidewall area increases only linearly with L , the overall growth rate should decrease. Note that, in reality, diffusion constants on different facets and materials differ, as has been considered in more extensive models for nanowire growth rates [163,164]. If nanowire length exceeds the diffusion length

of the species (Figure 3.8b), the collection area will remain constant with further growth and thus growth rate should stay constant.

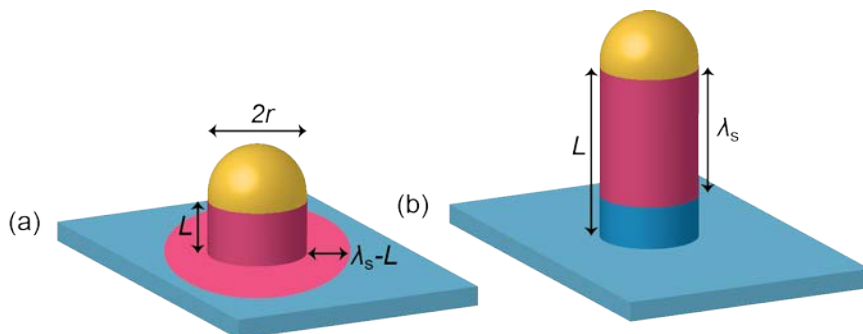


Figure 3.8. Schematics of surface diffusion contribution to the growth of nanowires, with the pink color representing collection area where adsorbed atoms can diffuse to the growth interface.

For the simplified picture, described above, we have assumed that nanowires are separated at a distance larger than any surface or gas diffusion lengths. Such regime is called the independent growth regime, and Johansson et al. [163] give a more extensive description with a mass transport model for nanowire growth in this case. If the nanowires are instead very densely packed and surface diffusion lengths overlap, the growth rate is expected to be lower and decrease with decreased nanowire separation, as the nanowires need to compete for shared material [165]. In between such independent and competitive regimes, however, a third, synergetic regime has been observed [155]. Synergetic regime happens when the surface diffusion collection areas do not overlap, but the larger gas phase diffusion areas for precursors decomposed at the Au particles do overlap. These precursors, partially decomposed at the catalyst particles, can then diffuse and reach growth fronts of other nanowires, thus increasing total available material for growth. In such a regime, nanowire growth rate actually increases with decreased nanowire separation, as well as increased diameter (whereas in the competitive regime thin nanowires grow faster). The nanowire arrays used in this thesis are fairly densely packed with pitch of 500 nm and thus most likely face the competitive growth regime, although synergetic effects could also be in play. The actual regime and the strength of the effect depend on pitch of the array, size of the particles, and the temperature dependent diffusion lengths of the used materials.

3.2.3 Shell growth

As we discussed in Section 3.1.4, the particle assisted growth of the nanowires typically takes place in the kinetically limited regime, whereas planar epitaxial layers are typically grown at a higher temperature in the mass-transport limited regime. Shell growth mostly resembles the planar growth of layers and thus requires higher temperatures to overcome kinetic limitations. Such growth mechanism is no longer described by the VLS mechanism, but rather by a direct vapor solid growth at the side-facets.

Some shell growth often occurs even in the kinetically limited regime despite a considerably higher growth rate along the nanowire axis than on the nanowire side facets when growth conditions are optimized for axial growth. In this case, however, the shell is usually of poor quality, and it can short-circuit a *p-n* junction in axial nanowires for photovoltaic applications. Thus, in-situ etchants are sometimes used in order to prevent formation of such a shell during growth. In Paper II, we have used hydrogen bromide (HBr), as in Ref. [166], and in Papers I and III - hydrogen chloride (HCl), as in Refs. [167-170], to prevent parasitic radial growth for GaAs and GaInP nanowires respectively. In addition, in-situ use of HCl can widen the parameter space for non-tapered nanowire growth, reduce incorporation of carbon impurities, and affect crystal structure [167,170,171]. For ternary materials, it can also lead to a change in composition, possibly due to formation of indium chloride (InCl) and gallium chloride (GaCl) compounds that have different decomposition and desorption probabilities [168], [Paper I].

As discussed in Section 2.1.3, controlled epitaxial shell growth can be desirable for nanowire surface passivation. A shell can be grown (see Figure 3.5e) by increasing the growth temperature and moving to a thermodynamically limited regime, where growth rate for the side facets is considerably higher than the axial growth rate.

If the Au particle is not removed before the radial growth, some axial growth is expected, where the exact amount varies based on the growth parameters and precursors used [Paper II]. It is possible to etch away the Au particles (Section 3.2.4) ex-situ by wet chemical etching. However, if Au is etched away, the sample needs to be transferred from and back to the growth reactor, which exposes the sample to the surrounding environment. Such exposure can lead to oxidation of the material and potential deterioration of its optical quality, which might not be recovered by passivation procedure with the shell grown afterwards.

3.2.4 Preparation after growth

Au etch

Au-particle assisted nanowire growth, as described in Section 3.2.2, is still by far the most common. However, the Au particles are expected to increase reflection of the array [172,173] and thus are usually removed during solar cell processing. In Paper III, we have studied the effect of Au particles on the nanowire array optical response. For that study, the Au particles were removed from one sample ex-situ by wet chemical etching in a $\text{KI:I}_2\text{:H}_2\text{O}$ solution after growth (see Figure 3.9).

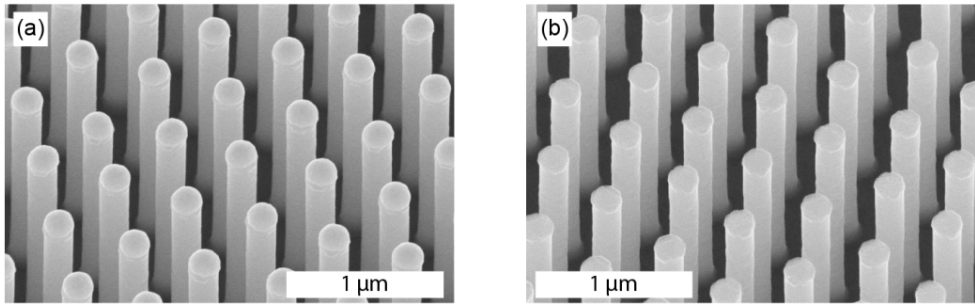


Figure 3.9. Scanning electron microscope images of an InP nanowire array sample (a) before, and (b) after the Au-etch procedure.

Peel-off

If nanowires are grown on a III-V semiconductor substrate, the costly substrate material significantly exceeds the amount of material used for the nanowires. In order to allow cheaper solar cell manufacturing, re-use of the substrate for multiple growths is highly desired. Furthermore, one of the tandem solar cell approaches, introduced in Section 2.2.3, requires nanowire arrays embedded in a transparent membrane, which could be also of interest for flexible devices. Peel-off [31,73,74] is a procedure where the nanowire array is embedded in a flexible polymer, which preferably shows negligible absorption of light for most of the relevant wavelengths. The polymer is applied to the nanowire array in a liquid form and then cured, after which it can be mechanically peeled-off from the substrate. This should result in nanowires mostly being broken close to the nanowire-bottom to substrate interface, although sometimes a small stub remains on the substrate. Peeled-off samples have been investigated experimentally in Papers II and III, and modelled theoretically in Paper IV.

4 Nanowire array optics

The use of nanowire arrays as solar cells offers intriguing benefits, where geometry dependent efficient absorption of light is the most cited one. In order to understand such benefits, we need to understand how nanowire array optics differs from the optics of bulk semiconductors. The understanding of nanowire array optics principles is a key in adapting the measurement methods and analyzing optical characterization of nanowire arrays. In this chapter, thus, we give a short description of why nanowire array optics is special, define main fundamental concepts and give examples of how nanowire geometry design can be used to obtain some optical effects.

4.1 From bulk to nanowires

In order to build up to the nanowire array optics, we start with a simpler and more familiar system – a thick bulk semiconductor. When light is incident on the thick bulk material in the form of a plane wave (see Figure 4.1a), it can be specularly reflected at the top interface or be transmitted into the bulk layer, where the light can travel as a plane wave until it reaches the bottom interface where it again can be reflected or transmitted. As the plane wave travels through the material, it can lose its coherence if the layer is thicker than the coherence length of the light. The forward propagating light, in such a case, cannot interfere with the backward propagating light, which simplifies the problem as the plane waves can then be described as optical rays propagating in different directions, and we need to keep track only of the intensity carried by each ray. Thus, bulk materials can be described by geometrical optics, and the Fresnel equations can be used to calculate the reflection and transmission of the rays at each interface.

If we instead make this layer thinner than the coherence length (Figure 4.1b), as could be the case for the simplest anti-reflective (AR) coating that is just a quarter wavelength film, interference effects show up and geometrical optics is not sufficient to describe the problem anymore. Even though in Figure 4.1b the path of the light is drawn by arrows, indicating the presence of plane waves just as in the case of a thick layer, the forward and backward propagating waves can now

interfere, and we need to keep track of the phase of the light in addition to the intensity. Thus, wave optics is required to solve the scattering problem. The multiple scattering of the plane wave between the top and the bottom interfaces within the thin film leads to a geometric series, which allows for an analytical solution for the reflection and transmission of light.

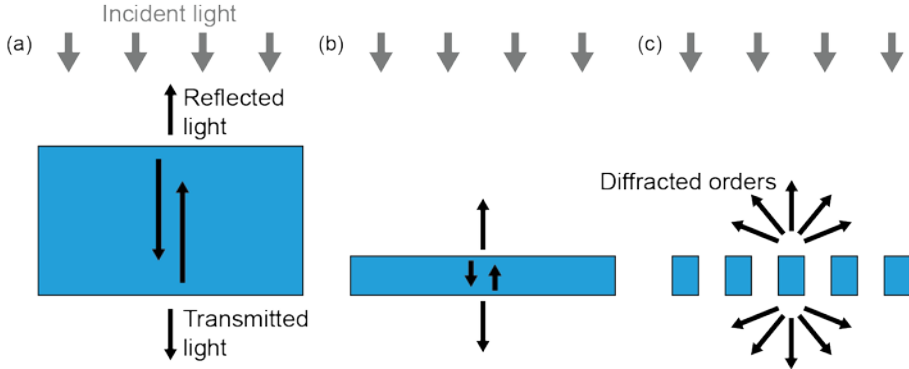


Figure 4.1. Schematic illustrations of pathways of light in (a) a thick bulk material, (b) a thin film, and (c) a diffraction grating. The arrows indicate plane waves and their propagation direction, whereas the optical modes inside the grating are more complicated and not shown here.

The nanowire array is essentially a diffraction grating and takes the light interaction one step further (Figure 4.1c) from the thin film case. The grating or nanowire array is typically thin enough so that the coherence of light is maintained as in the thin film case. However, due to the period which is on the order of the wavelength, we get additional diffracted orders at specific angles, defined by the grating period and materials surrounding the grating at the top and the bottom. These diffracted orders can be either propagating or evanescent (except for the 0th order which is always propagating), and a cutoff wavelength is defined for a diffracted order as the wavelength above which the diffracted order transforms from a propagating to an evanescent wave (note that the arrows in Figure 4.1c indicate only the propagating diffracted orders). Exactly at the cut-off wavelength, the diffracted order is a plane wave traveling purely along the surface of the grating. For normally incident light, the cutoff wavelength of the first diffracted order is given by $\lambda_{\text{cutoff}} = np$, where n is the refractive index of the homogeneous medium above/below the grating, and p is the period of the grating. This first diffracted order is the propagating diffracted order, beyond the specular one, that disappears (becomes evanescent) at the longest wavelength.

Inside the grating, the behavior of light is even more complicated, as light can bounce between the different features and give rise to new grating (array) modes.

As a result, in contrast to the bulk and thin film cases, analytical solutions are usually not available for the scattering of light by such diffraction gratings, and numerical modeling needs to be performed. The interaction of light with nanowire arrays will be described in more detail in the coming sections, whereas here we would like to mention one important additional connection point of the nanowire arrays to bulk concepts – the use of the bulk refractive index for our nanowires. Note that the nanowires that we are interested in for photovoltaics have relatively large diameters (around 200 nm) compared to the length scale at which quantum mechanical quantization effects show up in III-V nanowires. (For GaAs and InP nanowires, quantum confinement effects are observable at room temperature for diameters of less than around 20 nm as a rough estimate, obtained by comparing confinement energy of a one-dimensional infinite potential well model to thermal motion of the particles [174]. This rough estimate matches well with the experimental observation and the more accurate calculation for InP nanowires by Gudixsen et al. [175].) Therefore, we assume that the nanowire scatters light as a homogeneous bulk rod locally. Thus, we employ bulk refractive indices for the nanowires and we solve the classical Maxwell equations to take wave-optics diffraction/scattering effects into account. The use of the bulk refractive index for such nanowires has been shown to work well for analyzing the spectra of nanowire arrays, to the point where measured, complicated interference-dominated spectra could be quantitatively recreated by the modeling [176].

4.2 Geometric vs wave optics for nanowire arrays

The geometry of a vertical nanowire array is specified by four main parameters: nanowire diameter D and length L , array pitch p (center to center separation of the nanowires), and array symmetry with the most common being the square and hexagonal symmetries (see Figure 4.2). The symmetry of the nanowire cross-section is also sometimes taken into account with the most common ones being a round cylinder shape, a cylinder with hexagonal facets as well as tapered nanowire shapes.

In geometrical optics, a ray description of light is used, where the rays of light are assumed to be infinitesimally narrow and travel in straight lines. In such a picture, light would be able to pass through the gaps between the nanowires. However, considering the diffraction limit that originates from wave optics, we know that light can only be focused down to a spot size given by the Airy pattern, where the

full width at half maximum (FWHM) of the Airy disk in the center is around the size of the wavelength of light. Thus, if the dimensions of the nanowire array (diameter or pitch especially) are on the order of or less than the wavelength of incident light, the light will simultaneously interact with both the nanowires and the air, which would not be described by ray optics. Additionally, theoretical modeling has demonstrated cases where almost no light is transmitted through a sparse nanowire array with a low area filling factor [34], [Paper IV] and experimental measurements often show transmission values close to zero for certain wavelengths of various nanowire arrays [32], [Paper III]. Hence, geometrical optics is not applicable for understanding the physics of nanowires and nanowire arrays of subwavelength sizes, and wave optics should be used instead [34,39,40].

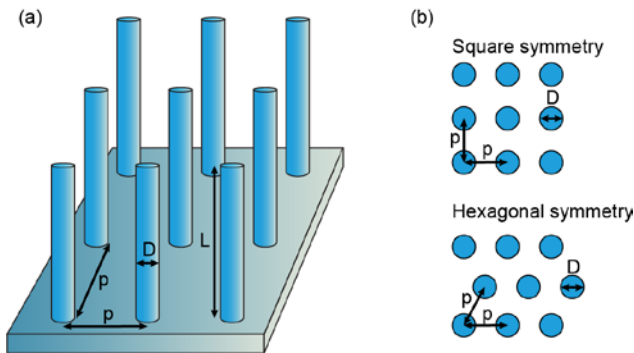


Figure 4.2. Illustration of vertical nanowire array geometry with the main parameters that specify the array: (a) nanowire diameter D , nanowire length L , array pitch p , and (b) the symmetry of the array with the most common square and hexagonal symmetries shown in the figure.

In fact, it was shown with full electrodynamic modeling that the results can be split into three optical regimes of (i) geometrical optics limit for $D \gg \lambda$, (ii) electrostatic limit for $D \ll \lambda$, and (iii) nanophotonic regime at $D \approx \lambda$ where optical resonances are observed and result in enhanced absorption [39], or resonant reflection [Paper IV]. Photovoltaic nanowire arrays typically fall within the nanophotonic regime and full electrodynamic modeling is used to understand the optical properties of such systems, as has been done in Paper IV, where we used both the finite-element method in COMSOL Multiphysics to solve the scattering problem in real space, as well as the scattering matrix method to solve for eigenmodes in reciprocal space. The two methods can provide complementary information in a convenient way: the finite-element method yields directly the electromagnetic field in real space, whereas the scattering matrix method yields directly information about the optical modes of the system.

4.3 Optical modes

Light is an electromagnetic wave that, in a homogeneous medium, can be described as a superposition of plane waves, where each plane wave has zero electric and magnetic field components along its propagation direction. For example, a plane wave incident towards a nanowire array from a direction parallel to the nanowire axis has zero electric and magnetic field components along the nanowire axis. When the incident light reaches the nanowires, however, the polarization is changed as new modes are excited. For example, transverse electric (TE) and transverse magnetic (TM) modes are supported by the nanowires, where for the TE modes the electric field is perpendicular to the nanowire axis and the magnetic field has a component parallel to the nanowire axis and vice versa for the TM modes. Additionally, hybrid electromagnetic modes (HE and EH) are also supported by the nanowires, where the electric and magnetic field components are now both non-zero along the propagation direction, that is, along the nanowire axis. In order to theoretically model optical properties of nanowires and nanowire arrays, generally, Maxwell equations are solved under certain boundary conditions for light incident on the system. When a modal method, such as the scattering matrix method [177], is used, solutions to the problem are usually described in terms of eigenmodes, or modes for short.

4.3.1 Single nanowire

A single vertical nanowire (Figure 4.3a) acts, in principle, as an absorbing optical fiber (for photon energies above the band-gap – otherwise like a non-absorbing fiber) and supports waveguide modes where coupled-in light propagates along the axis of the nanowire. Light that does not interact with the nanowire mode can be depicted to be reflected or transmitted at the substrate/air interface according to the Fresnel equations, whereas light that does interact with the nanowire mode can be scattered at the top air/nanowire interface, absorbed along the nanowire length, and reflected or transmitted at the bottom substrate/nanowire interface [178].

In general, a single, isolated nanowire can show guided HE_{mn} , EH_{mn} , TE_{0n} , and TM_{0n} modes [179], where $m=1, 2, \dots$ denotes the angular dependence of the mode, whereas n is related to the number of nodes in the radial direction within the core of the nanowire. More specifically, the electric and magnetic field

components of a mode show dependence of the form of $\cos(m\varphi)$ or $\sin(m\varphi)$, where $m=0$ for TE and TM modes in nanowires. Importantly, the normally incident, linearly polarized light shows $m=1$ dependence in the angular direction. Coupling between two modes is allowed only if their difference in m value is even. Hence, the incident light can excite only HE_{mn} and EH_{mn} modes with odd m , and excitation of TE_{0n} and TM_{0n} modes is not possible. The modes that show the strongest response to normally incident light in a vertical nanowire are the HE_{1n} guided modes, because the overlap with the incident plane wave is expected to be the largest for $m=1$, and the field patterns of the HE_{1n} modes are similar to the plane wave pattern outside the nanowire core, whereas the field patterns of the EH_{1n} modes differ considerably [179,180]. It is important to mention that for a fixed geometry, the fundamental mode HE_{11} is propagating for all photon energies, but the higher order propagating modes show up only at higher energies. The wavelength at which a mode changes from a leaky mode [181] to a bound, propagating one can be referred to as a cut-off wavelength. The cut-off wavelengths, and thus the number of propagating modes at a specific wavelength depend on the nanowire diameter (as well as the nanowire material and the material surrounding the nanowire).

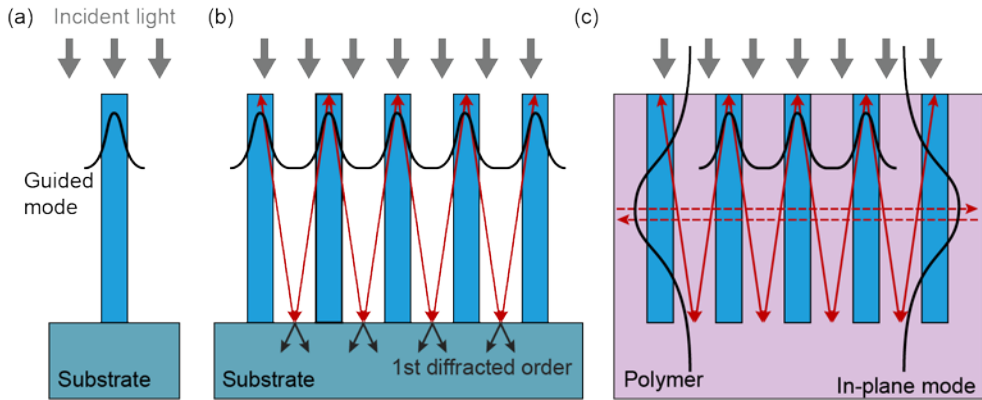


Figure 4.3. Schematic illustration of modes (a) in a single vertical nanowire on a substrate where a guided mode propagates along the nanowire axis, (b) in a vertical nanowire array on a substrate where similar guided modes as in a single nanowire are supported, but light can also scatter between the nanowires giving rise to array-modes that can leak into the substrate, and (c) without the substrate, where array modes are confined within the nanowire array and give rise to in-plane modes.

4.3.2 Nanowire array

Vertical nanowire arrays on a substrate (Figure 4.3b) support modes that follow similar behavior as the modes of a single vertical nanowire in some cases. For example, a mode similar to the fundamental single fiber HE_{11} mode can be found in an array. However, light can scatter between the nanowires, in addition to the top and bottom interfaces of the array, giving rise to array-modes with behavior deviating from the ones found in the individual nanowires. More specifically, for a low λ/D value, the array modes tend to converge towards the single nanowire modes, since the light becomes more and more confined to the nanowires [Paper IV] [182]. Just as in the single nanowire case, the array mode attributed to the single nanowire fundamental HE_{11} mode is propagating for all photon energies as well as any nanowire diameter and array pitch. Other modes change from propagating to evanescent modes at the cut-off wavelengths specific for each mode. The cut-off wavelengths and number of propagating modes in the case of arrays depend not just on the nanowire diameter, but also on the array pitch.

It is worth noting here that the nanowire array optical response depends on the geometry of the array as well as its surroundings. In the above case of a nanowire array on a substrate, the array-modes typically leak into the propagating diffracted orders of the substrate (only first diffracted order is indicated in Figure 4.3b, into which we have seen strong leakage of array modes [Paper IV]). In such a case, the array modes do not accumulate multiple roundtrips between the top and the bottom interfaces of the array.

However, if the array is embedded in a polymer and peeled-off from the substrate (Figure 4.3c), the cutoff wavelengths of the diffracted orders are much shorter due to the lower refractive indices surrounding the array, in which case, for a wide range of wavelengths, only the 0th diffracted order is propagating, and we have seen cases where an array mode does not leak efficiently into this 0th diffracted order [Paper IV]. Thus, the light bouncing between the nanowires and the top and bottom interfaces is instead confined within the array. This gives rise to a standing wave pattern that can result in reflectance or absorptance resonances [Paper III, IV] [183-188]. There are two ways to analyze these resonances: (i) as guided mode resonances that can form standing waves in the lateral direction (in-plane modes), which are similar to the modes obtained in dielectric slab waveguides [183,184,187,188], or (ii) as vertical, Fabry-Perot like array resonances that form a standing wave in the vertical direction, similar to thin films [185,186], [Paper IV]. The difference between these two ways stems from the way we choose to perceive the system, where in the first case, Maxwell equations are solved for waves

propagating in the nanowire-array plane, whereas in the second case, focus is on propagation along the nanowire axis. The two methods are complementary and highlight different aspects of the optical response. Note that the terms guided mode resonances, in-plane array modes and vertical Fabry-Perot array resonances all refer to the same standing wave phenomena that can lead to resonant effects.

Since such in-plane array modes rely on the waves bouncing between the top and bottom interfaces as well as between the nanowires, anything that hinders such pathways can suppress resonant excitation of such modes. As described above, the presence of a high refractive index substrate allows array modes to couple into the higher, propagating diffracted orders of the substrate thus disrupting roundtrips in the array. Additionally, in Paper III, we have shown that Au particles, on top of nanowires in a nanowire array, can absorb long wavelength light and suppress the resonant excitation of such in-plane modes. In Paper IV, we have used optical modeling to illustrate that such resonances would be suppressed efficiently with relatively low extinction coefficients. Thus, if the resonances fall in the absorbing region of III-V semiconductors, they would not be observed. However, as observed in Paper III, if Au particles are etched away and the substrate is removed, such guided mode resonances of the array can be observed below the semiconductor band-gap, where the nanowires are non-absorbing.

4.4 Geometry dependent optical response

While there has been a lot of research on absorption in horizontal single nanowires [189,190] that are extremely important for single nanowire device applications, in this thesis, we consider vertically oriented nanowire arrays that are most promising for solar cells where a large area is needed for power production. The optical properties of such nanowire arrays are typically investigated at normal incidence, which maximizes the projected area and gives the highest output power for most solar cells under direct solar illumination. We would like to also note that while there has been extensive research on the optical properties of Si nanowire arrays [34,178,183,185], this thesis focuses on direct band-gap III-V semiconductors. Since absorption characteristics of the indirect band-gap materials, such as Si, are significantly different from the direct band-gap materials studied in this thesis, the results of optical properties cannot always be directly transferred between the two systems. Thus, this section will be limited to reviewing some of the optical properties of vertically oriented III-V semiconductor nanowire arrays.

4.4.1 Enhanced absorption in nanowire arrays

It is commonly stated that nanowire arrays exhibit enhanced light absorption. In reality, absorption is typically strongly enhanced only for a certain wavelength range. For example, Anttu [39] has shown that the absorption per volume of semiconductor material in an InP nanowire array at $\lambda = 850$ nm can be varied by a factor of 200, ranging from 10 times weaker to 20 times stronger than in a bulk semiconductor sample. However, even when averaged over the solar spectrum, a subwavelength nanowire array can still absorb more light than a thin-film with the same amount of semiconductor material [33,183]. Such absorption enhancement in nanowire arrays occurs due to the geometry dependent modes. Hence, light absorption in the nanowire devices is not just a function of the intrinsic optical material properties, but can also be engineered through control of the nanowire array geometrical parameters [180,189].

In particular, the individual nanowire waveguide modes, introduced in the previous sections, have been shown to lead to strong absorption at a certain diameter dependent wavelength for each mode [180]. The constituent nanowires in an array support similar waveguiding modes and arrays show similar absorption peaks [180]. However, the array-modes can be excited too, and each mode can be either strongly or weakly absorbed by the nanowires, depending on the exact nanowire diameter and array pitch. A weakly absorbed mode can lead to noticeable transmission into the substrate as well as to detected reflection originating from the nanowire/substrate interface.

Design for efficient absorption

It has been shown, however, that the presence of absorption resonances of nanowire arrays are typically dominated by the characteristics of the individual nanowires, in which case the pitch and the length are tuned only to optimize overall absorption after the absorption resonance and its location is picked by the diameter. Specifically, the constituent nanowires can show absorption resonances due to the HE_{1n} modes, which lead to absorption peaks for the array. It was found that for direct band-gap semiconductor nanowires, the absorption and ultimate efficiency of a solar cell is maximized when the absorption resonance energy of an HE_{1n} mode is placed, by tuning the diameter, close to the band-gap of the material, where the absorption coefficient is smaller than at the higher energies [180].

When the diameter is fixed, the absorption of the nanowire array can be increased by increasing the length of the nanowires, but only until a saturation value is

reached. At this point, the absorption is limited by the insertion reflection loss – i.e., reflection loss at the top air/nanowire-array interface when there is no additional reflection at the nanowire-array/substrate interface since the light that enters the array is absorbed before reaching the substrate. In order to obtain the maximum ultimate efficiencies for the solar cells and the highest absorption values, the pitch should be increased with increasing length. As absorption increases with length, the array can be made sparser, which at the same time reduces the absorption and reduces the insertion reflection losses. Thus, when the length is increased, the pitch should also be increased until the reduction of the insertion reflection loss is balanced by the reduction in absorption.

We note that with respect to the symmetry of the array, the optical response of nanowire arrays does not seem to differ significantly between the hexagonal and the square arrays [43]. However, random/aperiodic nanowire arrays have also been investigated and suggested to potentially enhance the absorption in nanowire arrays [191].

4.4.2 Reduced reflection for tandem applications

For tandem applications, an important property is the nanowires' sub-wavelength dimensions and low surface coverage, which leads to a much lower reflection than for a thin film without an additional anti-reflective coating [192,193]. In a simplified picture, a nanowire array shows a low area coverage that leads to a better refractive index matching between the nanowire array and air, and between the nanowire array and a possible substrate, and thus a reduced reflection at both interfaces. In this case, we might expect high transmission of the low energy photons through the nanowire array top cell to a bottom cell.

Reflection resonances in a membrane

However, the above mentioned, simplified picture of reduced reflection does not always work. In Paper III, we have observed a reflection resonance peak after removal of the Au particles that were used as assisting particles for the nanowire growth. In such a case, as we explained in Section 4.3.2, in-plane modes are formed and they can scatter back into the incidence side causing a resonance. In Paper IV, we found that such resonances can lead to high reflectance values (up to 100%) for non-absorbing materials, or enhanced absorption with alternating reflectance and absorptance peaks for weakly absorbing materials.

In Paper IV, we have modelled nanowire arrays on a substrate and in a membrane, to confirm that resonant effects disappear in the presence of a high refractive index substrate but show up for the case of nanowires in a membrane (Figure 4.4). We have identified that the resonant wavelength-range lies between two cutoffs: (i) the 1st diffracted order cutoff in the polymer ($\lambda_{\text{cutoff,bot}} = pn_{\text{bot}}$, where $n_{\text{bot}} = 1.5$ is the refractive index of the polymer), and (ii) the 2nd mode cutoff in the nanowire array, obtained from the analysis of the eigenmodes. For nanowires on a substrate, $n_{\text{bot}} = 3.5$ and the 1st diffracted order cutoff in the substrate is pushed to much longer wavelengths, which thus allows the array modes to couple to the propagating diffracted order in the substrate, which, in turn, suppresses the occurrence of the in-plane mode resonances.

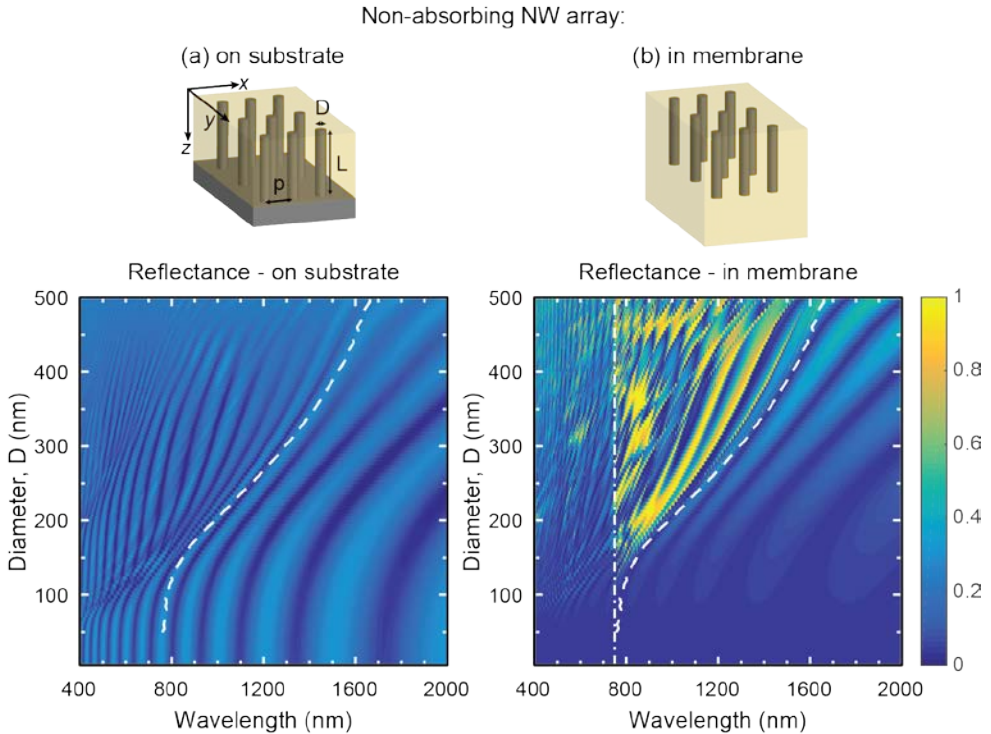


Figure 4.4. Geometry and dependence of reflectance spectra on diameter for non-absorbing nanowire array ($n = 3.5$) (a) on a semi-infinite substrate ($n = 3.5$) and (b) in an extended semi-infinite polymer ($n = 1.5$) membrane for light incident at normal angle from the top (air $n = 1$) side. The array geometry is set to $p = 500$ nm and $L = 2000$ nm. Resonant behavior is observed between two cutoffs in (b): the 1st diffracted order cutoff, in the membrane at the bottom, on the short-wavelength side (dash-dotted line) and the 2nd array-mode cutoff on the long-wavelength side (dashed line). In (a), the cutoff for the 1st diffracted order is at 1750 nm in the substrate, which results in the lack of resonant regime. Figure adapted from Paper IV.

Occurrence of such resonances can be detrimental for tandem solar cell applications, where, for example, a nanowire array embedded in a polymer could be used as a top cell. Such a configuration would rely on efficient transmission of below band-gap photons to the bottom cell, which would be diminished by the resonant reflection [Paper IV].

Design for high transmission by suppressing reflection resonances

Similar to the absorption enhancement, reflection resonances can be controlled by modifying the nanowire array geometry. However, unlike the absorption resonances that originate mostly from single nanowires and are mostly sensitive to the diameter, reflectance resonances arise from the array and thus are highly sensitive to both pitch and diameter. Furthermore, quite strong dependence on length, nanowire absorption coefficient, as well as surrounding materials is also observed [Paper IV].

In order to avoid reflectance resonances for tandem applications, the overall solar cell design needs to be considered. The resonances could be avoided if a 2 terminal configuration was made with a direct contact between the nanowires and the substrate, which would allow the array modes to leak to the substrate. However, if a transparent conductive layer is used and becomes too thick, or if a thick optical spacer is introduced between the array and bottom cell, as for example in 4-terminal devices, resonances could be a challenge, and the array geometry should be optimized. In particular, nanowires should be packed tighter and have smaller diameter in order to push the resonant regime into the absorbing regime of the nanowires, because the 2nd mode cutoff in the nanowire array blueshifts with reduced pitch and diameter [Paper IV].

5 Characterization techniques

In order to take advantage of the benefits of the nanowires described in the previous sections of this thesis, we need to link the growth control with the desired material properties. Optical modeling can help design the geometry and material compositions according to theory; however, various characterization techniques are needed to evaluate and optimize produced nanowire structures, as well as probe for any additional challenges. This chapter provides an overview of the main techniques used in this thesis in order to probe material morphology, dimensions and crystal structure (Sections 5.1, 5.5), composition (Sections 5.1.2, 5.2, 5.3), carrier dynamics and doping concentration (Section 5.3.2), and light interaction with the array (Sections 5.3, 5.4).

5.1 Microscopy

Resolution is the ability to distinguish two objects that are very close together. The resolution limit thus estimates a distance between two points that can still be told apart as distinct. A human eye is able to distinguish two objects only when they are separated roughly by at least 0.1 mm. In Figure 1.1a, we saw how nanowire array sample looks to the naked eye, where the nanowires themselves are not resolved. Hence, various microscopy tools are used to investigate nanowires, with the most common being the optical microscope, the scanning electron microscope (SEM), and the transmission electron microscope (TEM) (Figure 5.1).

The resolution of an optical microscope can be estimated by the Abbe's diffraction limit. In Section 4.2, we mentioned that light can, in best case, be focused to a spot described by the Airy pattern with the FWHM of the central spot on the order of the wavelength of the light. The resolution of an optical microscope, where visible light is used to image structures, can thus be estimated to be roughly $\lambda/2NA$, where NA is the numerical aperture of an objective, given by $NA = n \sin \theta$ with n the refractive index of the medium in which the objective is working, and θ is the maximum half-angle of the cone of light that can enter or exit the objective. Thus, assuming $NA = 1$, an optical microscope could resolve features down to 200 nm

scale for $\lambda = 400$ nm, which is the lower end of the wavelengths visible by human eye.

As seen in Figure 5.1a, optical microscopy can be used to locate single broken-off nanowires for single nanowire characterization. Alternatively, depending on the array pattern, the overall homogeneity of the pattern can be observed. However, finer details of the nanowire structure are not resolved.

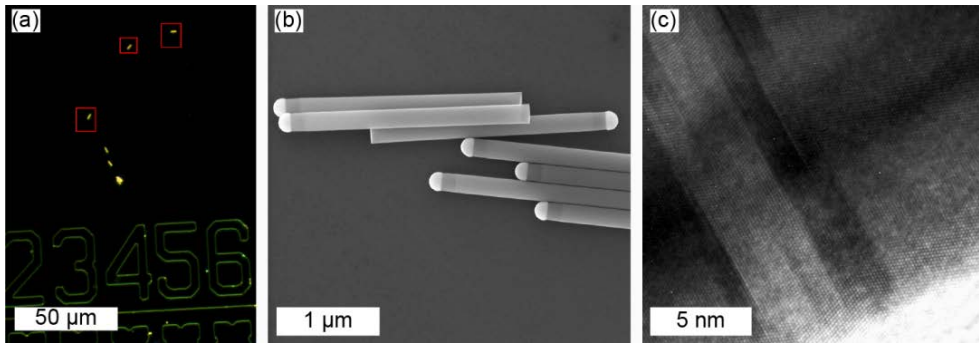


Figure 5.1. Broken-off nanowires with three different microscopy techniques: (a) a dark field optical microscope image where single nanowires are marked by red squares, (b) an SEM image, (c) a TEM image zoomed in to a small part of the nanowire.

Electron microscopy is typically used to go beyond the 200 nm limit of the visible light used in optical microscopes. Just like light, the electrons also have a wavelength, which is determined by the applied acceleration voltage. The energy of electrons is typically thousands of times larger than for the visible wavelength photons, and the wavelength of electrons is thus substantially shorter. Although the numerical aperture of electron microscopes is typically smaller than for the optical microscopes, the overall spatial resolution is much higher.

The two most common electron microscopes are the SEM and TEM, where the best SEMs typically have resolution on the order of 1-10 nm, whereas the best TEMs can go down to roughly 0.1 nm, i.e. the scale of atoms. The main differences between the SEM and TEM that allow for different resolution are the higher voltage used in a TEM, and different sample preparation as well as a different detection method. In an SEM, we detect scattered electrons that have a certain interaction volume with the material where the volume increases with the acceleration voltage. When electrons enter a sample, they spread and the emitted signal comes from an effectively larger area than the initial beam size, thus reducing the resolution of the SEM. To reduce the spreading, accelerating voltage can be reduced so that electrons penetrate the material less deeply and are thus

spread less. Alternatively, for a TEM, as the name suggests, we detect electrons transmitted through the sample. In order to be able to detect transmitted electrons, the sample has to be thin enough so that electrons do not interact and spread too much when passing through the material.

5.1.1 Scanning electron microscopy

The above differences result in different applications of the two microscopes. The SEM with a slightly lower resolution allows to measure on as-grown samples without any extra preparation steps. This makes SEM an essential and quick post-growth technique that is used to check the overall morphology of the sample, including distribution of the nanowires, their surface texture and facets, shape of the nanowires in terms of their diameter and length, and possible kinking or other deviations from the desired geometry. In some cases, SEM can even resolve different materials (e.g., in Figure 5.1b the top bright part of the nanowire is the Au-In alloy particle, the short darker segment under the particle is GaP, while most of the nanowire is GaInP), whereas from the facet formation it might be possible to tell the crystal structure. Thus, SEM gives crucial and quick feedback on the morphology of the materials that give insight into the growth mechanism.

5.1.2 Transmission electron microscopy

TEM, with a higher resolution, can give information about the crystal structure of the semiconductor and any defects present (e.g., in Figure 5.1c the contrast differences indicate presence of defects). It can give information about the composition of materials and interface quality of a heterostructure as well as strain caused by different materials. For TEM imaging, however, sample preparation is required. Nanowires are usually thin enough to be investigated by TEM, but they need to be mechanically broken off from the growth substrate and transferred to an electron transparent substrate, like a lacey carbon film covered Cu-grid. However, if information is wanted on the facets and composition of the cross-section, then nanowires are too thick (too long) and have to be thinned down before imaging, similarly to bulk samples. This is often known as focused ion beam milling, where a focused ion beam is used to thin down the nanowire to the required thickness and at a wanted distance along the nanowire length. Such a technique can be invaluable for investigating the cross-section of radial nanowire structures.

5.2 X-ray diffraction

Challenge of ternary development lies in chemical composition variation within each nanowire due to complex interactions between precursors as well as across the sample due to edge effects. Ternary material composition can be extremely sensitive to every growth parameter as well as to substrate and reactor preparation and any drifts. For this reason, material composition evaluation is a necessary addition to the characterization techniques used for binary materials.

X-ray diffraction (XRD) is one such tool, where an x-ray beam is incident on the sample at an angle θ (see Figure 5.2a) and the scattered x-rays are collected as a function of the scattering angle 2θ . Due to the short wavelength of the x-ray beam (in our case $\lambda = 1.541 \text{ \AA}$), which is shorter than the crystal lattice spacing, the beam diffracts at the periodic crystal structure, creating interference fringes. In most directions, the x-ray waves cancel each other out due to destructive interference; however, constructive interference occurs at specific angles, determined by the Bragg law:

$$2d_{hkl} \sin(\theta) = m\lambda, \quad (5.1)$$

where d_{hkl} is the spacing between adjacent (hkl) lattice planes, θ is the incident angle, m is an integer giving the order of diffraction, and λ is the x-ray wavelength. The (hkl) is the Miller index notation for lattice planes. As our nanowires are grown in the $[\bar{1}\bar{1}\bar{1}]$ direction, we have measured diffraction between the $(\bar{1}\bar{1}\bar{1})$ planes, in which case $d_{hkl} = a/\sqrt{h^2 + k^2 + l^2} = a/\sqrt{3}$, where a is the lattice constant of the crystal.

For ternary materials, Vegard's law (see Eq. (2.1)) can be used to express the ternary lattice constant through the composition x (for example for $\text{Ga}_x\text{In}_{1-x}\text{P}$) and the lattice constant of the respective binaries. We can thus obtain composition as a function of the angle:

$$x = \frac{\sqrt{3}\lambda/2 \sin(\theta) - a_{\text{InP}}}{a_{\text{GaP}} - a_{\text{InP}}}. \quad (5.2)$$

An example of XRD data is shown in Figure 5.2b where both the scattering angle and the material composition are given as axes for comparison.

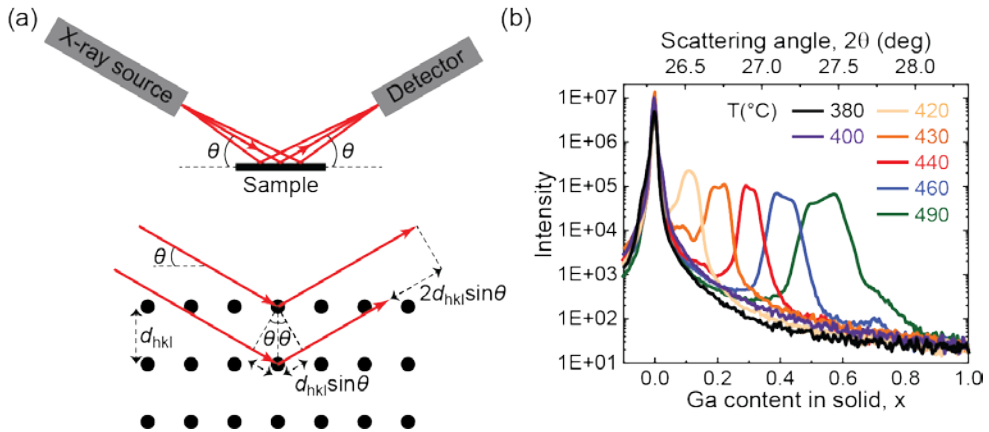


Figure 5.2. (a) Schematic illustration of an XRD measurement setup (top) and Bragg constructive interference condition in a crystal (bottom) as well as (b) an example of XRD data for $\text{Ga}_x\text{In}_{1-x}\text{P}$ nanowires grown on an InP substrate with varied growth temperatures [Paper I].

In addition to the actual composition variation, the width of peaks measured by XRD depends on several factors, such as the finite size of the scattering objects, strain gradients in the scattering objects, and instrumental resolution [194]. However, in our samples, the peak width is mostly determined by the composition variation along the nanowire [195][Paper I], unless samples were small compared to the x-ray beam spot size, in which case the edge effects would contribute as well. It is worth mentioning that the size effect, where the peak width tends to be inversely proportional to the size of the object in the measured direction, can be used, in some cases, to differentiate between the substrate or thin layer and the nanowires [196]. The method is based on the fact that along the growth direction, nanowires tend to look like bulk, without additional broadening effects. However, in the perpendicular direction, nanowire diameters are small enough to cause broadening effects, while substrate and layer peaks would be narrow, allowing to extract nanowire signal by measuring at an offset [196].

5.3 Photoluminescence

As described in Section 2.1.2, semiconductors are, to a large extent, characterized by their band structure, which defines a lot of the significant semiconductor properties. One way to extract these properties and probe the band structure is by photoluminescent experiments. If external excitation is applied to a sample, an electron gets excited from the VB to the CB, leaving a hole behind in the VB and

creating an e-h pair. Typically, this e-h pair is excited with energy higher than the band-gap and undergoes nonradiative relaxation processes before recombining, where only radiative recombination leads to emission of a photon with energy lower than the one of the excitation (see Figure 2.1). When the excitation is achieved with light incident on the sample, the process is called photoluminescence (PL), whereas some other relevant techniques, which are not described in this thesis, are cathodoluminescence, where the carriers are excited by an electron beam, and electroluminescence, where excess electrons and holes are injected from electrical contacts under a voltage bias. Here, we describe the general operation principles of steady state and time-resolved photoluminescence (SSPL and TRPL) measurement setups.

5.3.1 Steady state photoluminescence

A typical SSPL measurement setup is illustrated in Figure 5.3. It consists of an external light source, typically a continuous wave laser with variable excitation intensity achievable by the use of attenuators. The laser can then be focused on the sample through an objective if a beamsplitter is used. In this case, unless the sample holder is tilted, normal incidence excitation is typically used and quite small spot sizes are achieved, in ideal case, limited by the diffraction limit. Alternatively, the laser can be focused to the sample through a side where a long focal length lens is used. In the side excitation method, the spot size is larger and thus the power density is lower than with the excitation through the objective case. The benefit of the side excitation mainly lies within easier and quicker alignment, especially in the case of measurements on single nanowires due to the small dimensions. When the sample is excited, it emits light that is collected by an objective and focused onto a spectrometer (or a monochromator) where it gets dispersed by a diffraction grating and detected by a cooled CCD camera. A band-pass filter is typically used after the laser to make sure that only the wavelengths in the vicinity of the laser line pass through, whereas a longpass filter is used before the spectrometer in order to filter out this laser light. The sample is typically placed on a translational stage, allowing to measure on different spots over the sample as well as, in the case of single nanowire measurements, to locate and measure specific single nanowires. Additionally, if temperature dependent measurements are needed, the sample can be loaded into a liquid Helium cooled cryostat and placed on the translational stage.

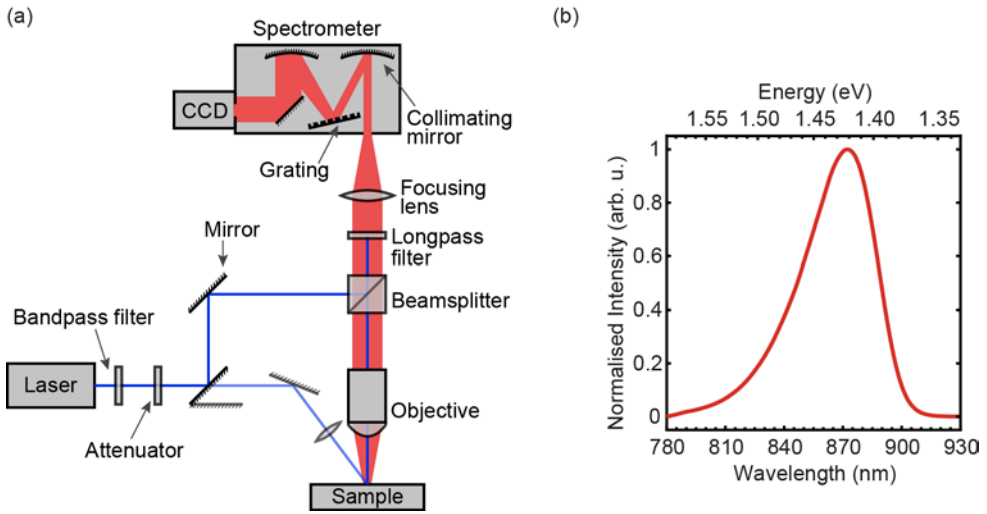


Figure 5.3. (a) Schematic illustration of a typical SSPL measurement setup, and (b) a GaAs substrate spectrum obtained with such a setup [Paper II].

PL measurements are often performed in order to identify dominating radiative transitions and their energies, material composition, presence of defects, crystal structure changes and doping concentration to mention a few possibilities. Often, single nanowire measurements are performed in order to investigate fundamental properties of a semiconductor nanowire without obscuring the result by the variation between the different nanowires. However, there is also a strong desire and a clear benefit in being able to perform PL measurements on as-grown nanowire arrays as well. SSPL, in principle, can be used similarly as SEM, as a basic first hand tool for probing nanowires immediately after growth. For that purpose, PL could be used to quickly check composition of the material, inhomogeneity in the composition and optical quality of the devices in terms of the strength of their luminescence. Additionally, such non-destructive measurements would be especially beneficial for solar cell development where optical quality could be nondestructively investigated before processing full devices. However, as we present in Paper II, in some cases, depending on the nanowire material grown and the substrate chosen, substrate PL signal can raise a challenge in interpreting the data.

While PL measurements can also be used to evaluate material composition, and typically XRD and PL provide a good agreement for the average composition, significant differences are expected in the two methods in some cases, such as degenerate doping, which affects band structure, but not the lattice spacing.

Additionally, indirect band-gap transitions might be too weak to observe in PL. Furthermore, some parts of the material could be optically inactive, or alternatively, additional peaks due to impurities could be present. Thus, XRD provides a much more accurate evaluation of material composition, whereas PL can be used as a quick estimate, as well as to obtain additional information.

5.3.2 Time-resolved photoluminescence

Radiative recombination transition energies can be detected by SSPL experiments. However, such measurements do not show the intricacies of carrier dynamics. In order to understand what happens after excitation in more detail, additional transient measurements, such as TRPL, are needed.

The main difference between the SSPL and TRPL measurements is the light source and the detection system, which together allow TRPL to probe some different physics and complement SSPL data. TRPL has been used widely in order to probe the transient carrier dynamics. TRPL can help identify which recombination process is dominating at different times and identify minority carrier lifetimes. These values can then be used to estimate the maximum limit of the open circuit voltage that is relevant for solar cell performance. TRPL can also estimate the surface recombination velocity and thus the surface quality. Furthermore, in Paper II, we have tentatively suggested a method for extracting doping values from TRPL data.

A typical TRPL setup is schematically shown in Figure 5.4. Although it looks more complicated than the typical SSPL setup, the main differences are that a pulsed rather than a continuous wave laser is used and a streak camera is used in order to obtain temporal resolution in addition to the spectral resolution created by the spectrometer. Other approaches for TRPL measurements exist, where the most common alternative is a time correlated single photon counting system where, instead of a streak camera, an avalanche photodiode is used. However, this system will not be further discussed in this thesis.

When a light pulse hits the sample, it creates a high density of e-h pairs in the sample and this density decays over time by various recombination processes (see Section 2.1.4) until a new pulse comes in and new e-h pairs are excited. Here, it is important to pick the laser repetition rate in such a way, that the excited carrier concentration has time to decay to a sufficiently low level. Otherwise, the tail of the first pulse decay curve can create an offset to the second one and complicate interpretation of the data. After the excitation of the excess carriers, part of the

beam goes to a photodiode in order to send a trigger to the streak camera as will be described later, and part of the beam goes through an optical path, similar to the SSPL setup, as described in the previous section. The sample is excited and its luminescence is collected and focused onto a spectrometer that spreads different wavelengths spatially (i.e., in a horizontal direction). This light is then incident on the streak camera (see Figure 5.5).

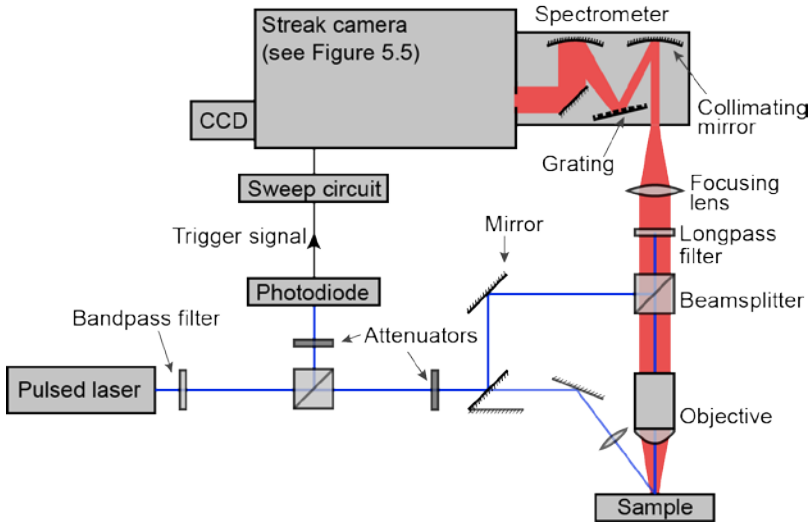


Figure 5.4. Schematic illustration of a typical TRPL measurement setup.

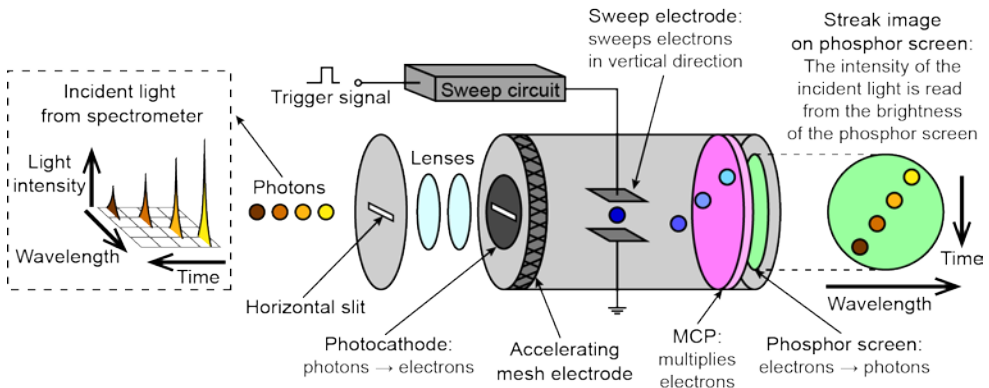


Figure 5.5. Schematic diagram of a streak camera, based on Ref. [197].

The streak camera is an ultra-high speed detector that spatially displaces electrons that come at different times resulting in temporal resolution. The operating principle is shown in Figure 5.5. The streak camera consists of an entrance slit, a

lens to focus photons onto a photocathode, which converts photons to electrons, an accelerating electrode where electrons are accelerated while keeping their energy proportional to the intensity of incident light, and a pair of sweep electrodes where a time-varying voltage is applied to create a high-speed sweep that displaces electrons in vertical direction, such that typically, the early time electrons give the signal at the top of the image, whereas the later electrons give rise to the signal lower on the screen (see Figures 5.5 and 5.6b). The control of the periodic voltage sweep is achieved by sending a trigger signal from the laser pulse split with a beamsplitter. Electrons are now spatially displaced in two dimensions – horizontally due to wavelength spreading in a spectrometer, and vertically due to the time spreading in the electric field between the sweep electrodes. This electron distribution then passes through a microchannel plate (MCP) that multiplies the electrons, which then hit a phosphor screen that converts electrons to light and the light is detected by a CCD camera attached to the streak camera.

Lifetime is a commonly used parameter when talking about TRPL results. We have introduced lifetime in Section 2.1.4 in terms of recombination. However, a simple way to visualize the lifetime is to define it as the time it takes for the carrier concentration to decay to $1/e$ value of its maximum concentration (see Figure 5.6c). Such lifetime is commonly called $1/e$ lifetime. Note that in Figure 5.6c the $1/e$ lifetime is actually the time it takes for the signal intensity to decay from its maximum value to $1/e$ of it. As discussed in Section 2.1.4, this estimate will be valid only in the low injection regime. In the high injection regime, the carrier concentration lifetime will actually be 2 times higher than the time it takes for the signal to decay to its $1/e$ value.

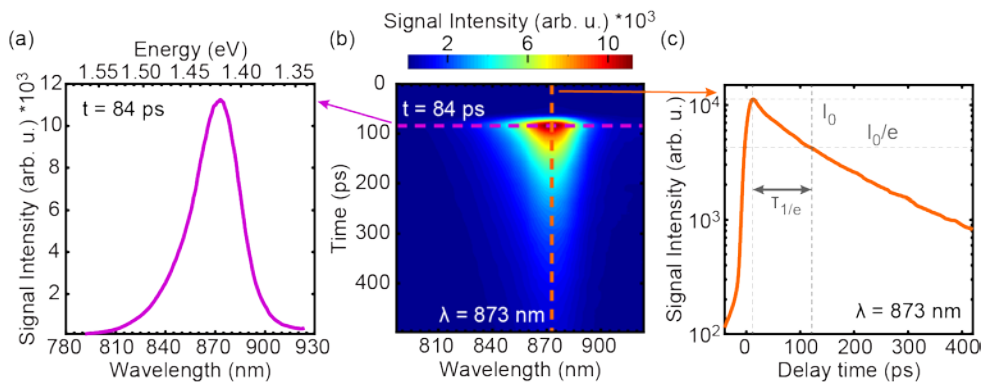


Figure 5.6. Example of a (b) streak image obtained by a TRPL setup with a streak camera, and linecuts that give (a) spectrum at a certain delay time, and (c) signal decay for a specific wavelength. The example shown is a measurement on a GaAs nanowire array capped with an AlInP shell, where 400 nm excitation wavelength was used.

In Paper II, we have also suggested that TRPL data could be used for estimating background carrier concentration in the nanowires. The method assumes that the luminescence is given by the regular bulk-like expression, that all the photons in the pulse are absorbed in the nanowires, and that the distribution of the photogenerated carriers is homogeneous in the volume of the nanowires. The main concept of the method is to use the peak counts just after the pulse and plot them as a function of excitation power (see Paper II for more details and examples). Fitting the power dependence with the bulk-like expression for luminescence intensity should allow extraction of the background carrier concentration as long as the excitation power has been swept over a range including the cross-over between the low and high injection regimes. For completeness, we note that there are various other techniques for doping evaluation, with both optical and electrical methods available [198-200]. Promising properties of our proposed TRPL method are: (i) it is a non-destructive method that can be applied on as-grown nanowire arrays; (ii) there is no need for additional measurement setups or complicated fits; (iii) it can be performed for arrays with complicated carrier dynamics; (iv) it should work for both low and high carrier concentrations. However, as the method has been introduced only tentatively, further experiments to compare this optical method to already established methods of known accuracy should be carried out to confirm the validity of the method.

5.4 Absorption, transmission and reflection

When light hits a large-area sample, the light can be reflected, absorbed or transmitted. The fraction of incident light reflected, absorbed and transmitted is then called reflectance (R), absorptance (A), and transmittance (T), respectively. In principle, transmitted and reflected light can be measured by simply placing a detector after the sample, or at a specular reflection angle respectively. However, such a measurement would only collect light arriving from a specified cone of angles, thus giving inaccurate values if the sample scatters light significantly beyond these angles. In order to capture full characteristics of how light interacts with the sample, an integrating sphere can be used.

An integrating sphere is a hollow spherical cavity with its interior covered with a diffuse reflective coating, with some holes for entrance and exit ports that, if not used, can usually be closed with plugs containing the same diffusive coating (Figure 5.7). Light incident on any point on the inner surface of the sphere is

diffusively scattered in all directions such that all light is homogeneously distributed on the surface of the sphere. Hence, a fiber-coupled detector, attached to the integrating sphere through one of the openings, measures this homogeneous intensity. The special benefit of the integrating sphere is collection of most of the light to the sphere independent of angular distribution of scattering. This advantage was used in Paper III to measure absorptance, transmittance and reflectance spectra of nanowire array samples (for an example, see Figure 5.8).

To measure transmittance, only one opening of the sphere is used and the sample is placed outside the integrating sphere so that it fully covers that opening. First, detector counts are measured with light passing through the sample ($C_{\text{sample},T}(\lambda)$, Figure 5.7a). Then, for calibration, the sample is removed and reference counts are measured, which are essentially proportional to the total incident light on the sample ($C_{\text{ref},T}(\lambda)$, Figure 5.7b). Additionally, the counts when light is switched off are measured ($C_{\text{dark}}(\lambda)$) in order to account for detector dark current. Transmittance is then calculated by:

$$T(\lambda) = \frac{C_{\text{sample},T}(\lambda) - C_{\text{dark}}(\lambda)}{C_{\text{ref},T}(\lambda) - C_{\text{dark}}(\lambda)}. \quad (5.3)$$

To measure reflectance, two of the openings are used. The sample is placed outside one of them, covering it fully, while the other opening is used to shine the light onto the sample at a small angle, so that specularly reflected light does not come straight back. In this case, the counts when light is reflected by the sample ($C_{\text{sample},R}(\lambda)$, Figure 5.7c) are measured first. Here, the calibration and normalization is performed by using a reference sample of known reflectance. Usually, this reference is some bulk substrate where literature parameters can be used in order to calculate reflectance spectrum $R_{\text{ref}}(\lambda)$. Hence, the same measurement is performed for the reference sample reflectance counts ($C_{\text{ref},R}(\lambda)$, Figure 5.7d). Finally, background calibration is done by removing the sample and letting the light pass straight through both openings. The background counts ($C_{\text{bg},R}(\lambda) = C_{\text{stray},R}(\lambda) + C_{\text{dark}}(\lambda)$, Figure 5.7e) then take into account both the stray light, which hits the wall of the sphere, as well as the detector dark current. Reflectance of the sample of interest is then given by:

$$R(\lambda) = R_{\text{ref}}(\lambda) \frac{C_{\text{sample},R}(\lambda) - C_{\text{bg},R}(\lambda)}{C_{\text{ref},R}(\lambda) - C_{\text{bg},R}(\lambda)}. \quad (5.4)$$

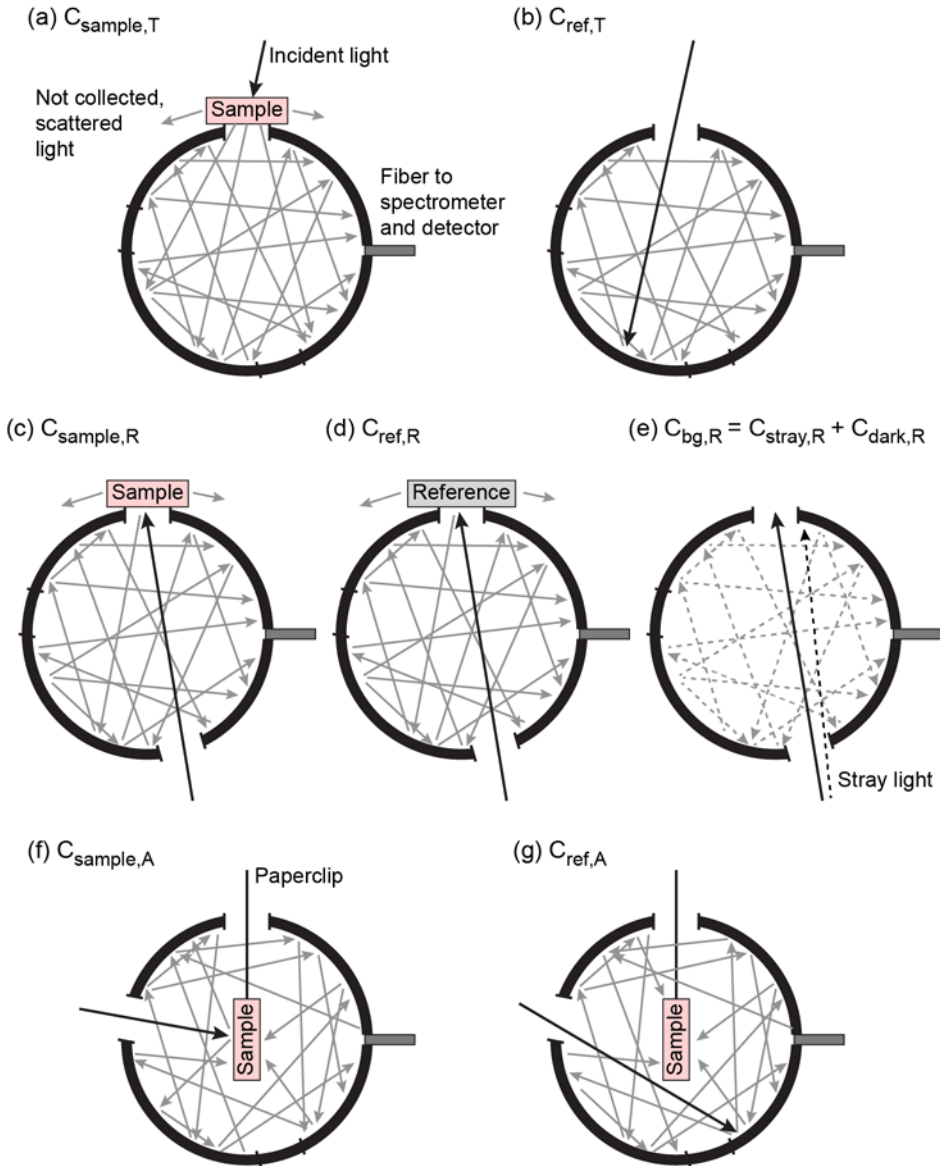


Figure 5.7. Schematic of an integrating sphere illustrating different measurement configurations and definitions of measured counts in each case. The first row illustrates measurement configurations for (a) transmittance through a sample and (b) the reference measurement. The second row illustrates measurement configurations for (c) reflectance from a sample, (d) the reflectance from a reference sample with known reflectance value, and (e) background measurement for reflectance which includes contribution from stray light and dark counts. The third row shows measurement configurations for (f) absorbance in a sample inserted inside the integrating sphere, and (g) reference measurement for absorbance.

In an ideal case, absorptance is given by $A(\lambda) = 1 - R(\lambda) - T(\lambda)$. However, as we illustrate in Figure 5.7, some light in the reflectance and transmittance measurements can be lost due to scattering in the sample, in which case R and T values are underestimated, and if the $A = 1 - R - T$ equation is used, absorptance would be overestimated. Instead, as shown in Figure 5.7f, g, we have modified the measurement configuration in order to measure absorptance directly [Paper III]. We have glued the sample to a paperclip and inserted it into the integrating sphere. In this case, all the scattered light is expected to be detected.

Thus, absorptance counts ($C_{\text{sample},A}(\lambda)$, Figure 5.7f) are measured with the light incident to the sample inside the sphere at a small angle so that specularly reflected light is not lost. Then, the direction of the incidence light is changed such that it does not hit the sample but passes by it and hits the wall of the sphere. Such measurement gives us reference counts essentially equivalent to the incident light intensity ($C_{\text{ref},A}(\lambda)$, Figure 5.7g). Finally, as for transmittance, the dark counts ($C_{\text{dark}}(\lambda)$) are measured with light switched off. Absorptance is then given by:

$$A(\lambda) = 1 - \frac{C_{\text{sample},A}(\lambda) - C_{\text{dark}}(\lambda)}{C_{\text{ref},A}(\lambda) - C_{\text{dark}}(\lambda)}. \quad (5.5)$$

Note that, in these measurements, we assume a homogeneous intensity distribution on the side walls of the integrating sphere as by the common definition of a well-functioning integrating sphere. However, when a sample is inserted inside the integrating sphere for absorptance measurements, the propagation of the diffusively scattered light can be affected. Hence, control measurements should be carried out, for example, on bulk substrates of varying size, in order to establish the size of the sample up to which the measured absorptance is independent of sample size for that specific integrating sphere [Paper III].

An example of transmittance, reflectance and absorptance spectra obtained by measurements performed in an integrating sphere and using Eqs. (5.3-5.5) is shown in Figure 5.8. The spectra are obtained from a GaInP nanowire array before removal of the Au particles, as studied in Paper III, where we have investigated how the presence or lack of Au particles affect the optical response of the nanowire array with respect to their absorption, transmission and reflection.

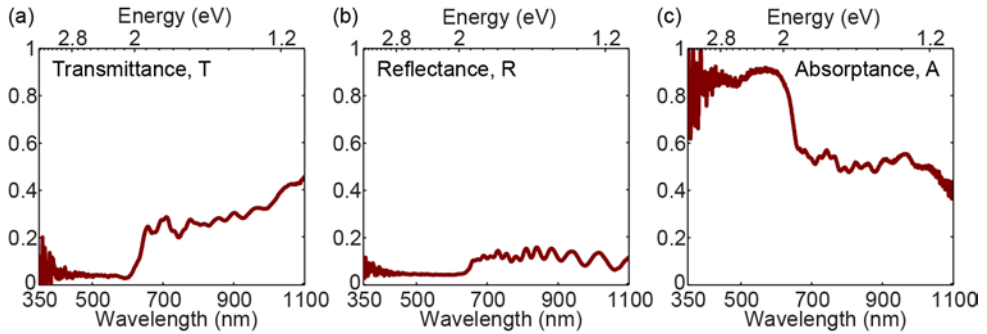


Figure 5.8. Example results obtained from the measurements performed in an integrating sphere using equations provided in the text for: (a) transmittance, (b) reflectance, and (c) absorbance spectra. The spectra are from GaInP nanowire array with Au particles, as studied in Paper III.

5.5 In-situ optical reflectometry

As we have discussed throughout this thesis, optical properties and performance of the nanowire array devices are expected to heavily depend on the size of the structures. It is thus important to be able to control and probe nanowire dimensions. We have seen already that pitch and to some extent diameter control can be obtained by NIL process, whereas array geometry can be measured by SEM. However, an in-situ probe significantly enhances the capability of optimizing and controlling nanowire dimensions, as well as aids in creating complex heterostructures.

Optical reflectometry is commonly used in the analysis of thin films to determine both the refractive index and the thickness of thin-film layers from interference fringes in reflectance spectrum [201], [202]. However, due to different light interaction with the nanowire array as compared to bulk, analysis schemes used for thin-films cannot be applied directly to nanowire systems. Only recently, Heurlin et al. [203] introduced in-situ characterization of nanowire dimensions and growth dynamics by optical reflectance, which we have used during the growth of every sample in this thesis. The main principle behind the method is the reflection of light at the nanowire/air and the nanowire/substrate interfaces (see Figure 5.9a) leading to interference effects. The method is in principle similar to the thin-film technique and uses the same equipment. However, unlike in bulk, where refractive indices of materials are known, nanowire refractive index is complicated, depicting the complex interaction with light. This refractive index can thus be estimated experimentally by calibration runs. Such in-situ method can be used to

determine both nanowire length and diameter [203], although we have only used in-situ length and growth rate determination in this thesis.

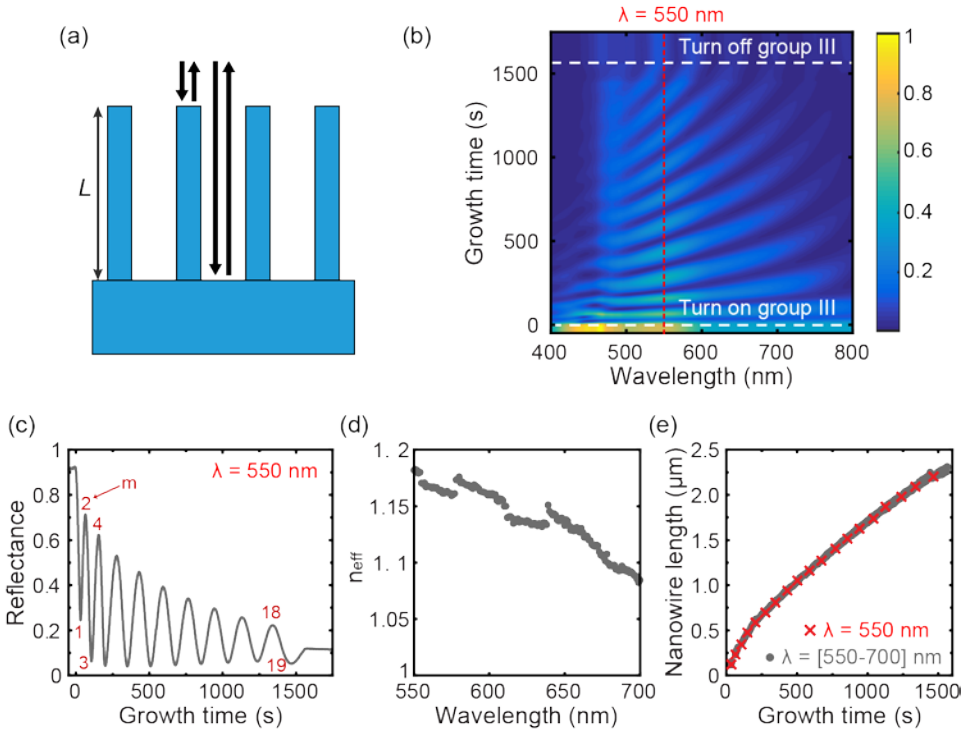


Figure 5.9. Description of an in-situ optical reflectometry technique. (a) Sketch of the nanowire array and light reflecting at the top and bottom surfaces of the array. (b) Example of time-dependent reflectance spectrum obtained during growth of *p-i-n* GaInP nanowires with an InP stub in the beginning and a GaP segment at the top (the same sample as the front cover image). (c) A linecut at $\lambda = 550$ nm (indicated by the red dashed line in figure (b)) showing reflectance oscillations with growth time. The numbers indicate extrema orders m as used in Eq. (5.6). (d) Effective refractive index obtained by averaging over 3 samples with 500 nm pitch and around 180 nm diameters. (e) Nanowire length as a function of time as extracted by applying Eq. (5.6) to figure (b). Red crosses indicate lengths extracted by using only $\lambda = 550$ nm as in figure (c), whereas grey dots indicate lengths extracted from 550-700 nm wavelength range.

The setup used in this thesis consists of a LayTec EpiR DA UV optical reflectometry system in the 400-800 nm wavelength range installed inside the MOVPE reactor, with the light incident and collected perpendicular to the substrate through a H_2 purged optical window (see schematics in Figure 3.1). The light reflected between the top and bottom surfaces of the nanowire array (Figure 5.9a) interfere and an interference pattern is obtained during growth (Figure 5.9b). Constructive interference occurs when the optical path difference (given by

$2Ln_{\text{eff}}$ where L is the nanowire length and n_{eff} is the effective refractive index of the array) is equal to an integer multiple of wavelength, whereas destructive interference occurs halfway between. Thus, the length can be calculated from the extrema points:

$$m \frac{\lambda}{2} = 2Ln_{\text{eff}} \Rightarrow L = \frac{m\lambda}{4n_{\text{eff}}}, \quad (5.6)$$

where λ is the wavelength of incident light and m is an integer where every odd integer ($m=1,3,5,\dots$) gives a minimum in the reflectance signal, and every even integer ($m=2,4,6,\dots$) gives a maximum in the reflectance signal, as indicated in Figure 5.9c for $\lambda = 550$ nm.

In order to calculate the length, however, we need to know the effective refractive index, which, as we previously said, cannot be taken as an effective medium refractive index. Instead, the effective refractive index is obtained experimentally by performing calibration runs where first reflectance spectra are measured for several different samples during growth, and then those samples are measured by SEM. Eq. (5.6) can then be applied in reverse to obtain a wavelength dependent refractive index (Figure 5.9d). After establishing the effective refractive index, reflectance spectra can be converted into nanowire length during growth (Figure 5.9e). If a broadband light source is used, multiple wavelengths can be used to obtain a higher temporal resolution (e.g., crosses in Figure 5.9e show data extracted from the extrema of 550 nm wavelength, whereas the grey points are from the 550-700 nm wavelength range), allowing real time tracking of the growth rate as well as the length. Note that since light interaction is affected by the array geometry, especially by the change of pitch, the procedure of calibrating the effective refractive index should be repeated in order to check the validity of the method whenever significant change is introduced in the grown samples.

6 Overview of results and outlook

As we have seen throughout this thesis, nanowire benefits originate solely from their low dimensions and spatial arrangement (e.g., a periodic array). Nanowires thus create a platform for devices very similar to the bulk semiconductor industry, but at the same time also very different. Although seemingly a small change, such low dimensions can result in different physics as well as different available techniques, where new challenges need to be considered for synthesis, characterization methods, and fundamental understanding of nanowire array behavior. Due to the similarity of the two platforms combined with various proposed nanowire platform benefits, a lot of research on nanowires focuses on adapting bulk devices into nanowires and understanding the benefits of this new platform for the specific applications. In this thesis, we have developed nanowire growth and investigated nanowire array optics of nominally intrinsic nanowires with solar cells in mind as our motivation and intended application. This thesis contributes to the knowledge of nanowire array synthesis and optics as well as to solar cell development through three main topics: (i) growth of ternary nanowire arrays (Section 6.1), (ii) non-destructive characterization of as-grown arrays (Section 6.2), and (iii) understanding optics of nanowire arrays embedded in a membrane (Section 6.3). The findings related to these topics as well as their relevance for solar cells are summarized in the coming sections. Note that although we chose to motivate and present our results, summarized in this chapter, in terms of solar cell perspective, the findings contribute to understanding of light interaction with nanostructures in general and could be applicable to other devices, as, for example, light emitting diodes and photodetectors.

6.1 Growth of ternary materials

Multi-junction structures are the most common pathway for achieving higher efficiency solar cells, which requires higher band-gap cells to be stacked at the top. Such higher band-gap cells are typically made from ternary materials, like $\text{Ga}_x\text{In}_{1-x}\text{P}$, in order to optimize the cell performance. As seen in this thesis, VLS growth of nanowires is a complex process on its own, and introduction of a third

precursor for ternary material growth makes it even more challenging, which results in lack of available information for controlling growth of ternary nanowires.

So far, most of the reported $\text{Ga}_x\text{In}_{1-x}\text{P}$ nanowire syntheses have been performed by using trimethylgallium (TMGa) as the Ga precursor [168,204-206]. However, during growth optimization, we have encountered ultra-long nanowires (several times longer than the majority of the nanowires in the sample), which would be detrimental for solar cell samples as the ultra-long nanowires could short-circuit the whole cell. We have identified that the presence of such ultra-long nanowires increases with increased Ga content in the nanowires, increased diethylzinc (DEZn, *p*-type dopant) content (note, however, that DEZn also leads to Ga-enrichment), and presence of SiN_x mask. From TEM investigations, the ultra-long nanowires contain many inclined twins. However, more in-depth understanding of the cause of this phenomenon is needed in order to gain control over it. As an alternative approach, we have investigated a different Ga precursor, triethylgallium (TEGa), in Paper I, where no ultra-long nanowires have been observed for nominally intrinsic samples, independent of Ga composition in the nanowires.

In addition to improved homogeneity by getting rid of the ultra-long nanowires, TEGa precursor is expected to be beneficial due to its lower pyrolysis temperature as compared to TMGa, which, at our low growth temperatures, results in a more efficient use of growth precursors since TEGa is expected to be fully pyrolysed, which is not the case for TMGa. In Paper I, we demonstrated that using TEGa as Ga precursor resulted in 5 times reduction in Ga precursor consumption as compared to TMGa grown nanowires in the same system with the same growth rate, material composition and other growth parameters. The versatility of TEGa is shown by synthesis of high homogeneity GaInP nanowire arrays, with a materials composition tunable by the group III input flows. Despite the complicated growth chemistry, discussed in the paper, growth series for every growth parameter provide a map between the growth parameters and achievable materials for everybody working with GaInP devices of similar geometry.

6.2 Characterization of as-grown arrays

After nanowires are grown, their properties need to be investigated to evaluate how various growth parameters influence fundamental properties of the nanowires

that then affect solar cell performance. Ideally, such measurements would be non-destructive and done on as-grown samples in order to allow faster feedback and further device processing. Photoluminescence is one of the main techniques for semiconductor materials characterization since it can give information about materials quality and doping concentration.

Measurements on the native substrate, however, cause issues as substrate and nanowire signals can overlap during photoluminescence measurements. In Paper II, we have evaluated TRPL characterization of dense periodic as-grown GaAs nanowire arrays. The nanowires were passivated with aluminum gallium arsenide (AlGaAs) shells of varied thickness and composition, with array dimensions designed for efficient light absorption and with relevance for PV. There, we showed that different nanowire array and substrate spectral behaviors with delay time in TRPL measurements can be used to determine which part of the sample dominates the detected spectrum. Additionally, as discussed in Section 5.3.2, we have tentatively proposed a method for extracting background doping from as-grown nanowire arrays by using excitation power dependence of the peak TRPL signal [Paper II]. However, the method still needs to be validated by comparing it to the already established methods. If validated, the method could provide a fast, non-destructive way to characterize doping level for both low and high carrier concentration values by a simple linear fit to the power dependent data.

We note that although all the samples in this study were nominally intrinsic, the measurements are still relevant for PV development as investigated aspects of TRPL should be applicable to measurements on *p-i-n* structures. We believe that modeling and measurements of *p-i-n* nanowire arrays will be an important step to in-depth nanowire solar cell characterization.

6.3 Optics of nanowire membrane

Another way to investigate nanowire array properties would be to look at the reflection, transmission and absorption of light in the arrays, as discussed in Section 5.4. However, these measurements are more suitable for arrays without the substrate underneath, which is achieved by embedding the nanowires into a polymer and peeling them off the substrate to obtain a flexible nanowire membrane sample. Such samples could be of interest on their own for flexible devices. However, it is also one of the pathways to create tandem solar cells

integrated with bulk Si solar cells [126]. This way of creating multi-junction solar cells, in comparison to the multi-junction approach within the nanowire, has an advantage of less complex design of the cell, which could be compatible with the established Si planar solar cell technology, and possibly with the uprising low cost aerotaxy growth method for the nanowire solar cells. Such a system, however, requires understanding and control of light interaction, especially to make sure that the low energy photons are transmitted efficiently to the bottom cell.

We have thus investigated reflection, transmission and absorption of light in nanowire arrays embedded in a polymer and relevant for tandem solar cell applications experimentally in Paper III and theoretically in Paper IV. Experimentally, we have identified two mechanisms that could be detrimental for the performance of the tandem cell [Paper III]. First, the Au particles used in the nanowire synthesis can absorb $> 50\%$ of the low-energy photons, leading to a $< 40\%$ transmittance, even though the Au particles cover $< 15\%$ of the surface area. The removal of the Au particles can recover transmission of the low energy photons to $> 80\%$. Second, after the removal of the Au particles, a 40% reflectance peak shows up due to resonant back-scattering of light from the in-plane waveguiding modes. We believe that such effect has not been observed before, because first, for nanowires on the substrate such modes should leak into the substrate and second, previously studied materials had such band-gap that the reflection resonance wavelength fell into the absorbing region, which limits the possibility to resonantly excite the in-plane waveguide modes.

The origin and control of such resonances was investigated theoretically in Paper IV, where we found that the optical response is rather complicated with strong and possibly resonant dependence on nanowire length and diameter, array pitch, materials surrounding the nanowires, and absorption coefficient of nanowire material. This is in contrast to the peak wavelengths of the absorption resonances in single vertical nanowires that typically depend mostly just on the nanowire diameter. In Paper IV, we have defined simple boundaries for the wavelength range of resonant response, where resonances can occur only if there is more than 1 propagating mode in the array, and they disappear if the 1st diffracted order is propagating in the top or bottom material. When nanowires are on a high refractive index substrate, the 1st diffracted order in the substrate tends to be propagating for all the wavelengths where more than 1 propagating mode in the array is available, thus suppressing the excitation of the resonances.

Since such resonant reflection effects can be detrimental for tandem solar cell applications, we need to consider how to avoid them. Paper IV considers some

common approaches for solar cell design, where we show that if a spacer is introduced between the nanowire array and bulk Si cells, as could be done in the 4-terminal approach, the resonances are an issue as the decay length of the diffracted orders is on the order of a hundred nanometers and thus they cannot reach the substrate, into which they could otherwise leak to suppress the resonances. In order to avoid this issue, several different directions can be suggested: (i) a thin transparent contact without a spacer layer between the two cells, (ii) an Esaki diode joining the nanowire and bulk cells, (iii) both top and bottom cells defined in a nanowire, (iv) reduced pitch and diameter in order to push the resonances into the absorbing regime of the top cell. Furthermore, introducing randomness in the array, for example, by moving from a perfect square or hexagonal array to one with randomly positioned nanowires, could be another direction for future investigations.

All in all, the included papers should contribute towards better understanding of nanowire array synthesis and optical properties as well as their characterization. In particular, ternary growth and design considerations for nanowire array membranes discussed in this thesis should be considered for development of tandem solar cells, whereas characterization of as-grown arrays could play a role in aiding material optimization along the way.

References

- [1] Green M A, Hishikawa Y, Dunlop E D, Levi D H, Hohl-Ebinger J and Ho-Baillie A W Y, *Solar cell efficiency tables (version 52)*, Progress in Photovoltaics: Research and Applications **26**, 427 (2018)
- [2] Fraunhofer ISE, *Photovoltaics report* (updated: 19 June 2018)
<https://www.ise.fraunhofer.de/content/dam/ise/de/documents/publications/studies/Potovoltatics-Report.pdf>
- [3] Wagner R S, Ellis W C, Jackson K A and Arnold S M, *Study of the filamentary growth of silicon crystals from the vapor*, Journal of Applied Physics **35**, 2993 (1964)
- [4] Wagner R S and Ellis W C, *Vapor-liquid-solid mechanism of single crystal growth*, Applied Physics Letters **4**, 89 (1964)
- [5] Wagner R S and Doherty C J, *Mechanism of branching and kinking during VLS crystal growth*, Journal of the Electrochemical Society **115**, 93 (1968)
- [6] Givargizov E I, *Periodic instability in whisker growth*, Journal of Crystal Growth **20**, 217 (1973)
- [7] Givargizov E I, *Fundamental aspects of VLS growth*, Journal of Crystal Growth **31**, 20 (1975)
- [8] Haraguchi K, Katsuyama T, Hiruma K and Ogawa K, *GaAs p-n junction formed in quantum wire crystals*, Applied Physics Letters **60**, 745 (1992)
- [9] Gudiksen M S and Lieber C M, *Diameter-selective synthesis of semiconductor nanowires*, Journal of the American Chemical Society **122**, 8801 (2000)
- [10] Holmes J D, Johnston K P, Doty R C and Korgel B A, *Control of thickness and orientation of solution-grown silicon nanowires*, Science **287**, 1471 (2000)
- [11] Cui Y, Lauhon L J, Gudiksen M S, Wang J and Lieber C M, *Diameter-controlled synthesis of single-crystal silicon nanowires*, Applied Physics Letters **78**, 2214 (2001)
- [12] Gudiksen M S, Wang J and Lieber C M, *Synthetic control of the diameter and length of single crystal semiconductor nanowires*, The Journal of Physical Chemistry B **105**, 4062 (2001)
- [13] Ohlsson B J, Björk M T, Magnusson M H, Deppert K, Samuelson L and Wallenberg L R, *Size-, shape-, and position-controlled GaAs nano-whiskers*, Applied Physics Letters **79**, 3335 (2001)
- [14] Hiruma K, Murakoshi H, Yazawa M and Katsuyama T, *Self-organized growth of GaAs/InAs heterostructure nanocylinders by organometallic vapor phase epitaxy*, Journal of Crystal Growth **163**, 226 (1996)

- [15] Wu Y, Fan R and Yang P, *Block-by-block growth of single-crystalline Si/SiGe superlattice nanowires*, Nano letters **2**, 83 (2002)
- [16] Björk M T, Ohlsson B J, Sass T, Persson A I, Thelander C, Magnusson M H, Deppert K, Wallenberg L R and Samuelson L, *One-dimensional steeplechase for electrons realized*, Nano letters **2**, 87 (2002)
- [17] Gudiksen M S, Lauhon L J, Wang J, Smith D C and Lieber C M, *Growth of nanowire superlattice structures for nanoscale photonics and electronics*, Nature **415**, 617 (2002)
- [18] Cui Y, Zhong Z, Wang D, Wang W U and Lieber C M, *High performance silicon nanowire field effect transistors*, Nano letters **3**, 149 (2003)
- [19] Tomioka K, Yoshimura M and Fukui T, *A III-V nanowire channel on silicon for high-performance vertical transistors*, Nature **488**, 189 (2012)
- [20] Cui Y, Wei Q, Park H and Lieber C M, *Nanowire nanosensors for highly sensitive and selective detection of biological and chemical species*, Science **293**, 1289 (2001)
- [21] Hahn J-i and Lieber C M, *Direct ultrasensitive electrical detection of DNA and DNA sequence variations using nanowire nanosensors*, Nano letters **4**, 51 (2004)
- [22] IEA, *Key world energy statistics* (2017)
- [23] Crabtree G W, Lewis N S, Hafemeister D, Levi B, Levine M and Schwartz P, *Solar energy conversion*, in AIP Conference Proceedings (AIP, 2008), pp. 309
- [24] IEA PVPS, *Snapshot of global PV markets 2017* (2018)
- [25] Ginley D, Green M A and Collins R, *Solar energy conversion toward 1 terawatt*, MRS Bulletin **33**, 355 (2008)
- [26] Shockley W and Queisser H J, *Detailed balance limit of efficiency of p-n junction solar cells*, Journal of Applied Physics **32**, 510 (1961)
- [27] Garnett E C, Brongersma M L, Cui Y and McGehee M D, *Nanowire solar cells*, Annual Review of Materials Research **41**, 269 (2011)
- [28] Kempa T J, Day R W, Kim S-K, Park H-G and Lieber C M, *Semiconductor nanowires: A platform for exploring limits and concepts for nano-enabled solar cells*, Energy & Environmental Science **6**, 719 (2013)
- [29] Cao L, Fan P, Vasudev A P, White J S, Yu Z, Cai W, Schuller J A, Fan S and Brongersma M L, *Semiconductor nanowire optical antenna solar absorbers*, Nano letters **10**, 439 (2010)
- [30] Beard M C, Luther J M and Nozik A J, *The promise and challenge of nanostructured solar cells*, Nature Nanotechnology **9**, 951 (2014)
- [31] Otnes G and Borgström M T, *Towards high efficiency nanowire solar cells*, Nano Today **12**, 31 (2017)
- [32] Anttu N, Abrand A, Asoli D, Heurlin M, Åberg I, Samuelson L and Borgström M, *Absorption of light in InP nanowire arrays*, Nano Research **7**, 816 (2014)
- [33] Kupec J, Stoop R L and Witzigmann B, *Light absorption and emission in nanowire array solar cells*, Optics Express **18**, 27589 (2010)

- [34] Hu L and Chen G, *Analysis of optical absorption in silicon nanowire arrays for photovoltaic applications*, Nano letters **7**, 3249 (2007)
- [35] Hu S, Chi C-Y, Fountaine K T, Yao M, Atwater H A, Dapkus P D, Lewis N S and Zhou C, *Optical, electrical, and solar energy-conversion properties of gallium arsenide nanowire-array photoanodes*, Energy & Environmental Science **6**, 1879 (2013)
- [36] Anttu N and Xu H Q, *Coupling of light into nanowire arrays and subsequent absorption*, Journal of Nanoscience and Nanotechnology **10**, 7183 (2010)
- [37] Kim S-K, Day R W, Cahoon J F, Kempa T J, Song K-D, Park H-G and Lieber C M, *Tuning light absorption in core/shell silicon nanowire photovoltaic devices through morphological design*, Nano letters **12**, 4971 (2012)
- [38] Kästner G and Gösele U, *Stress and dislocations at cross-sectional heterojunctions in a cylindrical nanowire*, Philosophical Magazine **84**, 3803 (2004)
- [39] Anttu N, *Geometrical optics, electrostatics, and nanophotonic resonances in absorbing nanowire arrays*, Optics letters **38**, 730 (2013)
- [40] Wallentin J, Anttu N, Asoli D, Huffman M, Åberg I, Magnusson M H, Siefer G, Fuss-Kailuweit P, Dimroth F, Witzigmann B, Xu H Q, Samuelson L, Deppert K and Borgström M T, *InP nanowire array solar cells achieving 13.8% efficiency by exceeding the ray optics limit*, Science **339**, 1057 (2013)
- [41] Åberg I, Vescovi G, Asoli D, Naseem U, Gilboy J P, Sundvall C, Dahlgren A, Svensson K E, Anttu N, Björk M T and Samuelson L, *A GaAs nanowire array solar cell with 15.3% efficiency at 1 sun*, IEEE Journal of Photovoltaics **6**, 185 (2016)
- [42] Yao M, Huang N, Cong S, Chi C-Y, Seyedi M A, Lin Y-T, Cao Y, Povinelli M L, Dapkus P D and Zhou C, *GaAs nanowire array solar cells with axial p-i-n junctions*, Nano letters **14**, 3293 (2014)
- [43] Mariani G, Scofield A C, Hung C-H and Huffaker D L, *GaAs nanopillar-array solar cells employing in situ surface passivation*, Nature communications **4**, 1497 (2013)
- [44] Cui Y, Wang J, Plissard S R, Cavalli A, Vu T T T, van Veldhoven R P J, Gao L, Trainor M, Verheijen M A, Haverkort J E M and Bakkers E P A M, *Efficiency enhancement of InP nanowire solar cells by surface cleaning*, Nano letters **13**, 4113 (2013)
- [45] Cui Y, van Dam D, Mann S A, van Hoof N J J, van Veldhoven P J, Garnett E C, Bakkers E P A M and Haverkort J E M, *Boosting solar cell photovoltage via nanophotonic engineering*, Nano letters **16**, 6467 (2016)
- [46] Boulanger J P, Chia A C E, Wood B, Yazdi S, Kasama T, Aagesen M and LaPierre R R, *Characterization of a Ga-assisted GaAs nanowire array solar cell on Si substrate*, IEEE Journal of Photovoltaics **6**, 661 (2016)
- [47] Nakai E, Chen M, Yoshimura M, Tomioka K and Fukui T, *InGaAs axial-junction nanowire-array solar cells*, Japanese Journal of Applied Physics **54**, 015201 (2014)
- [48] Nakai E, Yoshimura M, Tomioka K and Fukui T, *GaAs/InGaP core-multishell nanowire-array-based solar cells*, Japanese Journal of Applied Physics **52**, 055002 (2013)

- [49] van Dam D, van Hoof N J J, Cui Y, van Veldhoven P J, Bakkers E P A M, Gómez-Rivas J and Haverkort J E M, *High-efficiency nanowire solar cells with omnidirectionally enhanced absorption due to self-aligned Indium–Tin–Oxide Mie scatterers*, ACS Nano **10**, 11414 (2016)
- [50] Otnes G, Barrigón E, Sundvall C, Svensson K E, Heurlin M, Siefer G, Samuelson L, Åberg I and Borgström M T, *Understanding InP nanowire array solar cell performance by nanoprobe-enabled single nanowire measurements*, Nano letters **18**, 3038 (2018)
- [51] Czaban J A, Thompson D A and LaPierre R R, *GaAs core–shell nanowires for photovoltaic applications*, Nano letters **9**, 148 (2008)
- [52] Joyce H J, Docherty C J, Gao Q, Tan H H, Jagadish C, Lloyd-Hughes J, Herz L M and Johnston M B, *Electronic properties of GaAs, InAs and InP nanowires studied by terahertz spectroscopy*, Nanotechnology **24**, 214006 (2013)
- [53] Yablonoitch E, Sandroff C J, Bhat R and Gmitter T, *Nearly ideal electronic properties of sulfide coated GaAs surfaces*, Applied Physics Letters **51**, 439 (1987)
- [54] Mauk M G, Xu S, Arent D J, Mertens R P and Borghs G, *Study of novel chemical surface passivation techniques on GaAs pn junction solar cells*, Applied Physics Letters **54**, 213 (1989)
- [55] Christesen J D, Zhang X, Pinion C W, Celano T A, Flynn C J and Cahoon J F, *Design principles for photovoltaic devices based on Si nanowires with axial or radial p–n junctions*, Nano letters **12**, 6024 (2012)
- [56] Ahtapodov L, Todorovic J, Olk P, Mjåland T, Slåttnes P, Dheeraj D L, van Helvoort A T J, Fimland B-O and Weman H, *A story told by a single nanowire: Optical properties of wurtzite GaAs*, Nano letters **12**, 6090 (2012)
- [57] Boland J L, Casadei A, Tütüncüoğlu G, Matteini F, Davies C L, Jabeen F, Joyce H J, Herz L M, Fontcuberta i Morral A and Johnston M B, *Increased photoconductivity lifetime in GaAs nanowires by controlled n-type and p-type doping*, ACS Nano **10**, 4219 (2016)
- [58] Demichel O, Heiss M, Bleuse J, Mariette H and Fontcuberta i Morral A, *Impact of surfaces on the optical properties of GaAs nanowires*, Applied Physics Letters **97**, 201907 (2010)
- [59] Jiang N, Parkinson P, Gao Q, Breuer S, Tan H H, Wong-Leung J and Jagadish C, *Long minority carrier lifetime in Au-catalyzed GaAs/Al_xGa_{1-x}As core-shell nanowires*, Applied Physics Letters **101**, 023111 (2012)
- [60] Perera S, Fickenscher M A, Jackson H E, Smith L M, Yarrison-Rice J M, Joyce H J, Gao Q, Tan H H, Jagadish C, Zhang X and Zou J, *Nearly intrinsic exciton lifetimes in single twin-free GaAs/AlGaAs core-shell nanowire heterostructures*, Applied Physics Letters **93**, 145302 (2008)
- [61] Titova L V, Hoang T B, Jackson H E, Smith L M, Yarrison-Rice J M, Kim Y, Joyce H J, Tan H H and Jagadish C, *Temperature dependence of photoluminescence from single core-shell GaAs–AlGaAs nanowires*, Applied Physics Letters **89**, 173126 (2006)
- [62] Jiang N, Gao Q, Parkinson P, Wong-Leung J, Mokkapati S, Breuer S, Tan H H, Zheng C L, Etheridge J and Jagadish C, *Enhanced minority carrier lifetimes in*

- GaAs/AlGaAs core-shell nanowires through shell growth optimization*, Nano letters **13**, 5135 (2013)
- [63] Chang C-C, Chi C-Y, Yao M, Huang N, Chen C-C, Theiss J, Bushmaker A W, LaLumondiere S, Yeh T-W, Povinelli M L and Zhou C, *Electrical and optical characterization of surface passivation in GaAs nanowires*, Nano letters **12**, 4484 (2012)
- [64] Chia A C E, Tirado M, Li Y, Zhao S, Mi Z, Comedi D and LaPierre R R, *Electrical transport and optical model of GaAs-AllnP core-shell nanowires*, Journal of Applied Physics **111**, 094319 (2012)
- [65] Chia A C E, Tirado M, Thouin F, Leonelli R, Comedi D and LaPierre R R, *Surface depletion and electrical transport model of AllnP-passivated GaAs nanowires*, Semiconductor science and technology **28**, 105026 (2013)
- [66] Sköld N, Karlsson L S, Larsson M W, Pistol M-E, Seifert W, Trägårdh J and Samuelson L, *Growth and optical properties of strained GaAs-Ga_xIn_{1-x}P core-shell nanowires*, Nano letters **5**, 1943 (2005)
- [67] Lin A, Shapiro J N, Senanayake P N, Scofield A C, Wong P-S, Liang B and Huffaker D L, *Extracting transport parameters in GaAs nanopillars grown by selective-area epitaxy*, Nanotechnology **23**, 105701 (2012)
- [68] Darbandi A and Watkins S P, *Measurement of minority carrier diffusion lengths in GaAs nanowires by a nanoprobe technique*, Journal of Applied Physics **120**, 014301 (2016)
- [69] Polman A and Atwater H A, *Photonic design principles for ultrahigh-efficiency photovoltaics*, Nature Materials **11**, 174 (2012)
- [70] Mårtensson T, Svensson C P T, Wacaser B A, Larsson M W, Seifert W, Deppert K, Gustafsson A, Wallenberg L R and Samuelson L, *Epitaxial III-V nanowires on silicon*, Nano letters **4**, 1987 (2004)
- [71] Dhaka V, Haggren T, Jussila H, Jiang H, Kauppinen E, Huhtio T, Sopanen M and Lipsanen H, *High quality GaAs nanowires grown on glass substrates*, Nano letters **12**, 1912 (2012)
- [72] Jafari Jam R, Heurlin M, Jain V, Kvennefors A, Graczyk M, Maximov I, Borgström M T, Pettersson H and Samuelson L, *III-V nanowire synthesis by use of electrodeposited gold particles*, Nano letters **15**, 134 (2014)
- [73] Spurgeon J M, Plass K E, Kayes B M, Brunschwigg B S, Atwater H A and Lewis N S, *Repeated epitaxial growth and transfer of arrays of patterned, vertically aligned, crystalline Si wires from a single Si (111) substrate*, Applied Physics Letters **93**, 032112 (2008)
- [74] Zeng X, *InP/GaInP nanowires for tandem junction solar cells: Growth, processing, and characterization*, PhD Thesis, Lund University (2018)
- [75] Deppert K, Bovin J-O, Malm J-O and Samuelson L, *A new method to fabricate size-selected compound semiconductor nanocrystals: Aerotaxy*, Journal of Crystal Growth **169**, 13 (1996)
- [76] Heurlin M, Magnusson M H, Lindgren D, Ek M, Wallenberg L R, Deppert K and Samuelson L, *Continuous gas-phase synthesis of nanowires with tunable properties*, Nature **492**, 90 (2012)

- [77] Otnes G, Heurlin M, Graczyk M, Wallentin J, Jacobsson D, Berg A, Maximov I and Borgström M T, *Strategies to obtain pattern fidelity in nanowire growth from large-area surfaces patterned using nanoimprint lithography*, Nano Research **9**, 2852 (2016)
- [78] Sze S M and Ng K K, *Physics of semiconductor devices* (John Wiley & Sons, 2006)
- [79] Yu P Y and Cardona M, *Fundamentals of semiconductors: Physics and materials properties* 4th edn. (Springer, 2010)
- [80] Klingshirn C F, *Semiconductor optics* 4th edn. (Springer, 2012)
- [81] Adachi S, *Optical properties of crystalline and amorphous semiconductors: Materials and fundamental principles* (Springer Science & Business Media, 2012)
- [82] Koguchi M, Kakibayashi H, Yazawa M, Hiruma K and Katsuyama T, *Crystal structure change of GaAs and InAs whiskers from zinc-blende to wurtzite type*, Japanese Journal of Applied Physics **31**, 2061 (1992)
- [83] Hiruma K, Yazawa M, Katsuyama T, Ogawa K, Haraguchi K, Koguchi M and Kakibayashi H, *Growth and optical properties of nanometer-scale GaAs and InAs whiskers*, Journal of Applied Physics **77**, 447 (1995)
- [84] Caroff P, Bolinsson J and Johansson J, *Crystal phases in III-V nanowires: From random toward engineered polytypism*, IEEE Journal of selected topics in quantum electronics **17**, 829 (2011)
- [85] Joyce H J, Wong-Leung J, Gao Q, Tan H H and Jagadish C, *Phase perfection in zinc blende and wurtzite III-V nanowires using basic growth parameters*, Nano letters **10**, 908 (2010)
- [86] Algra R E, Verheijen M A, Borgström M T, Feiner L-F, Immink G, van Enckevort W J P, Vlieg E and Bakkers E P A M, *Twinning superlattices in indium phosphide nanowires*, Nature **456**, 369 (2008)
- [87] Lehmann S, Wallentin J, Jacobsson D, Deppert K and Dick K A, *A general approach for sharp crystal phase switching in InAs, GaAs, InP, and GaP nanowires using only group V flow*, Nano letters **13**, 4099 (2013)
- [88] Joyce H J, Gao Q, Tan H H, Jagadish C, Kim Y, Zhang X, Guo Y and Zou J, *Twin-free uniform epitaxial GaAs nanowires grown by a two-temperature process*, Nano letters **7**, 921 (2007)
- [89] Joyce H J, Gao Q, Tan H H, Jagadish C, Kim Y, Fickenscher M A, Perera S, Hoang T B, Smith L M, Jackson H E and Yarrison-Rice J M, *Unexpected benefits of rapid growth rate for III-V nanowires*, Nano letters **9**, 695 (2008)
- [90] Akiyama T, Yamashita T, Nakamura K and Ito T, *Band alignment tuning in twin-plane superlattices of semiconductor nanowires*, Nano letters **10**, 4614 (2010)
- [91] Bao J, Bell D C, Capasso F, Wagner J B, Mårtensson T, Trägårdh J and Samuelson L, *Optical properties of rotationally twinned InP nanowire heterostructures*, Nano letters **8**, 836 (2008)
- [92] Mishra A, Titova L V, Hoang T B, Jackson H E, Smith L M, Yarrison-Rice J M, Kim Y, Joyce H J, Gao Q and Tan H H, *Polarization and temperature dependence*

- of photoluminescence from zincblende and wurtzite InP nanowires*, Applied Physics Letters **91**, 263104 (2007)
- [93] Pohl U W, *Epitaxy of semiconductors: Introduction to physical principles* (Springer, 2013)
- [94] Vurgaftman I, Meyer J R and Ram-Mohan L R, *Band parameters for III–V compound semiconductors and their alloys*, Journal of Applied Physics **89**, 5815 (2001)
- [95] Varshni Y P, *Temperature dependence of the energy gap in semiconductors*, Physica **34**, 149 (1967)
- [96] Smith L M, Jackson H E, Yarrison-Rice J M and Jagadish C, *Insights into single semiconductor nanowire heterostructures using time-resolved photoluminescence*, Semiconductor science and technology **25**, 024010 (2010)
- [97] Parkinson P, Lloyd-Hughes J, Gao Q, Tan H H, Jagadish C, Johnston M B and Herz L M, *Transient terahertz conductivity of GaAs nanowires*, Nano letters **7**, 2162 (2007)
- [98] Shockley W, *On the surface states associated with a periodic potential*, Physical Review **56**, 317 (1939)
- [99] Sun M H, Joyce H J, Gao Q, Tan H H, Jagadish C and Ning C Z, *Removal of surface states and recovery of band-edge emission in InAs nanowires through surface passivation*, Nano letters **12**, 3378 (2012)
- [100] Bessolov V N and Lebedev M V, *Chalcogenide passivation of III–V semiconductor surfaces*, Semiconductors **32**, 1141 (1998)
- [101] Tajik N, Peng Z, Kuyanov P and LaPierre R R, *Sulfur passivation and contact methods for GaAs nanowire solar cells*, Nanotechnology **22**, 225402 (2011)
- [102] Woo R L, Xiao R, Kobayashi Y, Gao L, Goel N, Hudait M K, Mallouk T E and Hicks R F, *Effect of twinning on the photoluminescence and photoelectrochemical properties of indium phosphide nanowires grown on silicon (111)*, Nano letters **8**, 4664 (2008)
- [103] Parkinson P, Joyce H J, Gao Q, Tan H H, Zhang X, Zou J, Jagadish C, Herz L M and Johnston M B, *Carrier lifetime and mobility enhancement in nearly defect-free core–shell nanowires measured using time-resolved terahertz spectroscopy*, Nano letters **9**, 3349 (2009)
- [104] Thelander C, Caroff P, Plissard S, Dey A W and Dick K A, *Effects of crystal phase mixing on the electrical properties of InAs nanowires*, Nano letters **11**, 2424 (2011)
- [105] Joyce H J, Wong-Leung J, Yong C-K, Docherty C J, Paiman S, Gao Q, Tan H H, Jagadish C, Lloyd-Hughes J, Herz L M and Johnston M B, *Ultralow surface recombination velocity in InP nanowires probed by terahertz spectroscopy*, Nano letters **12**, 5325 (2012)
- [106] Ahrenkiel R K, *Minority-carrier lifetime in III–V semiconductors*, Semiconductors and semimetals **39**, 39 (1993)
- [107] Ren D, Scofield A C, Farrell A C, Rong Z, Haddad M A, Laghumavarapu R B, Liang B and Huffaker D L, *Exploring time-resolved photoluminescence for*

- nanowires using a three-dimensional computational transient model*, *Nanoscale* **10**, 7792 (2018)
- [108] Pankove J I, *Optical processes in semiconductors* (New York, Dover Publications, Inc., 1971)
- [109] Kivisaari P, Oksanen J and Tulkki J, *Effects of lateral current injection in GaN multi-quantum well light-emitting diodes*, *Journal of Applied Physics* **111**, 103120 (2012)
- [110] Heikkilä O, Oksanen J and Tulkki J, *Ultimate limit and temperature dependency of light-emitting diode efficiency*, *Journal of Applied Physics* **105**, 093119 (2009)
- [111] Chen Y, Kivisaari P, Pistol M-E and Anttu N, *Optimization of the short-circuit current in an InP nanowire array solar cell through opto-electronic modeling*, *Nanotechnology* **27**, 435404 (2016)
- [112] Shockley W and Read Jr W T, *Statistics of the recombinations of holes and electrons*, *Physical Review* **87**, 835 (1952)
- [113] Hall R N, *Electron-hole recombination in germanium*, *Physical Review* **87**, 387 (1952)
- [114] Entner R, *Modeling and simulation of negative bias temperature instability*, PhD Thesis, Technical University Wien (2007)
- [115] Chen Y, Kivisaari P, Pistol M-E and Anttu N, *Optimized efficiency in InP nanowire solar cells with accurate 1D analysis*, *Nanotechnology* **29**, 045401 (2017)
- [116] Dan Y, Seo K, Takei K, Meza J H, Javey A and Crozier K B, *Dramatic reduction of surface recombination by in situ surface passivation of silicon nanowires*, *Nano letters* **11**, 2527 (2011)
- [117] Ahrenkiel R K, Keyes B M and Dunlavy D J, *Intensity-dependent minority-carrier lifetime in III-V semiconductors due to saturation of recombination centers*, *Journal of Applied Physics* **70**, 225 (1991)
- [118] Allen J E, Hemesath E R, Perea D E, Lensch-Falk J L, Li Z Y, Yin F, Gass M H, Wang P, Bleloch A L, Palmer R E and Lauhon L J, *High-resolution detection of Au catalyst atoms in Si nanowires*, *Nature Nanotechnology* **3**, 168 (2008)
- [119] van Weert M H M, Wunnicke O, Roest A L, Eijkemans T J, Yu Silov A, Haverkort J E M, 't Hooft G W and Bakkers E P A M, *Large redshift in photoluminescence of p-doped InP nanowires induced by Fermi-level pinning*, *Applied Physics Letters* **88**, 043109 (2006)
- [120] *Air mass 1.5 spectra (american society for testing and materials)*, <http://rredc.nrel.gov/solar/spectra/am1.5/>
- [121] Anttu N, Kivisaari P and Chen Y, *Effect of internal and external photon management on open-circuit voltage in solar cells*, submitted
- [122] Green M A, *Third generation photovoltaics: Ultra-high conversion efficiency at low cost*, *Progress in Photovoltaics: Research and Applications* **9**, 123 (2001)
- [123] Conibeer G, *Third-generation photovoltaics*, *Materials today* **10**, 42 (2007)
- [124] Esaki L, *New phenomenon in narrow germanium p-n junctions*, *Physical Review* **109**, 603 (1958)

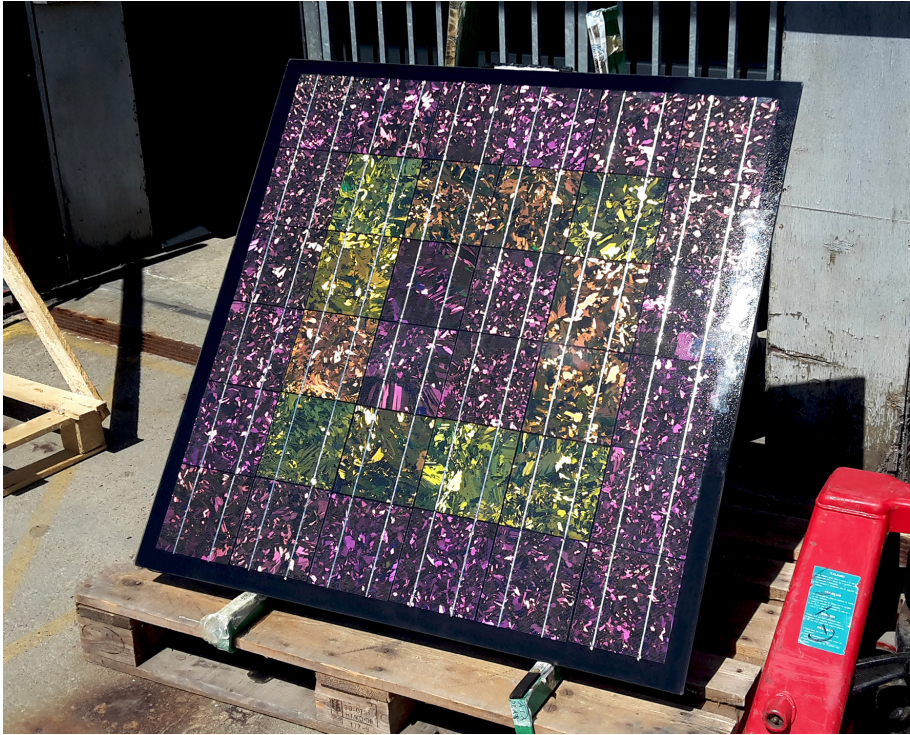
- [125] Zeng X, Otnes G, Heurlin M, Mourão R T and Borgström M T, *InP/GaInP nanowire tunnel diodes*, Nano Research **11**, 2523 (2018)
- [126] Borgström M T, Magnusson M H, Dimroth F, Siefer G, Höhn O, Riel H, Schmid H, Wirths S, Björk M and Åberg I, *Towards nanowire tandem junction solar cells on silicon*, IEEE Journal of Photovoltaics **8**, 733 (2018)
- [127] Hobbs R G, Petkov N and Holmes J D, *Semiconductor nanowire fabrication by bottom-up and top-down paradigms*, Chemistry of Materials **24**, 1975 (2012)
- [128] Lieber C M, *Nanoscale science and technology: Building a big future from small things*, MRS Bulletin **28**, 486 (2003)
- [129] Dick K A and Caroff P, *Metal-seeded growth of III–V semiconductor nanowires: Towards gold-free synthesis*, Nanoscale **6**, 3006 (2014)
- [130] Fontcuberta i Morral A, *Gold-free GaAs nanowire synthesis and optical properties*, IEEE Journal of selected topics in quantum electronics **17**, 819 (2011)
- [131] Colombo C, Spirkoska D, Frimmer M, Abstreiter G and Fontcuberta i Morral A, *Ga-assisted catalyst-free growth mechanism of GaAs nanowires by molecular beam epitaxy*, Physical Review B **77**, 155326 (2008)
- [132] Plissard S, Dick K A, Larrieu G, Godey S, Addad A, Wallart X and Caroff P, *Gold-free growth of GaAs nanowires on silicon: Arrays and polytypism*, Nanotechnology **21**, 385602 (2010)
- [133] Goto H, Nosaki K, Tomioka K, Hara S, Hiruma K, Motohisa J and Fukui T, *Growth of core–shell InP nanowires for photovoltaic application by selective-area metal organic vapor phase epitaxy*, Applied Physics Express **2**, 035004 (2009)
- [134] Inari M, Takeda J, Motohisa J and Fukui T, *Selective area MOVPE growth of InP and InGaAs pillar structures for InP-based two-dimensional photonic crystals*, Physica E: Low-dimensional Systems and Nanostructures **21**, 620 (2004)
- [135] Tomioka K, Kobayashi Y, Motohisa J, Hara S and Fukui T, *Selective-area growth of vertically aligned GaAs and GaAs/AlGaAs core–shell nanowires on Si (111) substrate*, Nanotechnology **20**, 145302 (2009)
- [136] Yao M, Cong S, Arab S, Huang N, Povinelli M L, Cronin S B, Dapkus P D and Zhou C, *Tandem solar cells using GaAs nanowires on Si: Design, fabrication, and observation of voltage addition*, Nano letters **15**, 7217 (2015)
- [137] Lee S T, Wang N, Zhang Y F and Tang Y H, *Oxide-assisted semiconductor nanowire growth*, MRS Bulletin **24**, 36 (1999)
- [138] Kodambaka S R M C, Tersoff J, Reuter M C and Ross F M, *Germanium nanowire growth below the eutectic temperature*, Science **316**, 729 (2007)
- [139] Persson A I, Larsson M W, Stenström S, Ohlsson B J, Samuelson L and Wallenberg L R, *Solid-phase diffusion mechanism for GaAs nanowire growth*, Nature Materials **3**, 677 (2004)
- [140] Zhang A, Zheng G and Lieber C M, *Nanowires: Building blocks for nanoscience and nanotechnology* (Springer, 2016)
- [141] Fan H J, Werner P and Zacharias M, *Semiconductor nanowires: From self-organization to patterned growth*, Small **2**, 700 (2006)

- [142] Mårtensson T, Carlberg P, Borgström M, Montelius L, Seifert W and Samuelson L, *Nanowire arrays defined by nanoimprint lithography*, Nano letters **4**, 699 (2004)
- [143] Stringfellow G B, *Organometallic vapor-phase epitaxy: Theory and practice* (Academic Press, 1999)
- [144] AkzoNobel, *TMIn SSG product data sheet*, HPMO 60453.03/January 2014
- [145] AkzoNobel, *TMGa SSG product data sheet*, HPMO 60452.04/September 2017
- [146] AkzoNobel, *TEGa SSG product data sheet*, HPMO 60448.03/January 2014
- [147] Otnes G, Heurlin M, Zeng X and Borgström M T, *In_xGa_{1-x}P nanowire growth dynamics strongly affected by doping using diethylzinc*, Nano letters **17**, 702 (2017)
- [148] Seifert W, Borgström M, Deppert K, Dick K A, Johansson J, Larsson M W, Mårtensson T, Sköld N, Svensson C P T and Wacaser B A, *Growth of one-dimensional nanostructures in MOVPE*, Journal of Crystal Growth **272**, 211 (2004)
- [149] Kim H, Ren D, Farrell A C and Huffaker D L, *Catalyst-free selective-area epitaxy of GaAs nanowires by metal-organic chemical vapor deposition using triethylgallium*, Nanotechnology **29**, 085601 (2018)
- [150] Buchan N I, Larsen C A and Stringfellow G B, *A mass spectrometric study of the simultaneous reaction mechanism of TMIn and PH₃ to grow InP*, Journal of Crystal Growth **92**, 605 (1988)
- [151] DenBaars S P, Maa B Y, Dapkus P D, Danner A D and Lee H C, *Homogeneous and heterogeneous thermal decomposition rates of trimethylgallium and arsine and their relevance to the growth of GaAs by MOCVD*, Journal of Crystal Growth **77**, 188 (1986)
- [152] Otnes G, *III-V nanowire solar cells: Growth and characterization*, PhD thesis, Lund University (2018)
- [153] Joyce H J, Gao Q, Tan H H, Jagadish C, Kim Y, Zou J, Smith L M, Jackson H E, Yarrison-Rice J M, Parkinson P and Johnston M B, *III-V semiconductor nanowires for optoelectronic device applications*, Progress in Quantum Electronics **35**, 23 (2011)
- [154] Verheijen M A, Immink G, de Smet T, Borgström M T and Bakkers E P A M, *Growth kinetics of heterostructured GaP-GaAs nanowires*, Journal of the American Chemical Society **128**, 1353 (2006)
- [155] Borgström M T, Immink G, Ketelaars B, Algra R and Bakkers E P A M, *Synergetic nanowire growth*, Nature Nanotechnology **2**, 541 (2007)
- [156] Kodambaka S, Tersoff J, Reuter M C and Ross F M, *Diameter-independent kinetics in the vapor-liquid-solid growth of Si nanowires*, Physical review letters **96**, 096105 (2006)
- [157] Dick K A, *A review of nanowire growth promoted by alloys and non-alloying elements with emphasis on Au-assisted III-V nanowires*, Progress in Crystal Growth and Characterization of Materials **54**, 138 (2008)
- [158] Wacaser B A, Dick K A, Johansson J, Borgström M T, Deppert K and Samuelson L, *Preferential interface nucleation: An expansion of the VLS growth mechanism for nanowires*, Advanced Materials **21**, 153 (2009)

- [159] Wen C-Y, Tersoff J, Hillerich K, Reuter M C, Park J H, Kodambaka S, Stach E A and Ross F M, *Periodically changing morphology of the growth interface in Si, Ge, and GaP nanowires*, Physical review letters **107**, 025503 (2011)
- [160] Dasgupta N P, Sun J, Liu C, Britzman S, Andrews S C, Lim J, Gao H, Yan R and Yang P, *25th anniversary article: Semiconductor nanowires—synthesis, characterization, and applications*, Advanced Materials **26**, 2137 (2014)
- [161] Glas F, Harmand J-C and Patriarche G, *Nucleation antibunching in catalyst-assisted nanowire growth*, Physical review letters **104**, 135501 (2010)
- [162] Wen C-Y, Tersoff J, Reuter M C, Stach E A and Ross F M, *Step-flow kinetics in nanowire growth*, Physical review letters **105**, 195502 (2010)
- [163] Johansson J, Svensson C P T, Mårtensson T, Samuelson L and Seifert W, *Mass transport model for semiconductor nanowire growth*, The Journal of Physical Chemistry B **109**, 13567 (2005)
- [164] Dubrovskii V G, Sibirev N V, Cirilin G E, Soshnikov I P, Chen W H, Larde R, Cadel E, Pareige P, Xu T and Grandidier B, *Gibbs-Thomson and diffusion-induced contributions to the growth rate of Si, InP, and GaAs nanowires*, Physical Review B **79**, 205316 (2009)
- [165] Jensen L E, Björk M T, Jeppesen S, Persson A I, Ohlsson B J and Samuelson L, *Role of surface diffusion in chemical beam epitaxy of InAs nanowires*, Nano letters **4**, 1961 (2004)
- [166] Berg A, Mergenthaler K, Ek M, Pistol M-E, Wallenberg L R and Borgström M T, *In situ etching for control over axial and radial III-V nanowire growth rates using HBr*, Nanotechnology **25**, 505601 (2014)
- [167] Borgström M T, Wallentin J, Trägårdh J, Ramvall P, Ek M, Wallenberg L R, Samuelson L and Deppert K, *In situ etching for total control over axial and radial nanowire growth*, Nano Research **3**, 264 (2010)
- [168] Jacobsson D, Persson J M, Kriegner D, Etzelstorfer T, Wallentin J, Wagner J B, Stangl J, Samuelson L, Deppert K and Borgström M T, *Particle-assisted $Ga_xIn_{1-x}P$ nanowire growth for designed bandgap structures*, Nanotechnology **23**, 245601 (2012)
- [169] Borgström M T, Wallentin J, Kawaguchi K, Samuelson L and Deppert K, *Dynamics of extremely anisotropic etching of InP nanowires by HCl*, Chemical Physics Letters **502**, 222 (2011)
- [170] Berg A, Lehmann S, Vainorius N, Gustafsson A, Pistol M-E, Wallenberg L R, Samuelson L and Borgström M T, *Growth and characterization of wurtzite GaP nanowires with control over axial and radial growth by use of HCl in-situ etching*, Journal of Crystal Growth **386**, 47 (2014)
- [171] Cavalli A, Cui Y, Kölling S, Verheijen M A, Plissard S R, Wang J, Koenraad P M, Haverkort J E M and Bakkers E P A M, *Influence of growth conditions on the performance of InP nanowire solar cells*, Nanotechnology **27**, 454003 (2016)
- [172] Lin C and Povinelli M L, *The effect of plasmonic particles on solar absorption in vertically aligned silicon nanowire arrays*, Applied Physics Letters **97**, 071110 (2010)

- [173] Hu Y, LaPierre R R, Li M, Chen K and He J-J, *Optical characteristics of GaAs nanowire solar cells*, Journal of Applied Physics **112**, 104311 (2012)
- [174] Fox M, *Optical properties of solids* 2nd edn. (Oxford University Press, 2010)
- [175] Gudiksen M S, Wang J and Lieber C M, *Size-dependent photoluminescence from single indium phosphide nanowires*, The Journal of Physical Chemistry B **106**, 4036 (2002)
- [176] Anttu N, Heurlin M, Borgström M T, Pistol M-E, Xu H Q and Samuelson L, *Optical far-field method with subwavelength accuracy for the determination of nanostructure dimensions in large-area samples*, Nano letters **13**, 2662 (2013)
- [177] Anttu N and Xu H Q, *Scattering matrix method for optical excitation of surface plasmons in metal films with periodic arrays of subwavelength holes*, Physical Review B **83**, 165431 (2011)
- [178] Seo K, Wober M, Steinvurzel P, Schonbrun E, Dan Y, Ellenbogen T and Crozier K B, *Multicolored vertical silicon nanowires*, Nano letters **11**, 1851 (2011)
- [179] Bures J, *Guided optics: Optical fibers and all-fiber components* (Weinheim, Wiley-VCH, 2009)
- [180] Anttu N and Xu H Q, *Efficient light management in vertical nanowire arrays for photovoltaics*, Optics Express **21**, A558 (2013)
- [181] Snyder A W and Love J D, *Optical waveguide theory* (Chapman and Hall, 1983)
- [182] Svensson J, Anttu N, Vainorius N, Borg B M and Wernersson L-E, *Diameter-dependent photocurrent in InAsSb nanowire infrared photodetectors*, Nano letters **13**, 1380 (2013)
- [183] Lin C and Povinelli M L, *Optical absorption enhancement in silicon nanowire arrays with a large lattice constant for photovoltaic applications*, Optics Express **17**, 19371 (2009)
- [184] Fan S and Joannopoulos J D, *Analysis of guided resonances in photonic crystal slabs*, Physical Review B **65**, 235112 (2002)
- [185] Sturmberg B C P, Dossou K B, Botten L C, Asatryan A A, Poulton C G, de Sterke C M and McPhedran R C, *Modal analysis of enhanced absorption in silicon nanowire arrays*, Optics Express **19**, A1067 (2011)
- [186] Lalanne P, Hugonin J P and Chavel P, *Optical properties of deep lamellar gratings: A coupled Bloch-mode insight*, Journal of Lightwave Technology **24**, 2442 (2006)
- [187] Ko Y H and Magnusson R, *Wideband dielectric metamaterial reflectors: Mie scattering or leaky Bloch mode resonance?*, Optica **5**, 289 (2018)
- [188] Ko Y H, Shokooh-Saremi M and Magnusson R, *Modal processes in two-dimensional resonant reflectors and their correlation with spectra of one-dimensional equivalents*, IEEE Photonics Journal **7**, 1 (2015)
- [189] Cao L, White J S, Park J-S, Schuller J A, Clemens B M and Brongersma M L, *Engineering light absorption in semiconductor nanowire devices*, Nature Materials **8**, 643 (2009)
- [190] Mokkaapati S and Jagadish C, *Review on photonic properties of nanowires for photovoltaics [invited]*, Optics Express **24**, 17345 (2016)

- [191] Lin C and Povinelli M L, *Optimal design of aperiodic, vertical silicon nanowire structures for photovoltaics*, Optics Express **19**, A1148 (2011)
- [192] Gu Z, Prete P, Lovergine N and Nabet B, *On optical properties of GaAs and GaAs/AlGaAs core-shell periodic nanowire arrays*, Journal of Applied Physics **109**, 064314 (2011)
- [193] Diedenhofen S L, Vecchi G, Algra R E, Hartsuiker A, Muskens O L, Immink G, Bakkers E P A M, Vos W L and Rivas J G, *Broad-band and omnidirectional antireflection coatings based on semiconductor nanorods*, Advanced Materials **21**, 973 (2009)
- [194] Kriegner D, Persson J M, Etzelstorfer T, Jacobsson D, Wallentin J, Wagner J B, Deppert K, Borgström M T and Stangl J, *Structural investigation of GaInP nanowires using x-ray diffraction*, Thin solid films **543**, 100 (2013)
- [195] Berg A, Lenrick F, Vainorius N, Beech J P, Wallenberg L R and Borgström M T, *Growth parameter design for homogeneous material composition in ternary Ga_xIn_{1-x}P nanowires*, Nanotechnology **26**, 435601 (2015)
- [196] Borg B M, Dick K A, Eymery J and Wernersson L-E, *Enhanced Sb incorporation in InAsSb nanowires grown by metalorganic vapor phase epitaxy*, Applied Physics Letters **98**, 113104 (2011)
- [197] Hamamatsu Photonics, *Guide to streak cameras*, Hamamatsu City, Japan, (2008)
- [198] Wallentin J and Borgström M T, *Doping of semiconductor nanowires*, Journal of Materials Research **26**, 2142 (2011)
- [199] Lindgren D, *Optical characterization of III-nitride and III-V semiconductor nanowires*, PhD Thesis, Lund University (2014)
- [200] Hultin O, *Nanostructures for optoelectronics: Device fabrication and characterization*, PhD Thesis, Lund University (2018)
- [201] Kushev D B, Zheleva N N, Demakopoulou Y and Siapakas D, *A new method for the determination of the thickness, the optical constants and the relaxation time of weakly absorbing semiconducting thin films*, Infrared physics **26**, 385 (1986)
- [202] Killeen K P and Breiland W G, *In situ spectral reflectance monitoring of III-V epitaxy*, Journal of Electronic Materials **23**, 179 (1994)
- [203] Heurlin M, Anttu N, Camus C, Samuelson L and Borgström M T, *In situ characterization of nanowire dimensions and growth dynamics by optical reflectance*, Nano letters **15**, 3597 (2015)
- [204] Wallentin J, Barrutia Poncela L, Jansson A M, Mergenthaler K, Ek M, Jacobsson D, Reine Wallenberg L, Deppert K, Samuelson L and Hessman D, *Single GaInP nanowire pin junctions near the direct to indirect bandgap crossover point*, Applied Physics Letters **100**, 251103 (2012)
- [205] Fakhr A, Haddara Y M and LaPierre R R, *Dependence of InGaP nanowire morphology and structure on molecular beam epitaxy growth conditions*, Nanotechnology **21**, 165601 (2010)
- [206] Ishizaka F, Ikejiri K, Tomioka K and Fukui T, *Indium-rich InGaP nanowires formed on InP (111)A substrates by selective-area metal organic vapor phase epitaxy*, Japanese Journal of Applied Physics **52**, 04CH05 (2013)



Me with a Si solar panel made at Gaia Solar.

This thesis describes epitaxial growth and optical studies of semiconductor nanowires with particular focus on implications and materials for solar energy applications. I wish I could show you a photo of a large scale nanowire solar cell device. However, the path of science is long, and this thesis does not contain any nanowire solar cell devices. I can only hope that the research in this thesis will contribute in some part along the way.

This back cover, thus, I would like to dedicate to the internship at Gaia Solar, where I spent 4 months of my PhD studies. There, among other topics, I investigated building integrated photovoltaics, where performance losses due to aesthetic changes need to be evaluated. I learnt about the solar cell market, real life solar module performance and manufacturing choices and challenges. I even got an opportunity to make solar panels with my own hands. The figure above is a multi-crystalline Si solar panel that I designed and made myself as a present from the company for my work there.